

AEDC-TR-80-32



Supplemental Calibration of the AEDC-PWT  
16-ft Transonic Tunnel Aerodynamic Test Section

M. L. Mills  
ARO, Inc.

July 1981

Final Report for Period December 1979 – June 1980

Approved for public release; distribution unlimited.

**ARNOLD ENGINEERING DEVELOPMENT CENTER  
ARNOLD AIR FORCE STATION, TENNESSEE  
AIR FORCE SYSTEMS COMMAND  
UNITED STATES AIR FORCE**

## NOTICES

When U. S. Government drawings, specifications, or other data are used for any purpose other than a definitely related Government procurement operation, the Government thereby incurs no responsibility nor any obligation whatsoever, and the fact that the Government may have formulated, furnished, or in any way supplied the said drawings, specifications, or other data, is not to be regarded by implication or otherwise, or in any manner licensing the holder or any other person or corporation, or conveying any rights or permission to manufacture, use, or sell any patented invention that may in any way be related thereto.

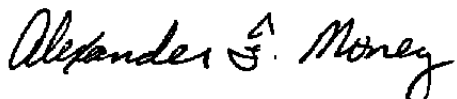
Qualified users may obtain copies of this report from the Defense Technical Information Center.

References to named commercial products in this report are not to be considered in any sense as an indorsement of the product by the United States Air Force or the Government.

This report has been reviewed by the Office of Public Affairs (PA) and is releasable to the National Technical Information Service (NTIS). At NTIS, it will be available to the general public, including foreign nations.

## APPROVAL STATEMENT

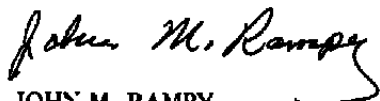
This report has been reviewed and approved.



ALEXANDER F. MONEY  
Directorate of Technology  
Deputy for Operations

Approved for publication:

FOR THE COMMANDER



JOHN M. RAMPY  
Director of  
Aerospace Flight Dynamics Test  
Deputy for Operations

**UNCLASSIFIED**

# UNCLASSIFIED

## 20. ABSTRACT (Continued)

acquired for Mach numbers from 0.6 to 1.6 at total pressures from 400 to 3,200 psfa. The calibration was conducted in the aerodynamic test section using a centerline pipe and wall pressure orifices to define the Mach number distributions. The results of an evaluation of alternate methods of calibration indicated that the current method is the most acceptable. Slightly changing the tunnel nozzle to eliminate the disturbances in the flow at supersonic Mach numbers indicated the need to investigate the entire nozzle system. Comparison of this calibration with previous calibration results indicates that a revision of the current tunnel calibration is not necessary.

## **PREFACE**

The work reported herein was conducted by the Arnold Engineering Development Center (AEDC), Air Force Systems Command (AFSC), at the request of the AEDC Directorate of Test (DOOP) and the AEDC Directorate of Technology (DOT). The Air Force project managers were Capt. Greg Cowley (AEDC/DOOP) and Mr. E. R. Thompson (AEDC/DOT). The results were obtained by ARO, Inc., AEDC Group (a Sverdrup Corporation Company), operating contractor for the AEDC, AFSC, Arnold Air Force Station, Tennessee, under ARO Project Numbers P41T-D4G and P32D-85C. The manuscript was submitted for publication on July 21, 1980.

## CONTENTS

	<u>Page</u>
<b>1.0 INTRODUCTION .....</b>	<b>7</b>
<b>2.0 APPARATUS</b>	
<b>2.1 Test Facility .....</b>	<b>8</b>
<b>2.2 Calibration Equipment .....</b>	<b>9</b>
<b>2.3 Instrumentation .....</b>	<b>9</b>
<b>3.0 PROCEDURE</b>	
<b>3.1 Test Conditions .....</b>	<b>10</b>
<b>3.2 Data Reduction .....</b>	<b>11</b>
<b>3.3 Uncertainty of Measurements .....</b>	<b>12</b>
<b>3.4 Flow Quality .....</b>	<b>12</b>
<b>4.0 RESULTS AND DISCUSSION</b>	
<b>4.1 Mach Number Distributions .....</b>	<b>13</b>
<b>4.2 Tunnel Calibration .....</b>	<b>17</b>
<b>5.0 CONCLUSIONS .....</b>	<b>20</b>
<b>REFERENCES .....</b>	<b>20</b>

## ILLUSTRATIONS

### Figure

<b>1. Tunnel 16T Test Section and Centerline Pipe Installation .....</b>	<b>23</b>
<b>2. Tunnel 16T Calibration Installation .....</b>	<b>24</b>
<b>3. Nozzle Static Pressure Orifice Locations .....</b>	<b>27</b>
<b>4. Test Section Wall Angle Schedules .....</b>	<b>29</b>
<b>5. Variation of Tunnel Pressure Ratio with <math>\theta = 0</math> .....</b>	<b>30</b>
<b>6. Tunnel 16T Mach Number Distributions at <math>M_{\infty} = 0.6</math> to 1.0 with <math>\lambda = \lambda^*</math>, <math>\theta = 0</math>, and <math>P_t = 1,600</math> psfa .....</b>	<b>31</b>
<b>7. Tunnel 16T Mach Number Distributions at <math>M_{\infty} = 1.1</math> to 1.6 with <math>\lambda = \lambda^*</math>, <math>\theta = 0</math>, and <math>P_t = 1,600</math> psfa .....</b>	<b>36</b>
<b>8. Effect of Orifice Selection on the Mach Number Deviations with <math>\lambda = \lambda^*</math>, <math>\theta = 0</math>, and <math>P_t = 1,600</math> psfa .....</b>	<b>41</b>
<b>9. Effect of Test Region Location on the Mach Number Deviations with <math>\lambda = \lambda^*</math>, <math>\theta = 0</math>, and <math>P_t = 1,600</math> psfa .....</b>	<b>42</b>
<b>10. Effect of Centerline Pipe Length on the Mach Number Distributions from <math>M_{\infty} = 1.1</math> to 1.6 with <math>\lambda = \lambda^*</math>, <math>\theta = 0</math>, and <math>P_t = 1,600</math> psfa .....</b>	<b>43</b>

<u>Figure</u>	<u>Page</u>
11. Effect of Centerline Pipe Length on the Mach Number Deviations with $\lambda = \lambda^*$ , $\theta = 0$ , and $P_t = 1,600$ psfa .....	44
12. Effect of Mach Number on the Centerline Mach Number Deviations with $\lambda = \lambda^*$ , $\theta = 0$ , and $P_t = 1,600$ psfa .....	45
13. Effect of Plenum Chamber Suction on the Centerline Mach Number Distributions at $P_t = 1,000$ psfa with $\theta = 0$ .....	46
14. Effect of Plenum Chamber Suction on the Centerline Mach Number Distributions at $P_t = 1,600$ psfa with $\theta = 0$ .....	49
15. Effect of Plenum Chamber Suction on the Centerline Mach Number Distributions at $P_t = 2,200$ psfa with $\theta = 0$ .....	52
16. Effect of Tunnel Pressure Ratio on the Total Power Factor at $M_\infty \leq 0.75$ with $\theta = 0$ .....	55
17. Effect of Test Section Humidity on the Mach Number Distributions with $\lambda = \lambda^*$ and $\theta = 0$ .....	56
18. Effect of Test Section Humidity on the Average Mach Number with $\lambda = \lambda^*$ and $\theta = 0$ .....	61
19. Effect of Test Section Humidity on the $2\sigma$ Mach Number Deviations with $\lambda = \lambda^*$ and $\theta = 0$ .....	63
20. Nozzle Wall Mach Number Distributions at $M_a = 0.6008$ and $M_c = 0.5912$ with $\lambda = \lambda^*$ , $\theta = 0$ , and $P_t = 1,600$ psfa .....	65
21. Nozzle Wall Mach Number Distributions at $M_a = 0.7996$ and $M_c = 0.7989$ with $\lambda = \lambda^*$ , $\theta = 0$ , and $P_t = 1,600$ psfa .....	66
22. Nozzle Wall Mach Number Distributions at $M_a = 0.9979$ and $M_c = 0.9859$ with $\lambda = \lambda^*$ , $\theta = 0$ , and $P_t = 1,600$ psfa .....	67
23. Nozzle Wall Mach Number Distributions at $M_a = 1.2023$ and $M_c = 1.1868$ with $\lambda = \lambda^*$ , $\theta = 0$ , and $P_t = 1,600$ psfa .....	69
24. Nozzle Wall Mach Number Distributions at $M_a = 1.3994$ and $M_c = 1.3853$ with $\lambda = \lambda^*$ , $\theta = 0$ , and $P_t = 1,600$ psfa .....	71
25. Nozzle Wall Mach Number Distributions at $M_a = 1.5985$ and $M_c = 1.5847$ with $\lambda = \lambda^*$ , $\theta = 0$ , and $P_t = 1,600$ psfa .....	73
26. Tunnel 16T Mach Number Calibration with $\lambda = \lambda^*$ , $\theta = 0$ , and $P_t = 1,600$ psfa .....	75
27. Tunnel 16T Pressure Calibrations from $M_\infty = 0.6$ to 1.6 with $\lambda = \lambda^*$ , $\theta = 0$ , and $P_t = 1,600$ psfa .....	76
28. Effect of Nozzle Jack Perturbations on the Nozzle-Test Section Calibration with $\lambda = \lambda^*$ , $\theta = 0$ , and $P_t = 1,600$ psfa .....	79

<u>Figure</u>	<u>Page</u>
29. Effect of the Calibration Method on the Uncertainty of the Calibrated Free-Stream Static Pressure with $\theta = 0$ .....	80
30. Effect of the Calibration Method on the Uncertainty of the Calibrated Free-Stream Mach Number with $\theta = 0$ .....	83
31. Effect of Mach Number on the Calibration with $\lambda = \lambda^*$ , $\theta = 0$ , and $P_t = 1,600$ psfa .....	86
32. Effect of the Centerline Pipe Length on the Calibration with $\lambda = \lambda^*$ , $\theta = 0$ , and $P_t = 1,600$ psfa .....	87
33. Effect of Plenum Chamber Suction on the Calibration at $M_\infty \leq 0.75$ with $\lambda = \lambda^*$ , $\theta = 0$ , and $P_t = 1,600$ psfa .....	88
34. Effect of Test Section Humidity on the Mach Number Calibration with $\lambda = \lambda^*$ , $\theta = 0$ .....	89
 <b>APPENDIX</b>	
A. NOZZLE JACK PERTURBATIONS .....	93
NOMENCLATURE .....	108

## 1.0 INTRODUCTION

The AEDC Propulsion Wind Tunnel (16T) was put into operation in July 1956. Initially, tunnel calibrations were conducted for the two test sections (aerodynamic and propulsion) available for tests, but later tunnel or equipment modification, the resolution of the effect of some tunnel parameter, or the need for improved data quality precipitated several additional tunnel calibrations. Collectively, this early calibration work revealed that, within the existing data accuracy, only test section wall angle variation had a significant effect upon the tunnel calibration.

After the installation of fiberglass compressor blades in Tunnel 16T in 1965, a calibration was conducted with the aerodynamic test section. This calibration (Ref. 1) was based on pressure orifices located in a 2-ft-wide solid plate in the test section floor. The Ref. 1 calibration remained in use in Tunnel 16T until May 1977.

To support a program for improving nozzle/afterbody (NAB) test techniques, tests were conducted in the propulsion test section of Tunnel 16T to determine the tunnel calibration and centerline Mach number distributions at various test section wall porosities and Reynolds numbers. During the porosity calibration (Ref. 2), limited data obtained at  $M_\infty = 0.6$  and 0.8 indicated that the calibrated Mach number increased slightly (less than 0.001 per million) with increasing Reynolds number. Following the calibration reported in Ref. 2, an analysis of the effects of variation of the tunnel calibration with Reynolds number on NAB test data was conducted. This analysis revealed that a 0.2-percent error in static pressure attributed to use of the Ref. 1 calibration, which neglects the effects of Reynolds number, could cause a 70-drag-count (based on maximum model cross-sectional area) error in nozzle afterbody drag at  $M_\infty = 0.6$  and  $Re = 5.0 \times 10^6/\text{ft}$ . Consequently, a test was conducted to define completely the effects of Reynolds number variation on the Tunnel 16T calibration. The results of this calibration, which was conducted with the propulsion test section, are presented in Ref. 3.

Since nozzle afterbody data are sensitive to small changes in the tunnel calibration, the adequacy of using the same tunnel calibration for both the aerodynamic and propulsion test sections came into question. Data obtained parasitically during an NAB test in the aerodynamic test section showed that the effects of Reynolds number on the tunnel calibration were more pronounced in the aerodynamic test section than in the propulsion test section. These results precipitated two calibration entries in the aerodynamic test section. Calibration results, which are reported in Ref. 4, confirmed that the aerodynamic and propulsion test sections had different Reynolds number effects. Both the Refs. 3 and 4 calibration results are currently utilized for Tunnel 16T operation.

The data in Ref. 4 indicated anomalies in the centerline distributions at supersonic Mach numbers. These anomalies were assumed to be partially attributable to disturbances originating on the ogive nose of the calibration pipe. The Ref. 4 calibration also indicated that power savings were available by increasing plenum chamber suction at Mach numbers less than 0.75. However, the Ref. 4 data were insufficient for a complete definition of this effect. Because of the increasing costs of energy and the need to continually improve the calibration accuracy, the need for another calibration evolved. This calibration was conducted in the aerodynamic test section using the Ref. 4 calibration pipe and a longer version. In addition to the supersonic disturbances and the plenum suction study, several other effects in the aerodynamic test section were investigated. These included evaluating the effect of test section humidity on the calibration and defining the correlation between nozzle wall and centerline static pressures.

During the calibration, data were obtained at free-stream Mach numbers from 0.6 to 1.6 at free-stream stagnation pressures from 400 to 3,200 psfa. The effect of plenum chamber suction on power was determined at free-stream Mach numbers of 0.6, 0.7, and 0.75 for stagnation pressures of 1,000, 1,600, and 2,200 psfa. Test section humidity was varied from a maximum of 0.009 to a minimum of 0.0005 lb H<sub>2</sub>O/lb dry air, depending upon the test condition. Results from this calibration are presented in this report.

## 2.0 APPARATUS

### 2.1 TEST FACILITY

The AEDC Propulsion Wind Tunnel (16T) is a variable density, continuous-flow tunnel capable of being operated at Mach numbers from 0.2 to 1.6 and stagnation pressures from 120 to 4,000 psfa. The maximum attainable Mach number can vary slightly depending upon the tunnel pressure ratio requirements with a particular test installation. The maximum stagnation pressure attainable is a function of Mach number and available electrical power. The tunnel stagnation temperature can be varied from about 80 to 160°F depending upon the cooling water temperature. The tunnel is equipped with a scavenging system which removes combustion products when rocket motors or turbo-engines are tested. The test section is 16 ft square by 40 ft long; it is enclosed by 60-deg inclined-hole perforated walls of six-percent porosity. The test section sidewalls can be either converged 2 deg or diverged 1 deg. The general arrangement of the test section and perforated wall geometry is shown in Fig. 1.

To prevent tunnel choking in the transonic Mach number range, test section flow removal is accomplished with a plenum evacuation system (PES), which is also utilized to control tunnel pressure level. The PES compressors are driven by motors with a total power rating of 179,000 hp, and the tunnel main compressor drive system is rated at 226,000 hp.

Various Mach numbers in Tunnel 16T are established by regulation of tunnel pressure ratio, plenum pressure, and the contour of a flexible, two-dimensional Laval nozzle. Mach numbers below 0.55 are obtained by operating the compressor drive motors subsynchronously. Test section flow removal is normally required at  $M_{\infty} > 0.75$  and supersonic nozzle contours are used at  $M_{\infty} \geq 1.05$ . Additional details concerning Tunnel 16T and its capabilities are presented in Ref. 5.

## 2.2 CALIBRATION EQUIPMENT

A 6.5-in.-diam static pressure pipe was used to obtain the centerline static pressure distribution from tunnel station -5.9 to 24.1. The aft end of the calibration pipe was attached to the tunnel sting support system, and a mechanism was provided to counteract pipe sway and sag. Four cables, swept rearward at 30 deg to the tunnel centerline and spaced to produce a moment that would aid in removing pipe sag, provided pipe support. The pipe, which had an ogive tip, was subject to a tensile load by a cable which extended upstream into the tunnel nozzle and connected to a streamlined forebody and cable support system. The pipe installation is shown in Fig. 2. To improve the supersonic Mach number distributions, the nose of the existing static pressure pipe was extended from station -22 to -30. After the effect of pipe length on the test section Mach number distribution was determined, the 8-ft extension was removed so the final pipe configuration was the same as that used on previous calibration tests.

## 2.3 INSTRUMENTATION

The centerline pipe contained 75 static pressure orifices (0.127-in.-diam), fifty-four of which were located approximately 30 deg in a clockwise direction (facing upstream) from the vertical plane and referred to as the centerline pipe upper orifices. These orifices were spaced in 1-ft intervals from tunnel stations -5.9 to 0.1 and 0.5-ft intervals from tunnel stations 0.1 to 24.1. The remaining 21 orifices were located approximately 210 deg in a clockwise direction (facing upstream) from the vertical plane and referred to as the centerline pipe lower orifices. These orifices were spaced in 1-ft intervals from tunnel stations 0.1 to 20.1.

Test section wall static pressure distributions were obtained from three rows of orifices (Fig. 1). A row of 20 orifices (0.065-in.-diam) was located 1 ft west of the tunnel centerline in the porous floor plates and spaced in 1-ft intervals from tunnel stations 1 to 20. A row of 24 orifices (0.065-in.-diam) was located 1 ft east of the tunnel centerline in 2-ft-wide solid floor plates. The solid floor was extended upstream to tunnel station -9 by filling all holes in the single transition section taper strip as shown in Fig. 2. These orifices were spaced in 1-ft intervals from tunnel stations 0 to 20 and 2-ft intervals from stations 20 to 26. Another row

of 20 orifices (0.65-in.-diam) was located 1 ft west of the tunnel centerline in porous ceiling plates. These orifices were spaced in 1-ft intervals from tunnel stations 1 to 20.

Nozzle wall static pressures were measured with 12 orifices (0.125-in.-diam) at tunnel station -4, 5 orifices (0.125-in.-diam) at tunnel station -8, and 8 orifices (0.125-in.-diam) at tunnel station -12 as shown in Fig. 3.

The pipe, wall, and nozzle orifices were connected to differential pressure transducers referenced to the tunnel plenum chamber pressure. The tunnel stagnation pressure was determined by averaging measurements from two independent systems of total pressure probes installed in the tunnel stilling chamber. The plenum chamber and stagnation pressures were determined by measurements from Datametrics® pressure transducers.

### 3.0 PROCEDURE

#### 3.1 TEST CONDITIONS

The calibration was conducted over a Mach number range from 0.6 to 1.6, although special emphasis was placed on the effects of plenum suction at  $0.6 \leq M_{\infty} \leq 0.75$  and on the quality of the supersonic Mach number distributions at  $M_{\infty} \geq 1.2$ . Data were obtained at various stagnation pressures from 400 to 3,200 psfa and at a stagnation temperature of 110°F, which corresponds to a unit Reynolds number variation from  $0.6 \times 10^6/\text{ft}$  to  $4.9 \times 10^6/\text{ft}$ . The effects of tunnel pressure ratio, test section wall angle variation, and nozzle jack movements were evaluated at a stagnation pressure of 1,600 psfa. A stagnation pressure of 1,600 psfa was chosen as a baseline for data acquisition because previous calibrations (Refs. 3 and 4) were conducted primarily at 1,600 psfa. The effects of tunnel specific humidity variation were evaluated at Mach numbers of 0.6, 0.9, 1.2, and 1.5.

The test section wall angle was varied from 0.50 to -1.00 deg. Positive wall angles correspond to wall divergence from the tunnel centerline. The Tunnel 16T optimum wall angle schedule and the range of wall angles investigated during this calibration are shown in Fig. 4. The optimum wall angle schedule generally provides the "best" pressure distribution on long, slender bodies of revolution with a test section blockage of one percent.

On the basis of data presented in Refs. 3 and 4, a nominal pressure ratio schedule was used during variations of test section wall angle and Reynolds number. The nominal pressure ratio ( $\lambda^*$ ) schedule is shown in Fig. 5. To determine the effects of pressure ratio on the Mach number distributions, the pressure ratio was varied above and below the nominal

schedule at  $M_{\infty} = 0.8, 0.9$ , and  $1.0$ . To determine the effect of using plenum suction on tunnel power requirements at  $M_{\infty} = 0.6, 0.7$ , and  $0.75$ , the tunnel pressure ratio was decreased below the nominal schedule.

The effect of specific humidity variation on the calibration was obtained by "wetting" the tunnel to the maximum specific humidity obtainable and then taking data while the tunnel was drying. The maximum range of specific humidity was from  $9.0 \times 10^{-3}$  to  $0.5 \times 10^{-3}$  lb H<sub>2</sub>O/lb dry air. For most other test conditions the specific humidity was maintained at less than  $1.5 \times 10^{-3}$  lb/lb.

In an attempt to eliminate the data anomalies at supersonic Mach numbers reported in Ref. 4, the centerline pipe was extended to tunnel station -30 by placing an 8-ft extension immediately aft of the ogive tip. After observing that the "longer" pipe did not improve the Mach number distributions, the extension was removed for the remainder of the test. To investigate the influence that the Tunnel 16T nozzle has on the supersonic data anomalies, data were obtained with individual nozzle jacks perturbed slightly from the design contour. Nozzle jacks were moved up to 0.35-in. from the nominal contours.

### 3.2 DATA REDUCTION

The distribution of local Mach number in the test section was obtained from the centerline pipe and wall static pressure data with the assumption of isentropic flow through the nozzle. The average Mach numbers and the  $2\sigma$  Mach number deviations for three test section regions, tunnel stations 1 to 20, 3 to 19, and 6 to 18 were computed. The Mach number deviation,  $2\sigma$ , is the conventional two standard deviation parameter used in statistical analysis. Nozzle average Mach numbers were computed using rings of nozzle wall static pressure orifices located at tunnel stations -12, -8, and -4.

The calibration of Tunnel 16T is based on the measured pressure differential between the test section and the plenum chamber at various operating conditions. An equivalent plenum chamber Mach number is calculated from plenum chamber and tunnel stagnation pressure measurements using the isentropic relationship. A calibration parameter, defined as the difference between the free-stream and plenum chamber Mach numbers ( $M_a - M_c$ ), is used to express the tunnel calibration for various operating conditions.

To aid in evaluating potential improvements in the accuracy of the calibration, three other calibration parameters were computed. A calibration factor, defined as the difference between the free-stream static and plenum chamber pressures normalized by free-stream stagnation pressure ( $P_a - P_c$ )/ $P_t$ , was used. This calibration factor provides static pressure

directly as a function of the plenum chamber pressure. Mach number is determined using isentropic relationships between  $p_\infty$  and  $p_t$ . The calibration factor  $(P_a - P_{\text{nozzle}})/P_t$ , which would make the tunnel calibration independent of the plenum chamber pressure and the calibration factor  $(P_a/P_t)$ , was also investigated.

### 3.3 UNCERTAINTY OF MEASUREMENTS

A Taylor series method of error propagation was used to estimate the uncertainty in the calibration parameters which could be attributed to instrumentation errors and data acquisition techniques. Uncertainties in the instrumentation systems were estimated from repeat calibration of the systems against secondary standards whose uncertainties are traceable to the National Bureau of Standards calibration equipment. For a confidence level of 95.4 percent, the estimated uncertainties are:

<u>Parameter</u>	<u>Uncertainty</u>
$\lambda$	$\pm 0.002$
$\theta$	$\pm 0.04$ deg
$M_{\text{local}}$	$\pm 0.003$
$M_a$	$\pm 0.0006$
$P_a$	$\pm 0.73$ psf
$Re$	$\pm 0.02 \times 10^{-6}$ /ft
$(M_a - M_c)$	$\pm 0.0014$
$(P_a - P_c)/P_t$	$\pm 0.0009$
$P_a/P_t$	$\pm 0.0008$
$(P_a - P_{\text{nozzle}})/P_t$	$\pm 0.0008$

### 3.4 FLOW QUALITY

One of the primary objectives of a tunnel calibration is to ascertain that adequate flow quality exists for acquisition of test data for various locations of test models and various combinations of tunnel conditions. Tunnel flow quality encompasses several parameters, such as flow angularity and turbulence, which were not investigated during this calibration.

Past calibrations have indicated that axial pressure gradients requiring the application of buoyancy corrections to test data do not exist in Tunnel 16T for normal operating conditions. This report, therefore, is concerned only with the uniformity of the axial Mach number distributions.

A quantitative evaluation of the uniformity of a Mach number distribution, when no pressure gradients exist, can be provided by analysis of the  $2\sigma$  Mach number deviation. This deviation can also be used to evaluate the effects of various test parameters on the centerline Mach number distributions. The minimum Mach number deviation for a particular test section length and set of tunnel conditions is, of course, indicative of the "best" distribution. For purposes of this report and in conformity with Refs. 3 and 4,  $2\sigma$  Mach number deviations of  $0.005 M_\infty$  and  $0.01 M_\infty$  for subsonic and supersonic Mach numbers, respectively, will be used as criteria for relative evaluation of the various Mach number distributions. These criteria should not be confused with tunnel data quality goals and requirements, which are established by individual test objectives.

## 4.0 RESULTS AND DISCUSSION

### 4.1 MACH NUMBER DISTRIBUTIONS

#### 4.1.1 General

Typical short pipe centerline and wall Mach number distributions obtained at Mach numbers from 0.6 to 1.6 with  $\lambda = \lambda^*$ ,  $\theta = 0$ , and  $P_t = 1,600$  psfa are presented in Figs. 6 and 7. The data presented in Fig. 6 indicate that at subsonic Mach numbers, the Mach number distributions on the centerline and tunnel walls differ aft of tunnel station 20. The differences are attributed to different interference and plenum chamber suction effects. The centerline pipe pressures are predominantly affected by boom flare and support strut interference, which cause a deceleration of the flow. The wall distributions are predominantly affected by strut interference, wall bulge, and plenum suction. The local Mach number along the solid plate also increases aft of tunnel station 20 at  $M_\infty < 0.8$  and decreases at  $M_\infty > 0.8$ . This is attributed to the use of plenum chamber suction which began at  $M_\infty = 0.8$ .

The data presented in Fig. 7 indicate that at supersonic Mach numbers the forward portions of the centerline and wall distributions differ. According to Refs. 3 and 4, for which similar Mach number distributions were obtained, the supersonic centerline Mach number distributions were believed to be affected by disturbances which emanated from the forward portion of the calibration pipe and from near tunnel station 0. During this test, an

attempt was made to eliminate these anomalies by extending the calibration pipe. These results are discussed in Section 4.1.2 of this report.

The  $2\sigma$  Mach number deviations for various test regions may be used as an aid in evaluating the Mach number distributions. The effects of pressure orifice selection and test region length are illustrated in Figs. 8 and 9. The comparisons of the deviations for various test region lengths have the same variation, in general, as the Ref. 4 data. The upper centerline pipe data from tunnel stations 6 to 18 are considered the primary data to be used as the basis for the calibration for the same reasons as reported in Ref. 4.

The effects of varying tunnel pressure ratio and test section wall angle on the Mach number distributions and  $2\sigma$  Mach number deviations were essentially the same as those reported in Ref. 4 and are therefore not presented here.

#### 4.1.2 Effect of Calibration Pipe Length

In an attempt to eliminate the disturbances in supersonic Mach number distributions, the calibration pipe was extended 8 ft. This extension caused the pipe nose shock to impinge on the nozzle walls rather than the test section walls. Similarly, the shock reflection from the nozzle walls impinged on the calibration pipe upstream of station 0.

Comparisons of the Mach number distributions and  $2\sigma$  Mach number deviations for the calibration pipe with and without the pipe extension (hereafter referred to as the long and short pipe) are presented in Figs. 10 and 11. The data in Fig. 10 indicate pipe length has large effects on the distribution upstream of tunnel station 0 with smaller effects in the primary test region which are not noticeable in Fig. 10 but indicated by the  $2\sigma$  deviations in Fig. 11. The data in Fig. 11 indicate that there is no difference between the short and long pipe deviations at Mach numbers from 0.8 to 1.0. With the exception of  $M_\infty = 1.1$ , there are only small but inconsistent differences between the short and long pipe deviations at supersonic Mach numbers. Since the longer pipe did not significantly improve the centerline distributions, the short pipe configuration was used for most of the calibration test so that a direct comparison could be made with previous data. Data were not taken with the short calibration pipe configuration at  $M_\infty = 0.6, 0.7$ , and 0.75 after observing that no change occurred in the other subsonic Mach number distributions when using the long pipe.

#### 4.1.3 Effect of Mach Number

The effect of Mach number on the  $2\sigma$  Mach number deviations for the centerline distributions and a comparison with the Ref. 4 calibration are shown in Fig. 12. The data indicate that, except for  $M_\infty = 1.2$  and 1.6, the deviations are better than the relative criteria for "good" distributions. The disturbances causing the poor Mach number distributions were previously thought to originate on the calibration pipe, but the Ref. 4 data in Fig. 12 and the current data were obtained with the same centerline pipe installation. The fact that poorer quality data were obtained at  $M_\infty = 1.2$  and 1.6 indicates that other disturbances exist in Tunnel 16T which affect the quality of the Mach number distributions. This observation led to an attempt to eliminate the disturbances by perturbing individual nozzle jacks. These results are presented in Appendix A.

#### 4.1.4 Effect of Plenum Suction

The effect of using plenum suction on the centerline distributions at  $M_\infty \leq 0.75$  with  $P_t = 1,000, 1,600$ , and  $2,200$  psfa are shown in Figs. 13, 14, and 15. The flow decelerates aft of tunnel station 20 when tunnel pressure ratio is decreased to accommodate the increased plenum suction. The data quality is slightly improved when using plenum suction, except at  $M_\infty = 0.6$ ,  $P_t = 2,200$  psfa, as indicated by the  $2\sigma$  deviations.

The effect of plenum suction on tunnel power requirements at  $M_\infty \leq 0.75$  is presented in Fig. 16. These data were obtained with the plenum bypass valve (Valve 12) both opened and closed. For the Valve 12 open cases, the power data were not corrected by subtracting the power associated with flow recirculated through the PES via Valve 12. The data show a minimum power requirement when tunnel pressure ratio is reduced by 0.5 percent at  $M_\infty = 0.6$  and 0.7 and by 1.5 percent at  $M_\infty = 0.75$  for  $P_t = 1,600$  psfa. Further decreases of tunnel pressure ratio, which coincide with increasing plenum suction, cause an increase of total power. Based on the data at  $P_t = 1,600$  psfa, the data for  $P_t = 1,000$  and  $2,200$  psfa were taken at tunnel pressure ratios which were too low to define the minimum total power requirements. Thus, further data are required for a complete definition of the range of tunnel pressure ratios or wall suction which will minimize power.

#### 4.1.5 Effect of Humidity

The effect of test section humidity on the Mach number distributions, the average Mach number of the primary test region (tunnel stations 6 to 18), and the  $2\sigma$  Mach number deviations for various tunnel conditions is shown in Figs. 17, 18, and 19. The objectives of the humidity study were to determine if humidity has an effect on the tunnel calibration and

if the present dryness criteria for Tunnel 16T are acceptable. The data presented in Figs. 17, 18, and 19 indicate that, for the range of humidities investigated, humidity does not have a significant effect upon the Mach number distributions, except at  $M_{\infty} = 1.5$ .

The current dryness criteria are that the test section static temperature must be greater than or equal to the test section dew point temperature for subsonic operation, and the specific humidity must be less than 0.0015 lb H<sub>2</sub>O/lb dry air for supersonic operation.

The data in Figs. 18a-b and 19a-b show that data were not obtained at humidities which exceed the subsonic dryness criteria at  $M_{\infty} = 0.6$ ,  $P_t = 3,200$  psfa, and  $M_{\infty} = 0.9$ ,  $P_t = 1,200$  psfa. However, this is not significant because the full range of possible humidities encountered during tunnel operations was obtained. There is no observable humidity effect for this range at  $M_{\infty} = 0.6$ ,  $P_t = 3,200$  psfa, and  $M_{\infty} = 0.9$ ,  $P_t = 1,200$  psfa.

The data in Figs. 18c-d and 19c-d indicate that there is no humidity effect on the average Mach number or the  $2\sigma$  Mach number deviations at  $M_{\infty} = 0.9$ ,  $P_t = 2,400$  psfa and  $M_{\infty} = 1.2$ ,  $P_t = 1,600$  psfa while the tunnel is operating within or slightly above the dryness criterion limit.

The data presented in Fig. 17e indicate that humidity has an effect on the Mach number distribution at  $M_{\infty} = 1.5$ . There is a positive Mach number gradient through the test section with the local Mach number increasing to 1.5 in the downstream end of the test section. This effect is also indicated by decreasing average Mach numbers and increasing  $2\sigma$  deviations with increasing humidity as shown in Figs. 18e and 19e. Throughout the humidity run, the plenum chamber pressure and stagnation pressure were not allowed to vary. The probable explanation for the effects cited above is that a condensation shock formed in the tunnel nozzle, causing the flow to decelerate, as indicated by the distribution in Fig. 17e. The porous test section walls permit the flow to expand to the plenum chamber pressure, which causes a Mach number gradient through the test section. The Mach numbers calculated when a condensation shock is present are not valid, however, because the stagnation pressure used to calculate Mach number is measured upstream of the shock. The data in Figs. 18e and 19e indicate that the Mach number distributions are not affected when the humidity is less than the dryness criterion limit. Thus, the test section humidity should never be allowed to exceed the dryness criterion during testing at  $M_{\infty} = 1.5$ .

#### 4.1.6 Nozzle Wall Mach Number Distributions

Typical Mach number distributions measured on the tunnel nozzle walls at tunnel stations -4 and -12 are presented in Figs. 20 through 25. The data indicate that the local

Mach number varies less at tunnel station -12 than at -4 for subsonic Mach numbers as indicated by the  $2\sigma$  deviations. These variations may be due to orifice or local surface irregularities such as the porous hole patterns at tunnel station -4, paint roughness, and mounting bolts countersunk in wall plates upstream of tunnel station -4. At supersonic Mach numbers the  $2\sigma$  deviations are smaller at tunnel station -4 than at -12. The variations in wall Mach number at supersonic Mach numbers are caused by the same disturbances as for subsonic Mach numbers plus spurious wave patterns emanating from the centerline pipe or nozzle walls.

The  $2\sigma$  deviations indicated in Figs. 20 through 25 are larger in general than those of the calibration pipe data presented in Fig. 12. This makes a correlation between the nozzle and test section Mach numbers undesirable for use as a calibration of Tunnel 16T.

## 4.2 TUNNEL CALIBRATION

### 4.2.1 General

Analytic expressions of the Mach number calibration parameter ( $M_a - M_c$ ) as a function of equivalent plenum chamber Mach number, test section wall angle, and Reynolds number are currently used to express the Tunnel 16T calibration. These expressions were obtained by using a least-squares, multiple regression data fitting program and are incorporated into the facility computer.

The use of tunnel calibration factors  $(P_a - P_c)/P_t$ ,  $P_a/P_t$ , and  $(P_a - P_{nozzle})/P_t$ , to express the calibration was investigated in an attempt to improve the accuracy of the tunnel calibration and possibly remove the effects of test section wall angle and Reynolds number from the calibration. Pressure calibrations were used rather than Mach number calibrations to determine if the estimated uncertainty of the test section calibrated static pressure can be improved by calculating the static pressure directly.

The tunnel Mach number calibration parameter and the three tunnel pressure calibration factors are determined from measurements of the tunnel test section static, stagnation, and either plenum chamber or nozzle static pressures. These pressures have different control and measurement response characteristics. The plenum chamber and stagnation pressures are independently and manually controlled, but the control of all four pressures are interrelated because the test section and plenum chamber communicate through the ventilated walls. Thus, the calibration parameter and factors are very sensitive to transients in various tunnel parameters. Most of the data scatter exhibited in the calibration data presented herein is attributed to such control transients. During acquisition of data at each test condition, data

points were obtained until the tunnel calibration parameter had been repeated or the data scatter had been bracketed. Three data points were required for most test conditions. As indicated in Section 4.1.1, the calibration data presented herein are based on centerline pipe data obtained for the primary test region, tunnel stations 6 to 18.

#### 4.2.2 Alternate Calibration Factors

The current tunnel Mach number calibration parameter is presented in Fig. 26 and three alternate tunnel pressure calibration factors with  $\lambda = \lambda^*$ ,  $\theta = 0$ , and  $P_t = 1,600$  psfa are presented in Fig. 27. The factor  $(P_a - P_c)/P_t$ , (Fig. 27a) is the pressure equivalent of the Mach number calibration parameter  $(M_a - M_c)$ . The factor  $(P_a/P_t)$  (Fig. 27b) is monotonic, increasing as the ratio of  $P_c/P_t$  increases. The factors,  $(P_a - P_{\text{nozzle}})/P_t$ , relating the test section static to nozzle static pressure at tunnel stations -4 and -12 are presented in Figs. 27c and d, respectively. The points in Fig. 27c which correspond to Mach numbers of 1.2 and 1.5 and in Fig. 27d which correspond to Mach numbers 1.2, 1.4, and 1.5, deviate significantly from what would be expected. Some improvement was gained by perturbing nozzle jack 1 and by perturbing nozzle jacks 2 and 4 at  $M_\infty = 1.2$  as shown in Fig. 28. The data show more variation in the calibration factor at tunnel station -12 than at tunnel station -4. The cause of the data anomalies at the supersonic speeds needs to be found before a decision with regard to the utilization of tunnel stations -4 and -12 static pressures for the tunnel calibration can be made.

#### 4.2.3 Pressure and Mach Number Uncertainty

Pressure and Mach number uncertainties were estimated for the calibration parameters  $(M_a - M_c)$ ,  $(P_a - P_c)/P_t$ , and  $P_a/P_t$ . The estimated uncertainty of the calibrated free-stream static pressure and Mach number for stagnation pressures of 1,000, 1,600, and 2,500 psfa and Mach numbers from 0.7 to 1.6 are presented in Figs. 29 and 30, respectively. The estimated uncertainty of the calibrated static pressure increases with increasing stagnation pressure, whereas the estimated uncertainty of the calibrated Mach number decreases. The estimated uncertainty of the calibrated static pressure can be decreased from  $M_\infty = 0.8$  to 1.2 by using a pressure calibration rather than a Mach number calibration. However, the estimated uncertainty would increase at  $M_\infty \leq 0.8$  and  $M_\infty \geq 1.2$ .

For example, the estimated uncertainty of the calibrated static pressure is 0.05 psf less at  $M_\infty = 0.9$ ,  $P_t = 1,600$  psfa using the calibration factor  $(P_a - P_c)/P_t$  to express the calibration, but 0.04 psf greater at  $M_\infty = 1.4$ . There is not a significant effect of changing the method of calibration on the calibrated free-stream Mach number uncertainty. The

estimated uncertainty of the calibrated Mach number varies less than 0.0003 with the various methods of calibration, except at  $M_{\infty} = 0.6$  where the estimated uncertainty of the calibrated Mach number increases by 0.001 when using the pressure calibration methods.

Expressing the calibration of Tunnel 16T as a function of pressure instead of Mach number does not decrease the estimated uncertainty of free-stream static pressure or Mach number significantly or over a large enough Mach number range. Thus, the calibration of Tunnel 16T should continue based on the calibration parameter ( $M_a - M_c$ ).

#### **4.2.4 Effect of Mach Number on the Calibration Parameter ( $M_a - M_c$ )**

The calibration parameter as a function of equivalent plenum chamber Mach number from  $M_{\infty} = 0.6$  to 1.6 and the Ref. 4 data are presented in Fig. 31. Although the calibration has slightly changed, the difference between the current data and the Ref. 4 data is less than the uncertainty in either data set. The largest difference in Mach number, which is 0.003, occurs at  $M_{\infty} = 1.3$ . This difference in the calibrations at Mach number is not considered large enough to require a change in the tunnel calibration from that reported in Ref. 4.

#### **4.2.5 Effect of Calibration Pipe Length**

The effect of the calibration pipe length on the calibration is presented in Fig. 32. Pipe length has no effect on the calibration at  $M_{\infty} = 0.8$  to 1.0; thus, it is assumed that there is no effect at  $M_{\infty} = 0.6$  to 0.75. Small effects on the calibration parameter are attributable to pipe length at supersonic Mach numbers, with the largest causing a difference of 0.002 in Mach number at  $M_{\infty} = 1.6$ .

#### **4.2.6 Effect of Plenum Chamber Suction at $M_{\infty} \leq 0.75$**

The effect of using plenum chamber suction at  $M_{\infty} \leq 0.75$  on the calibration is shown in Fig. 33. The calibration parameter decreases by 0.001 and 0.0007 at  $M_{\infty} = 0.6$  and 0.7, respectively. There is no change in the calibration at  $M_{\infty} = 0.75$ . The changes cited at  $M_{\infty} = 0.6$  and 0.7 are considered insignificant since they are less than the measurement uncertainty in the calibration parameter.

#### **4.2.7 Effect of Humidity on the Calibration**

The effect of tunnel humidity on the Mach number calibration parameter is presented in Fig. 34. During drying of Tunnel 16T at  $M_{\infty} = 0.9$  with  $P_i = 1,200$  psfa (Fig. 34b), difficulty was encountered in stabilizing the control parameters. Consequently, the data

obtained at  $SH \times 10 + 3$  from 3.5 to 9.1 lb/lb are omitted because tunnel conditions were unsatisfactory. The data in Fig. 34 indicate that humidity does not have a significant effect on the tunnel calibration except at  $M_{\infty} = 1.5$ . However, there is no effect if the humidity is within the dryness criteria at  $M_{\infty} = 1.5$ . Thus, the available data indicate that the tunnel operation dryness criteria of Tunnel 16T are acceptable with respect to the tunnel calibration.

## 5.0 CONCLUSIONS

Based on the results of this Tunnel 16T centerline calibration, the following conclusions have been reached:

1. Extending the centerline calibration pipe by 8 ft did not eliminate the centerline data anomalies at supersonic Mach numbers (i.e.,  $M_{\infty} = 1.2$ ).
2. Tunnel humidity does not affect the tunnel calibration when operating within the tunnel humidity operating criteria.
3. A correlation between the test section static pressure and the nozzle static pressure does not appear feasible for expressing the calibration of Tunnel 16T until the data anomalies in the nozzle static pressures at supersonic Mach numbers are eliminated.
4. The calibration factors  $P_a/P_t$  and  $(P_a - P_c)/P_t$  do not improve the estimated uncertainty of the calibrated test section static pressure or Mach number. Thus, there is no clear advantage in using these to express the calibration.
5. Utilization of plenum suction at  $M_{\infty} \leq 0.75$  and  $P_t = 1,600$  psfa permitted a reduction of total power. Data at  $P_t = 1,000$  and 2,200 psfa were inconclusive. There is no reason to believe that a reduction in total power can be achieved at  $P_t = 1,000$  and 2,000 psfa and other pressure levels. Thus, further study is recommended.

## REFERENCES

1. Gunn, J. A. "Check Calibration of the AEDC 16-Ft Transonic Tunnel." AEDC-TR-66-80 (AD633277), May 1966.

2. Jackson, F. M. "Calibration of the AEDC-PWT 16-Ft Transonic Tunnel at Test Section Wall Porosities of Two, Four, and Six Percent." AEDC-TR-76-13 (AD-B008985L), January 1976.
3. Jackson, F. M. "Calibration of the AEDC-PWT 16-Ft Transonic Tunnel with the Propulsion Test Section at Various Reynolds Numbers." AEDC-TR-77-121 (AD-A057877), August 1978.
4. Jackson, F. M. "Calibration of the AEDC-PWT 16-Ft Transonic Tunnel Aerodynamic Test Section at Various Reynolds Numbers." AEDC-TR-78-60 (AD-A065112), February 1979.
5. *Test Facilities Handbook* (Eleventh Edition). "Propulsion Wind Tunnel Facility, Vol. 4." Arnold Engineering Development Center, June 1979.

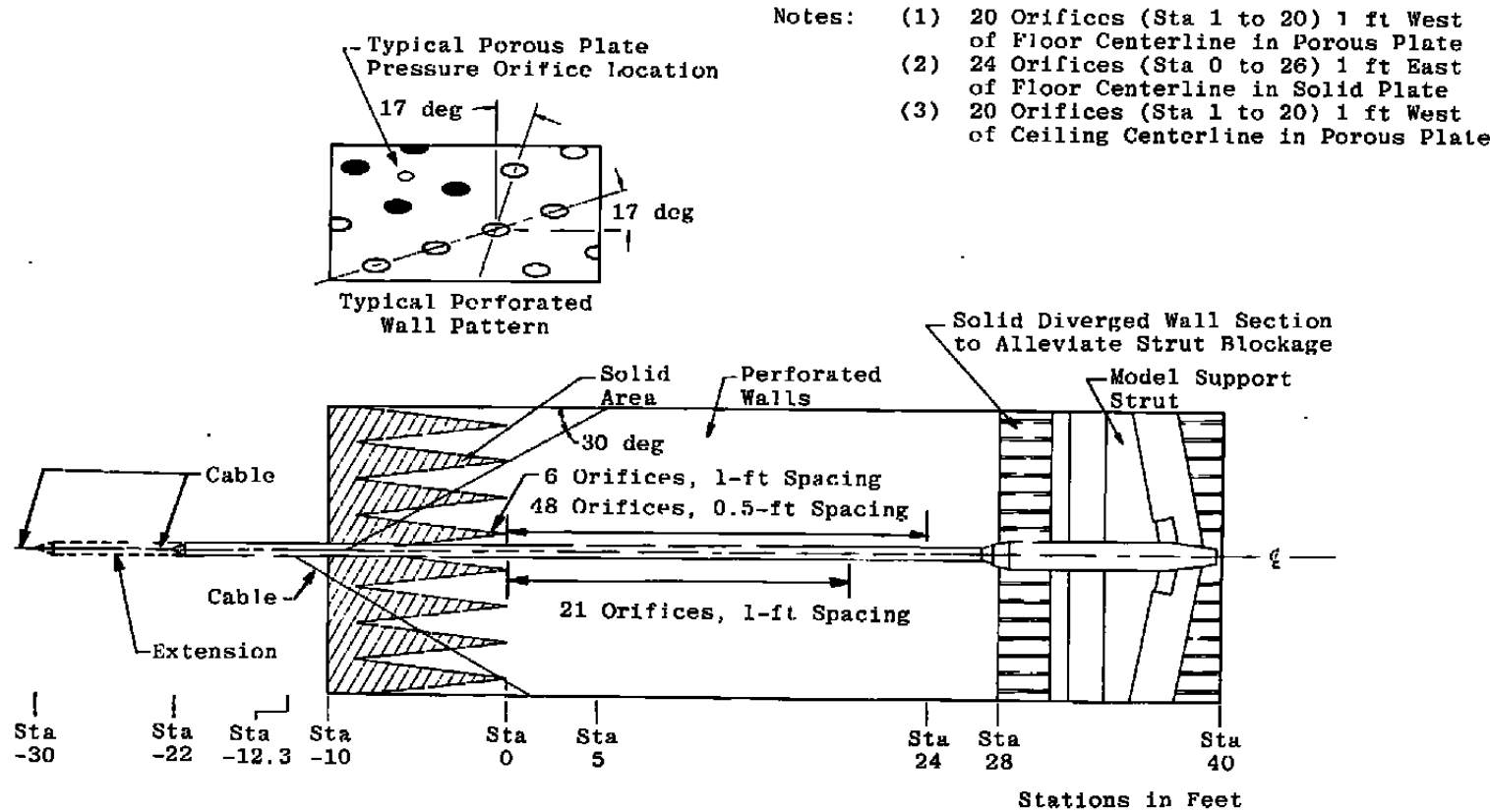
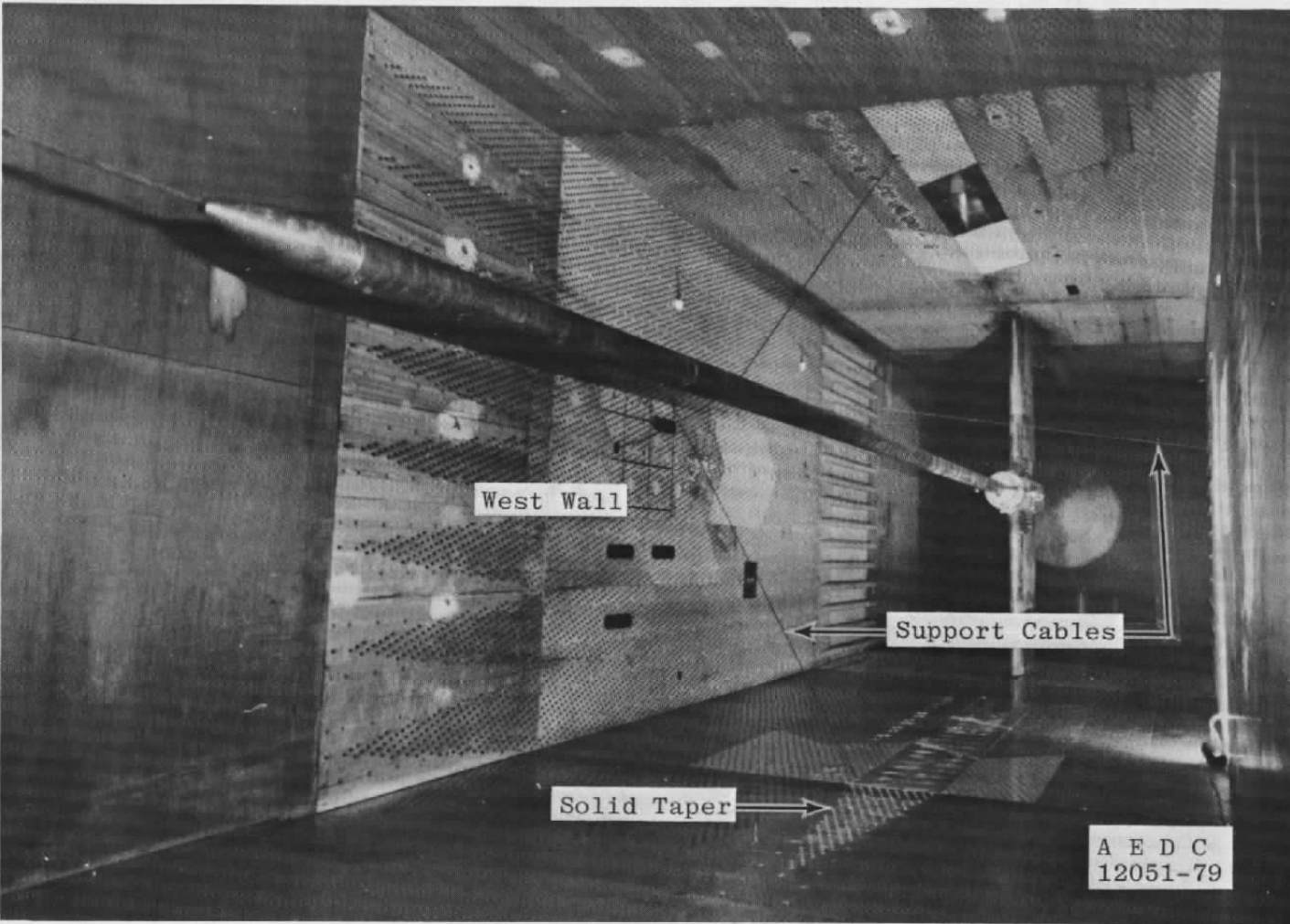
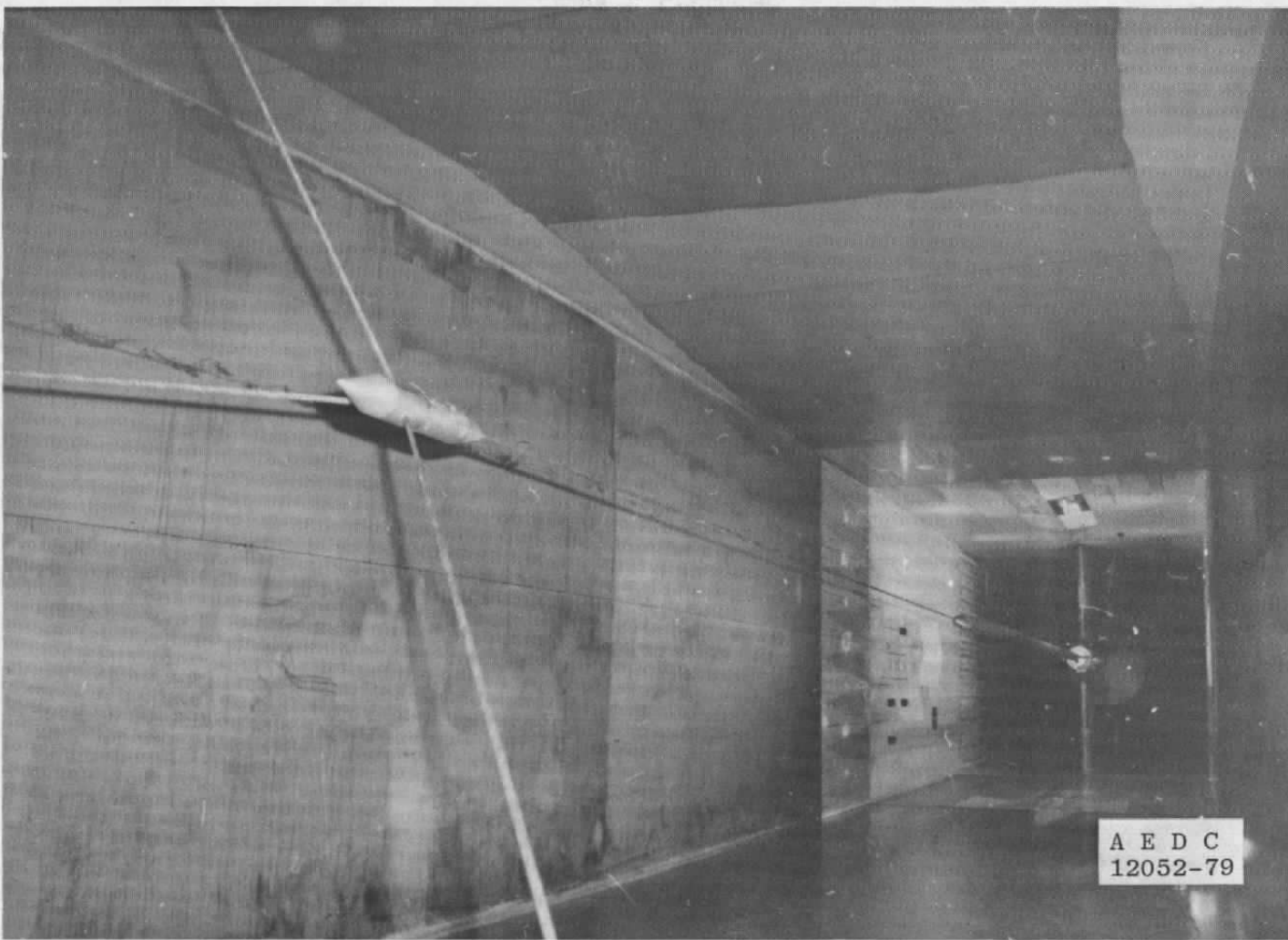


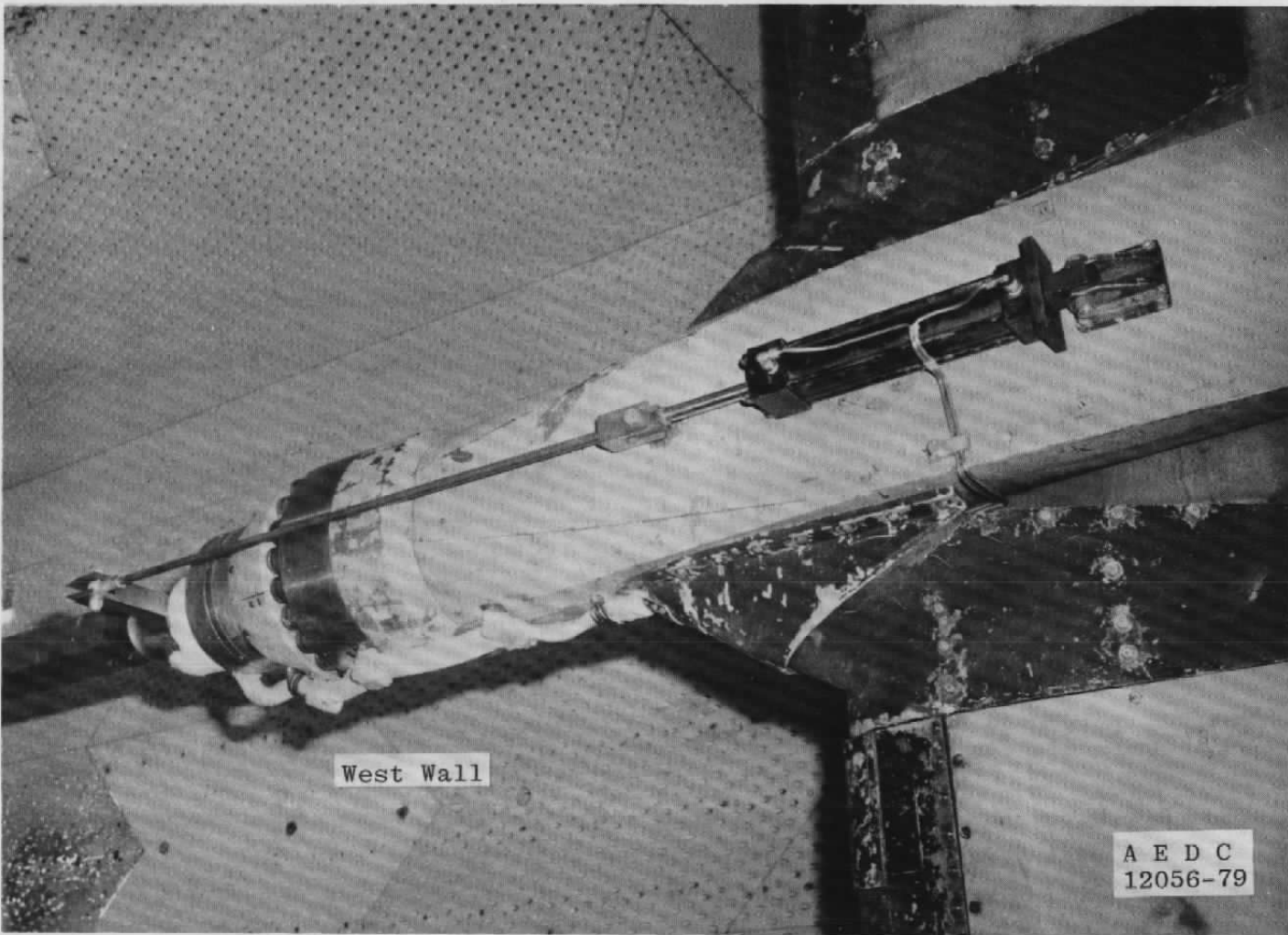
Figure 1. Tunnel 16T test section and centerline pipe installation.



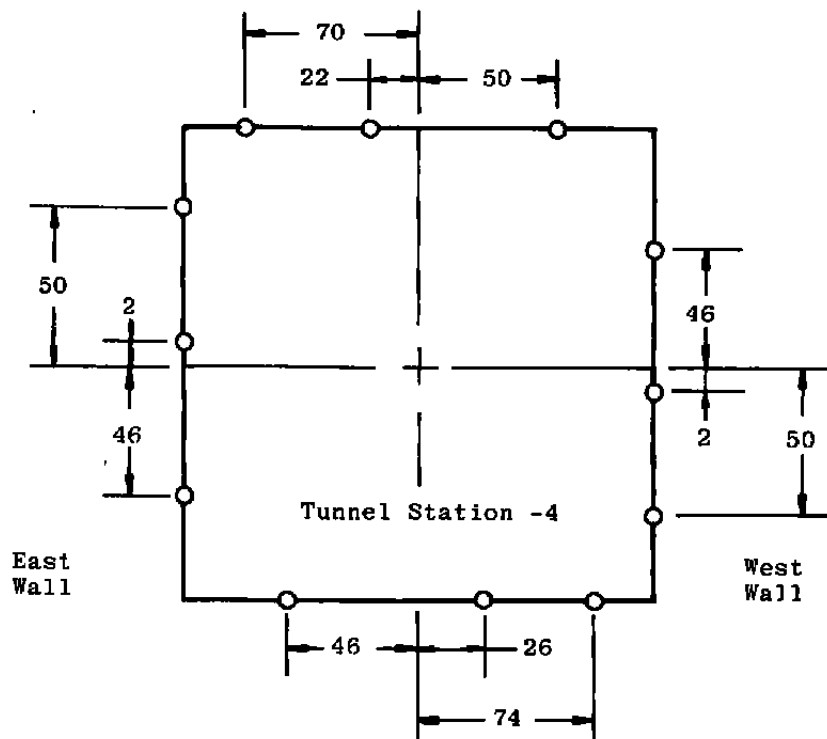
a. Pipe and main supporting cables  
Figure 2. Tunnel 16T calibration installation.



b. Pipe and forward cable system  
Figure 2. Continued.

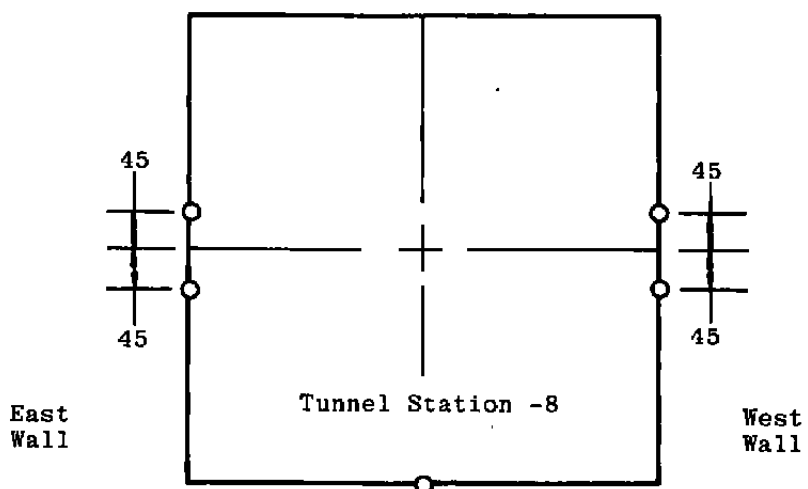


c. Pipe and aft mount system  
Figure 2. Concluded.



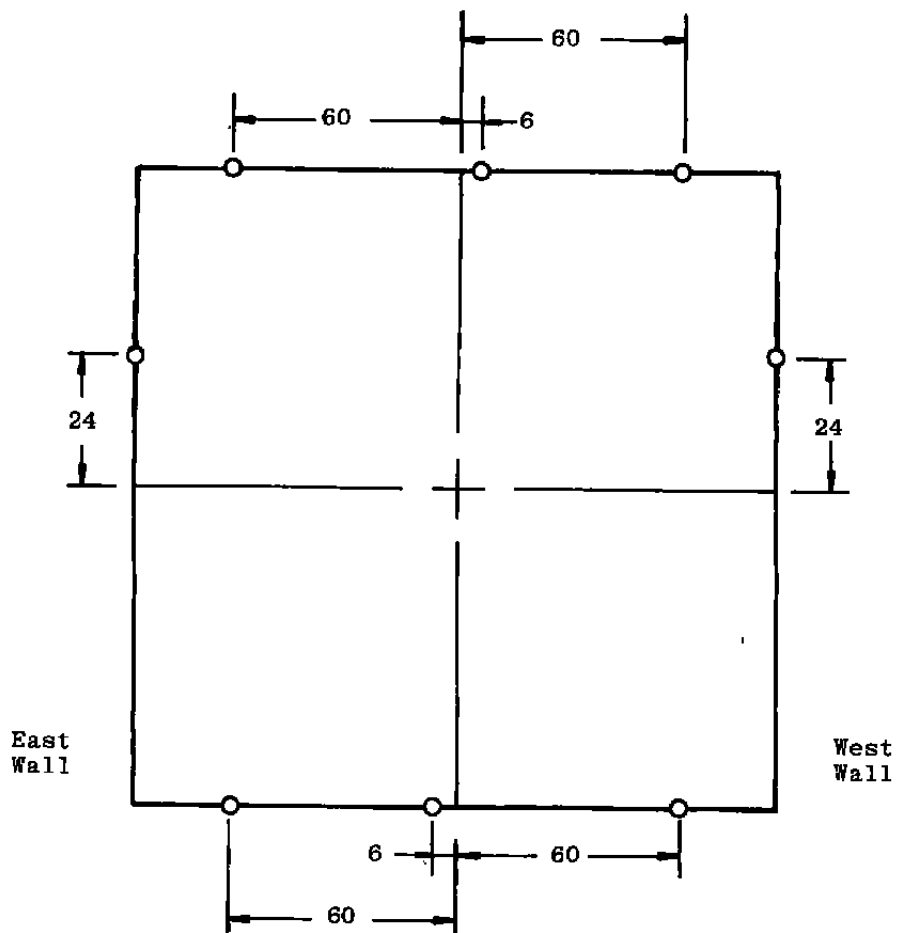
Note: All Dimensions in Inches

Sketch Not to Scale



a. Tunnel stations -4 and -8

Figure 3. Nozzle static pressure orifice locations.



Note: All Dimensions in Inches  
Sketch Not to Scale

b. Tunnel station -12  
Figure 3. Concluded.

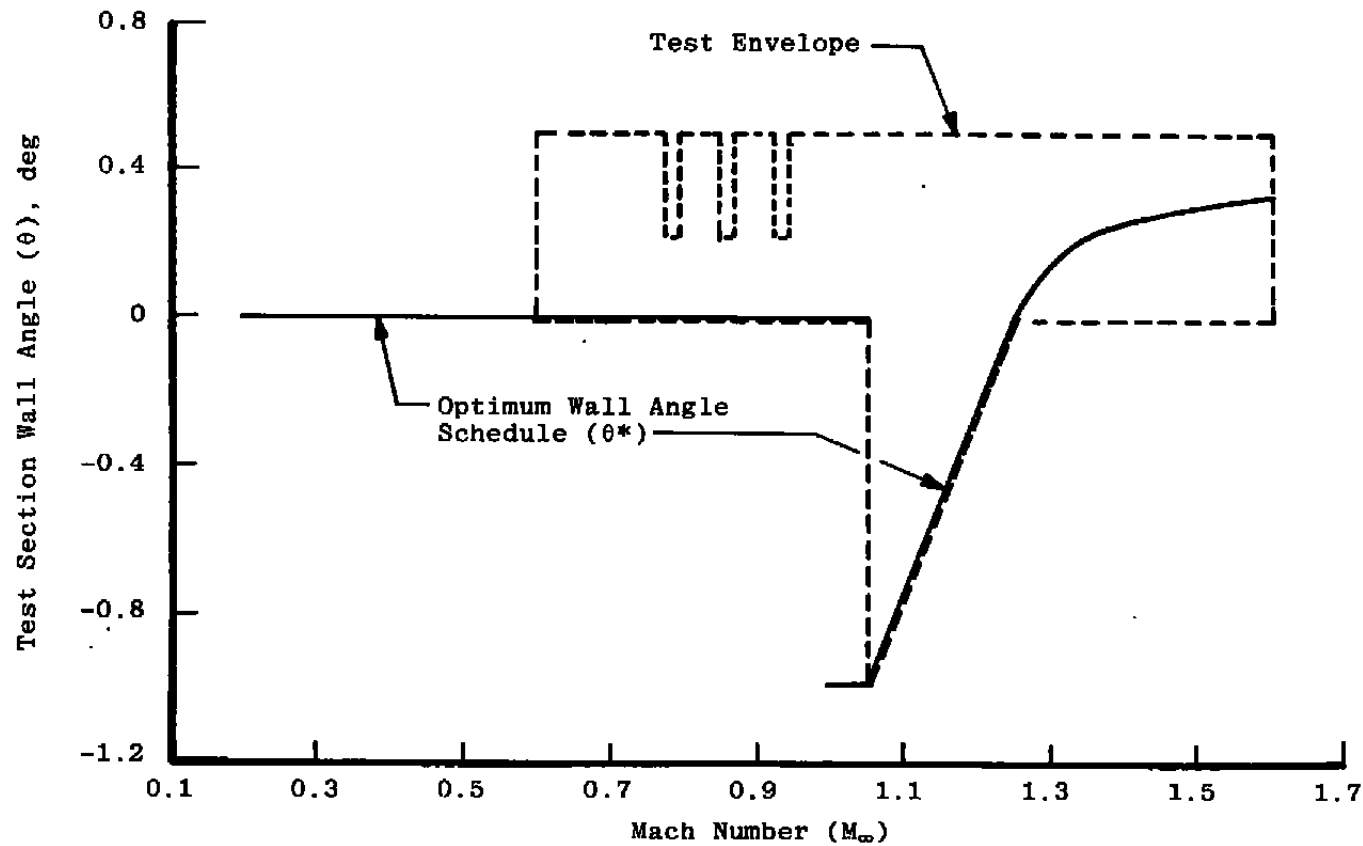


Figure 4. Test section wall angle schedules.

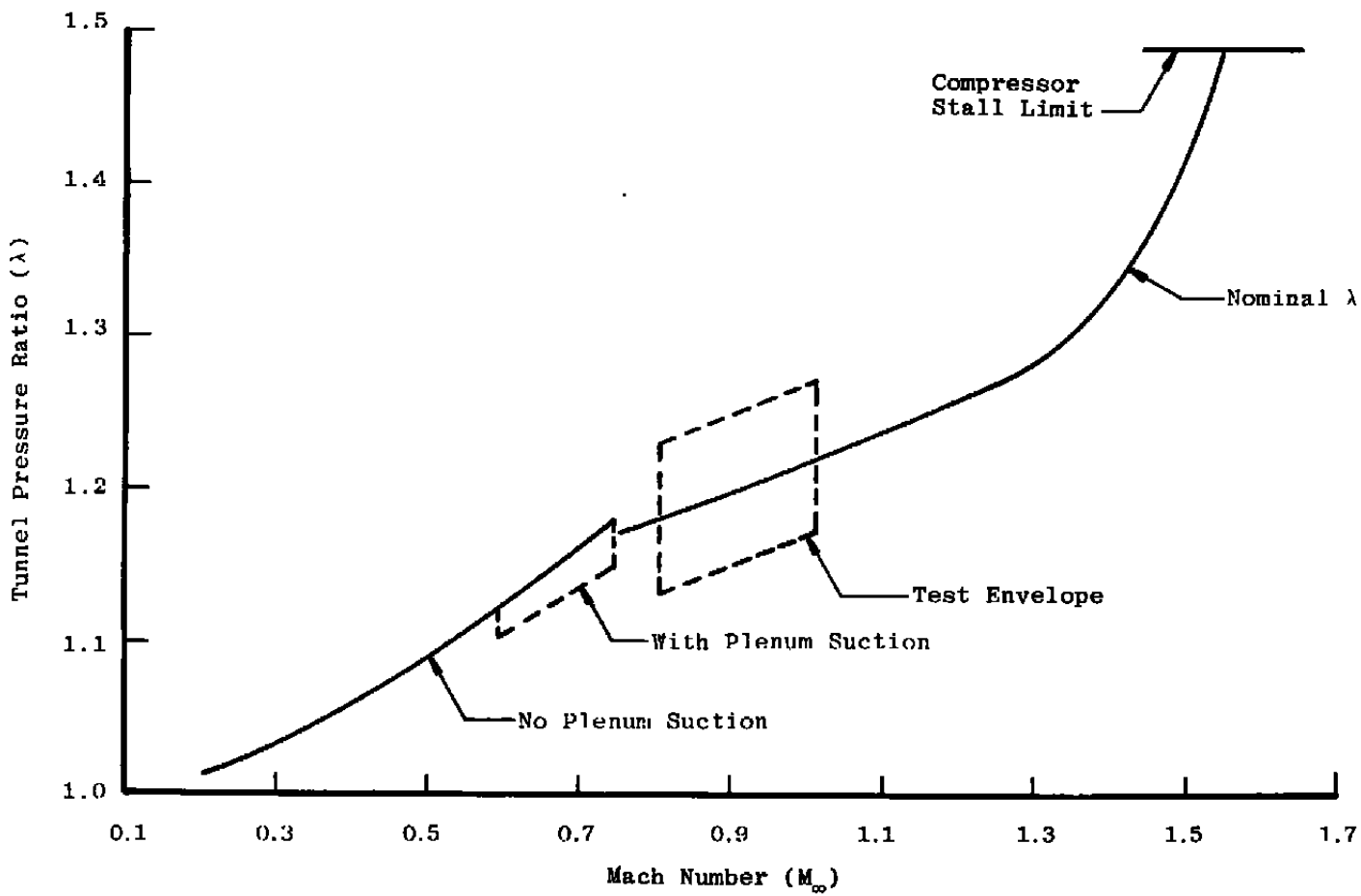
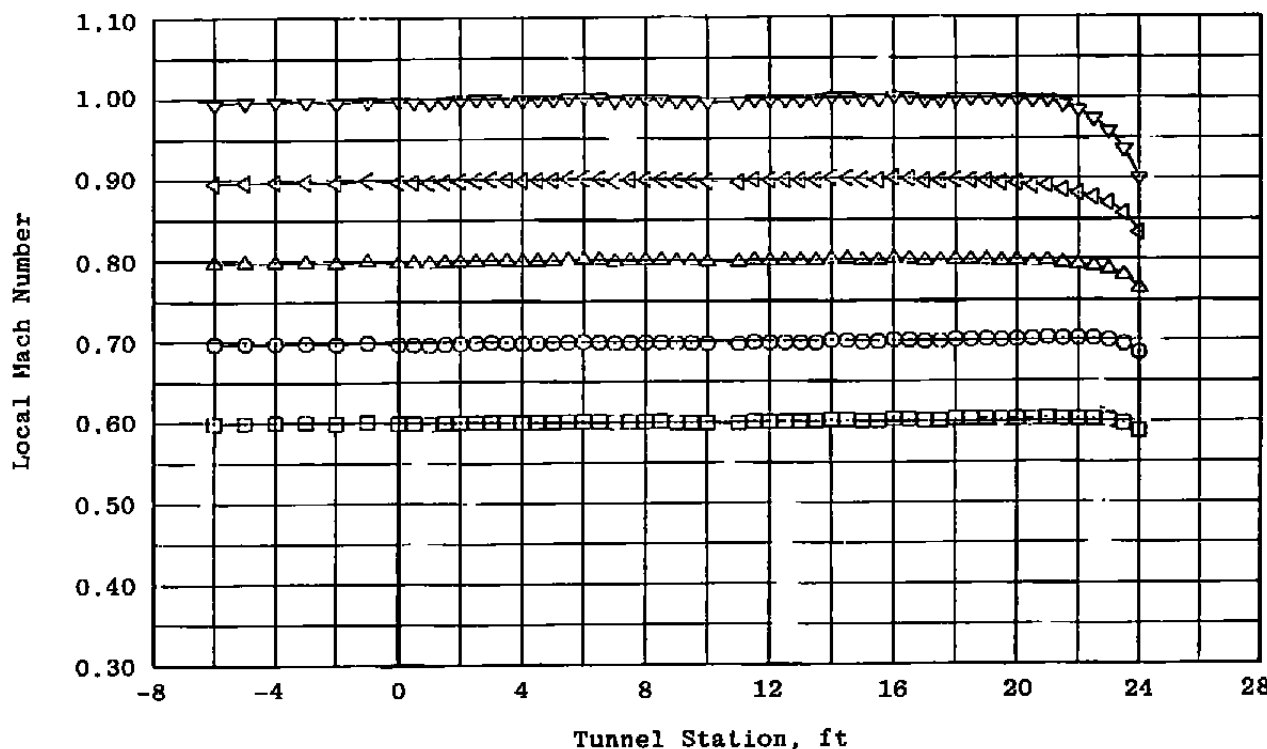


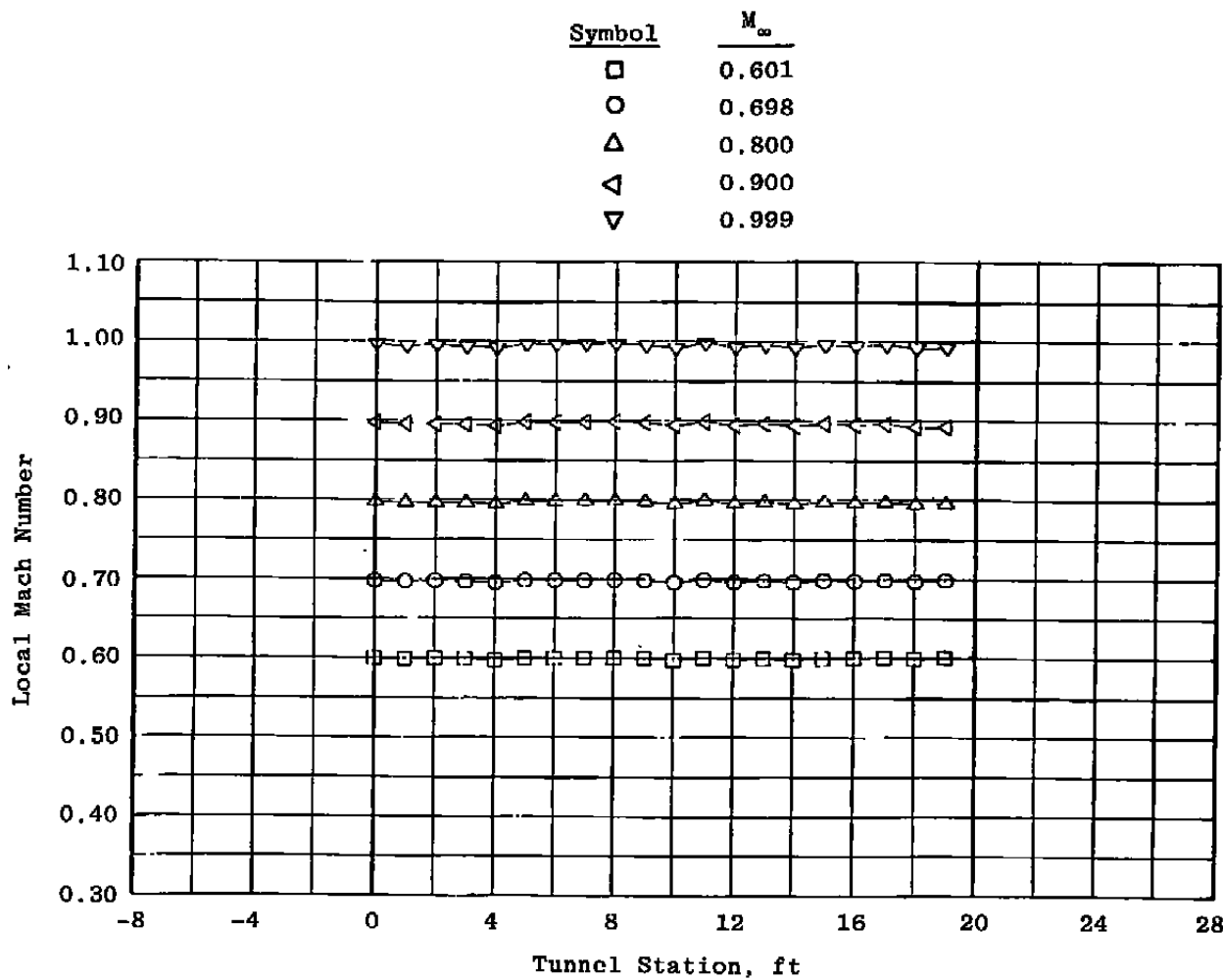
Figure 5. Variation of tunnel pressure ratio with  $\theta = 0$ .

Symbol	$M_\infty$
□	0.601
○	0.698
△	0.800
▽	0.900
▽	0.999

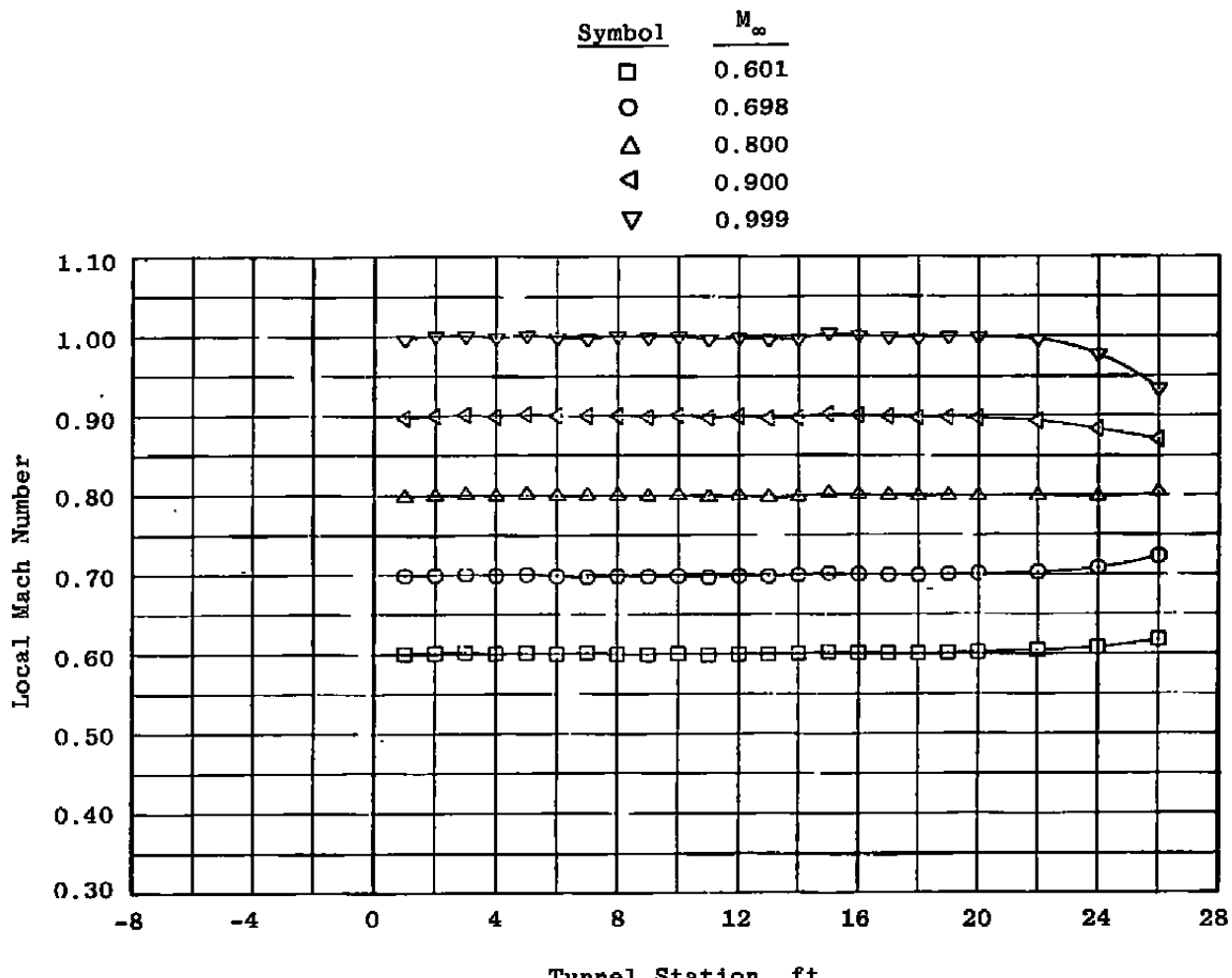


a. Upper centerline pipe

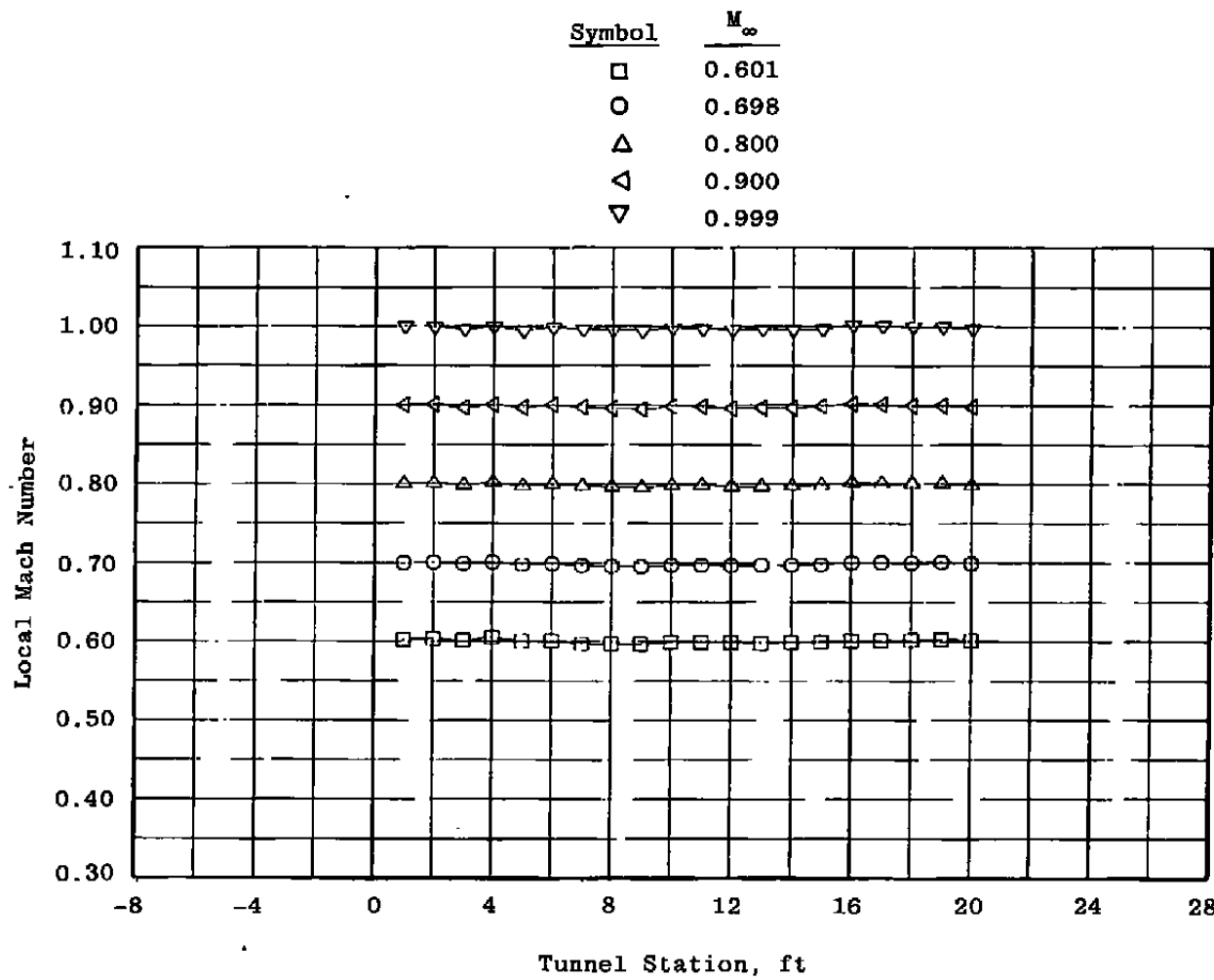
Figure 6. Tunnel 16T Mach number distributions at  $M_\infty = 0.6$  to 1.0 with  $\lambda = \lambda^*$ ,  $\theta = 0$ , and  $P_t = 1,600$  psfa.



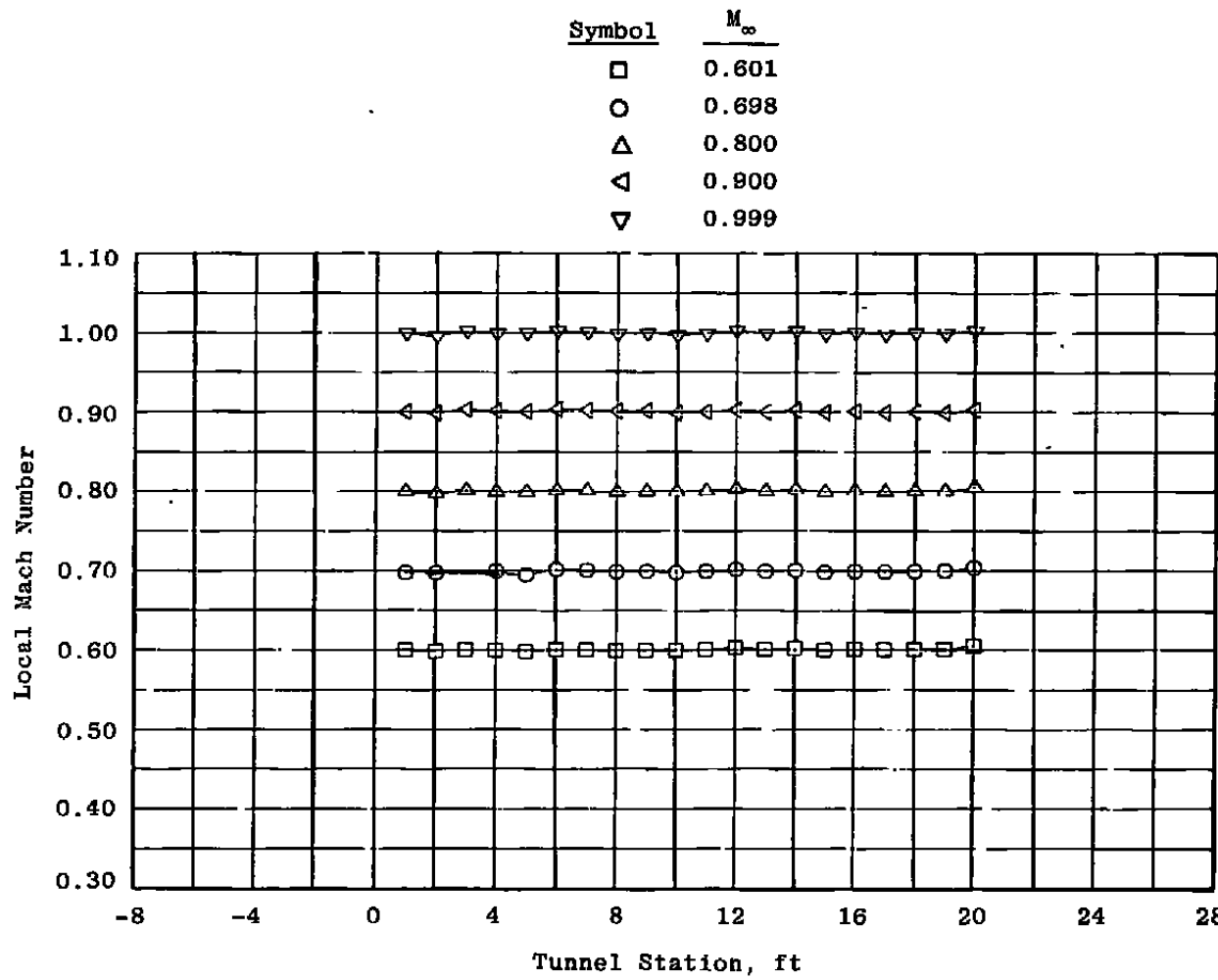
b. Lower centerline pipe  
Figure 6. Continued.



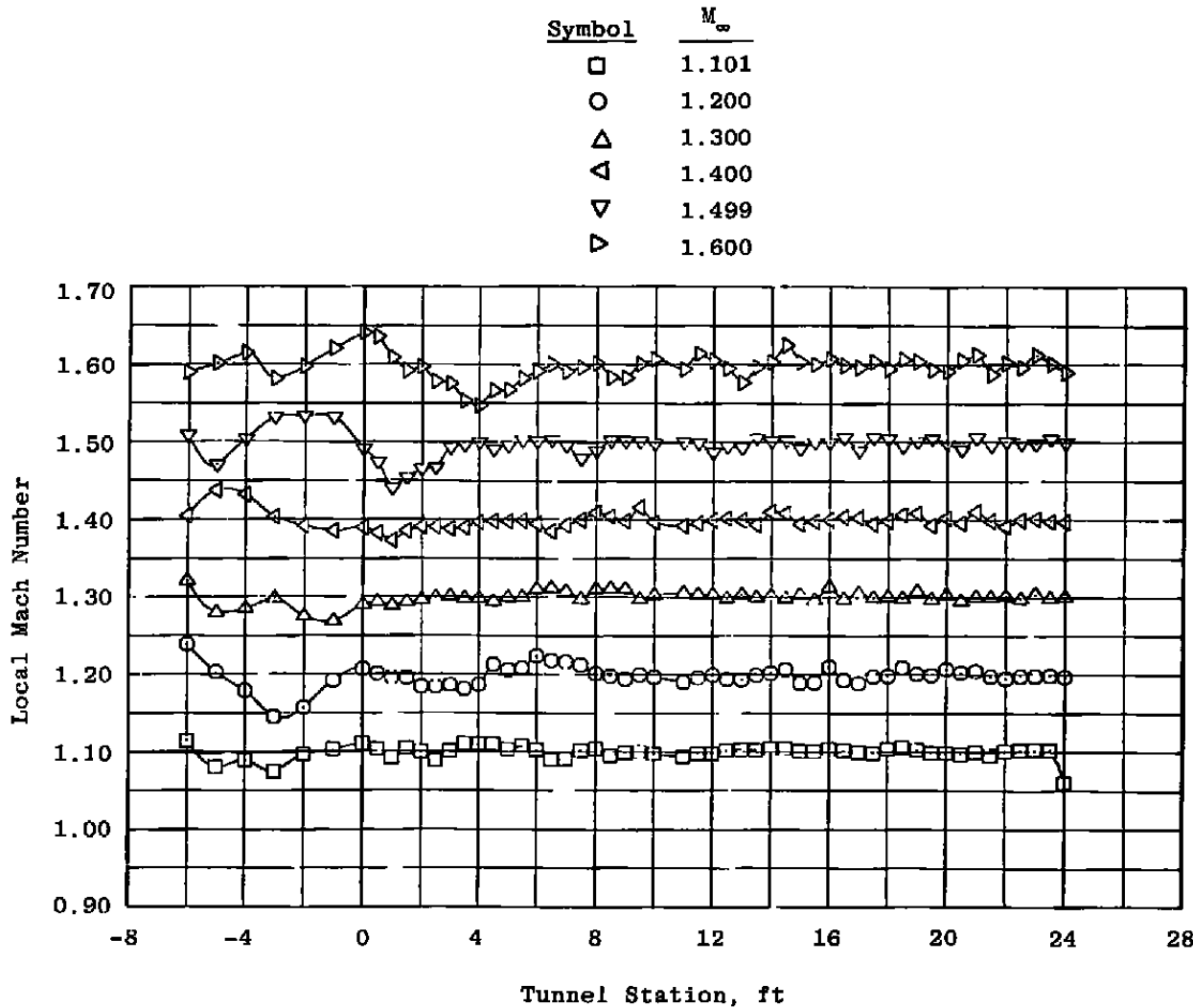
c. Bottom wall, solid plate  
Figure 6. Continued.



d. Bottom wall, porous plate  
Figure 6. Continued.

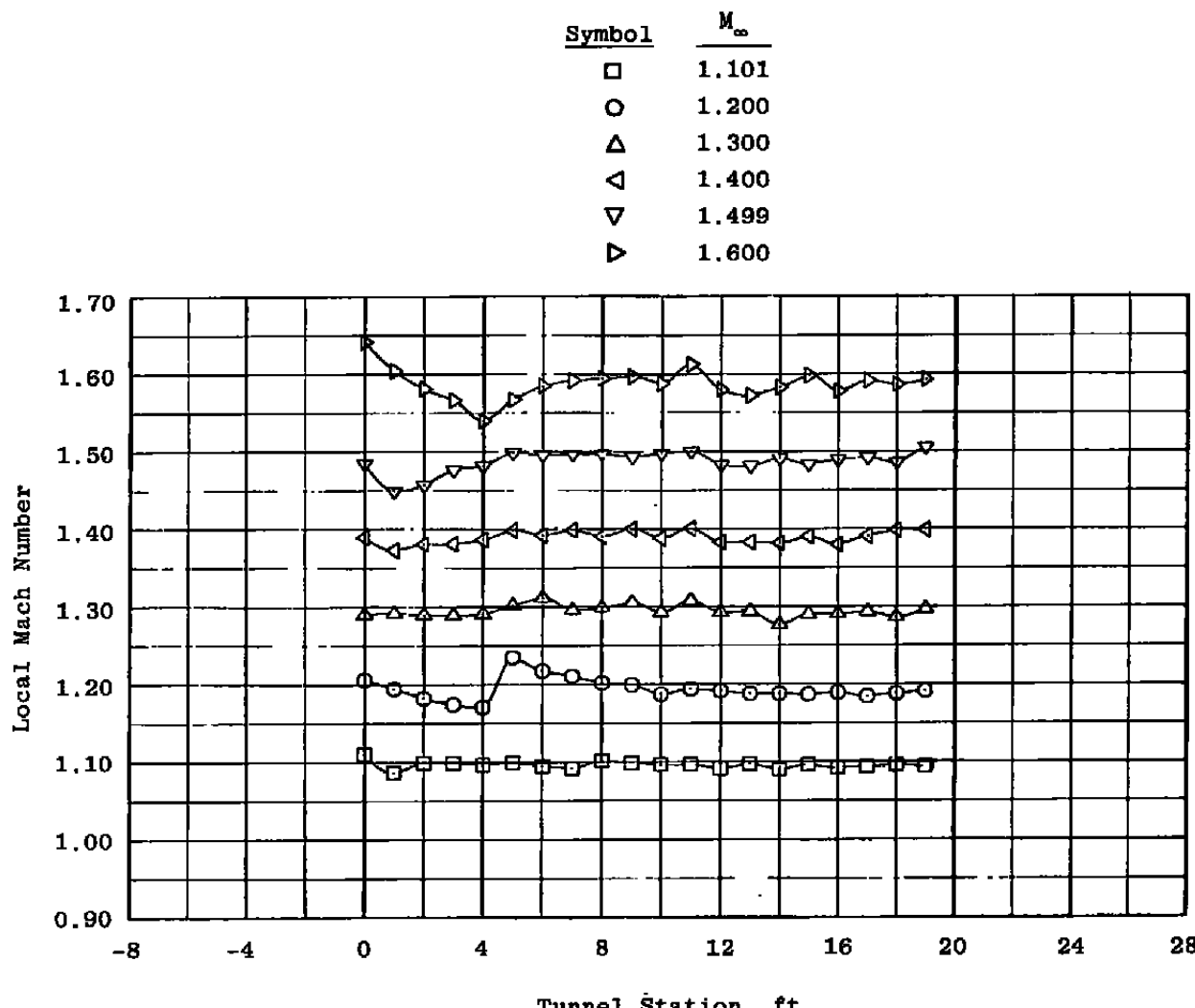


e. Top wall, porous plate  
Figure 6. Concluded.

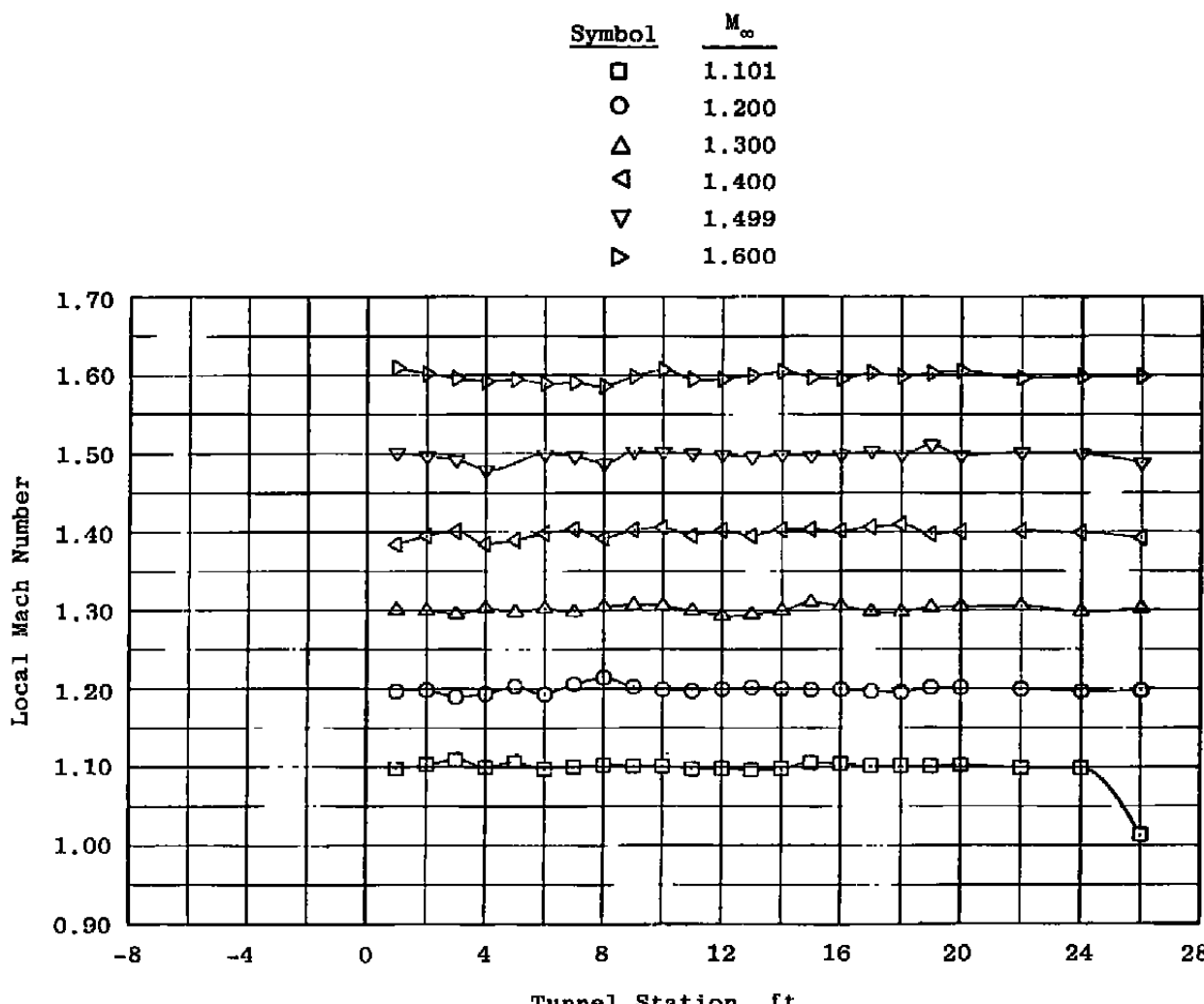


a. Upper centerline pipe

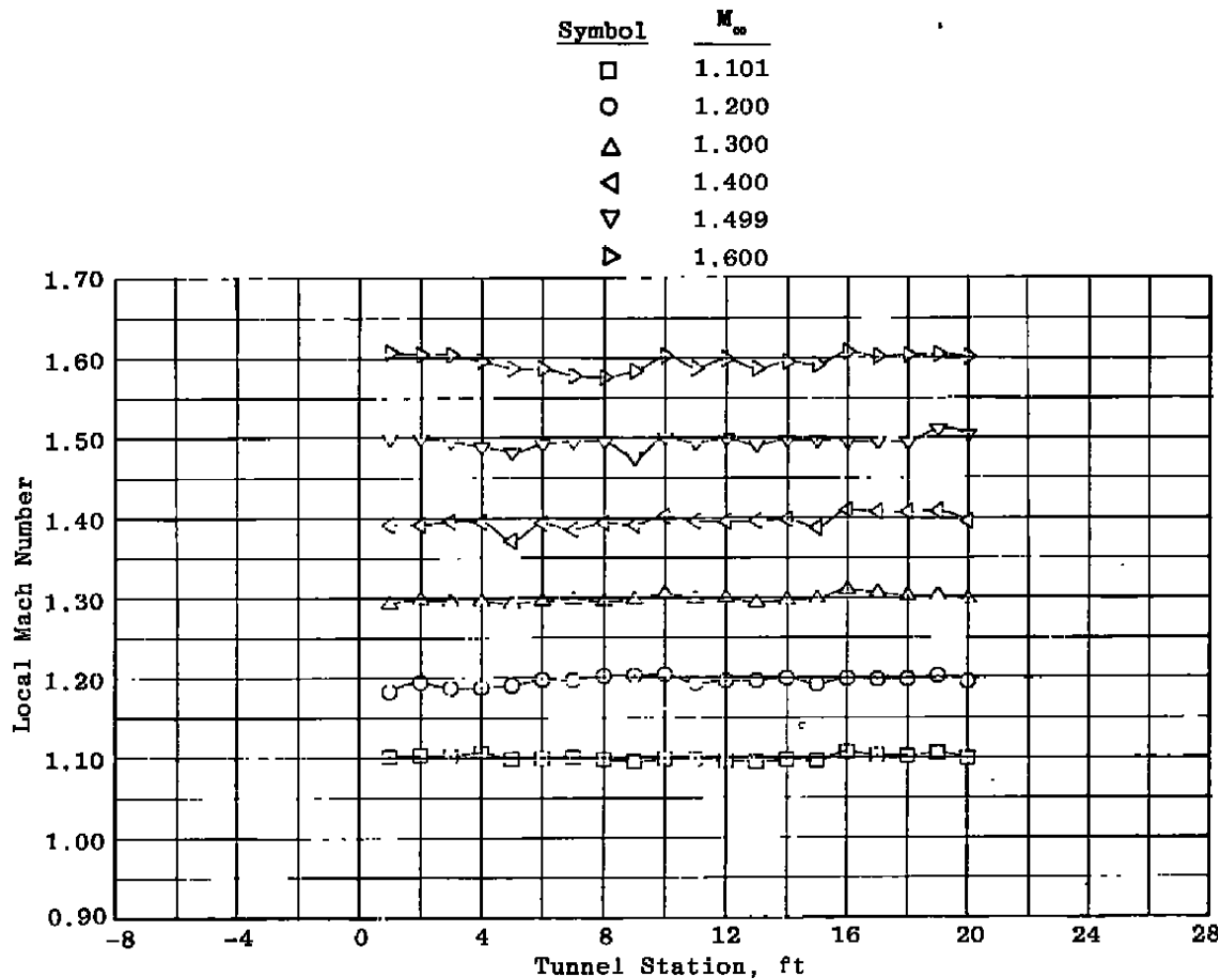
Figure 7. Tunnel 16T Mach number distributions at  $M_\infty = 1.1$  to 1.6  
with  $\lambda = \lambda^*$ ,  $\theta = 0$ , and  $P_t = 1,600$  psfa.



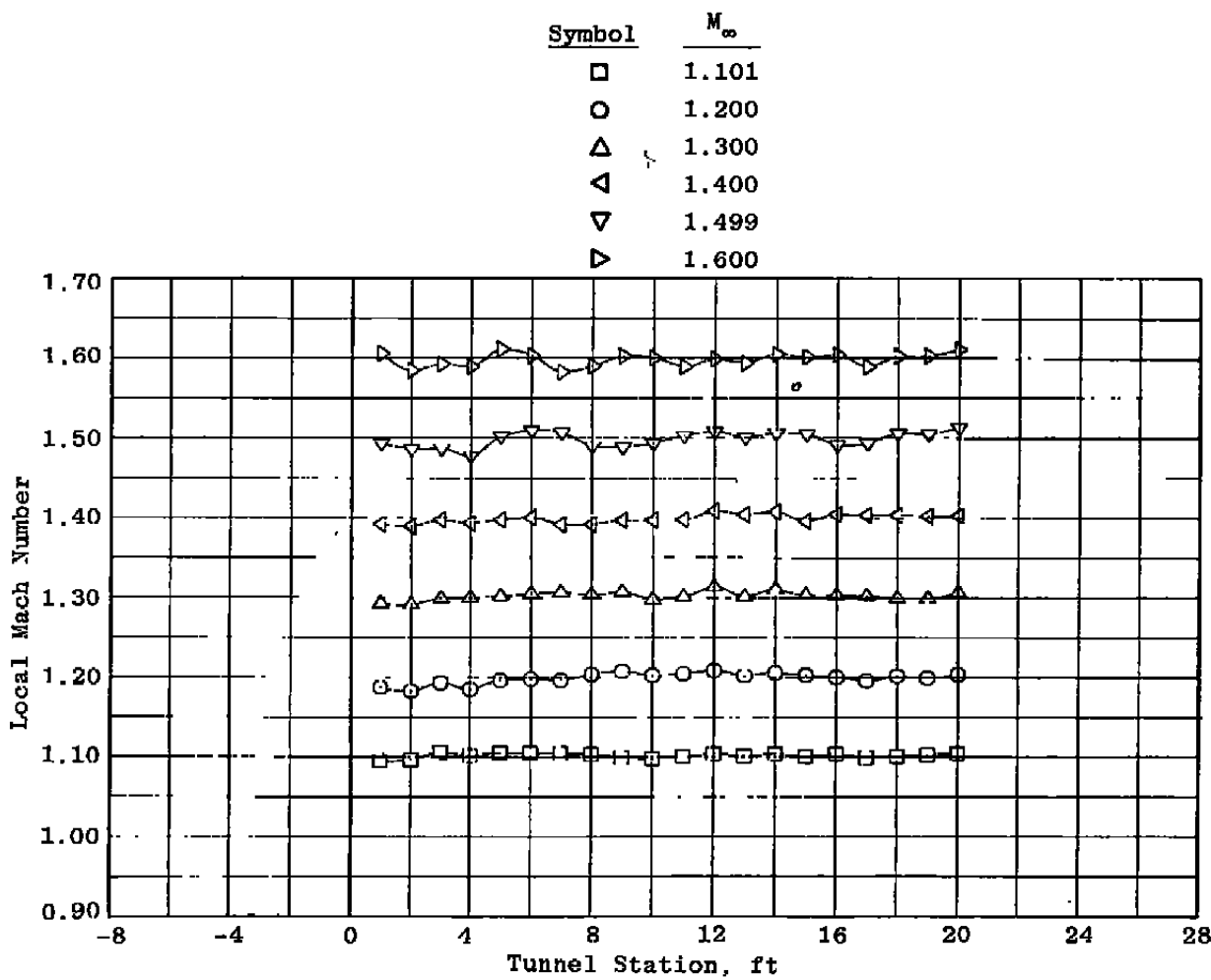
b. Lower centerline pipe  
Figure 7. Continued.



c. Bottom wall, solid plate  
 Figure 7. Continued.



d. Bottom wall, porous plate  
Figure 7. Continued.



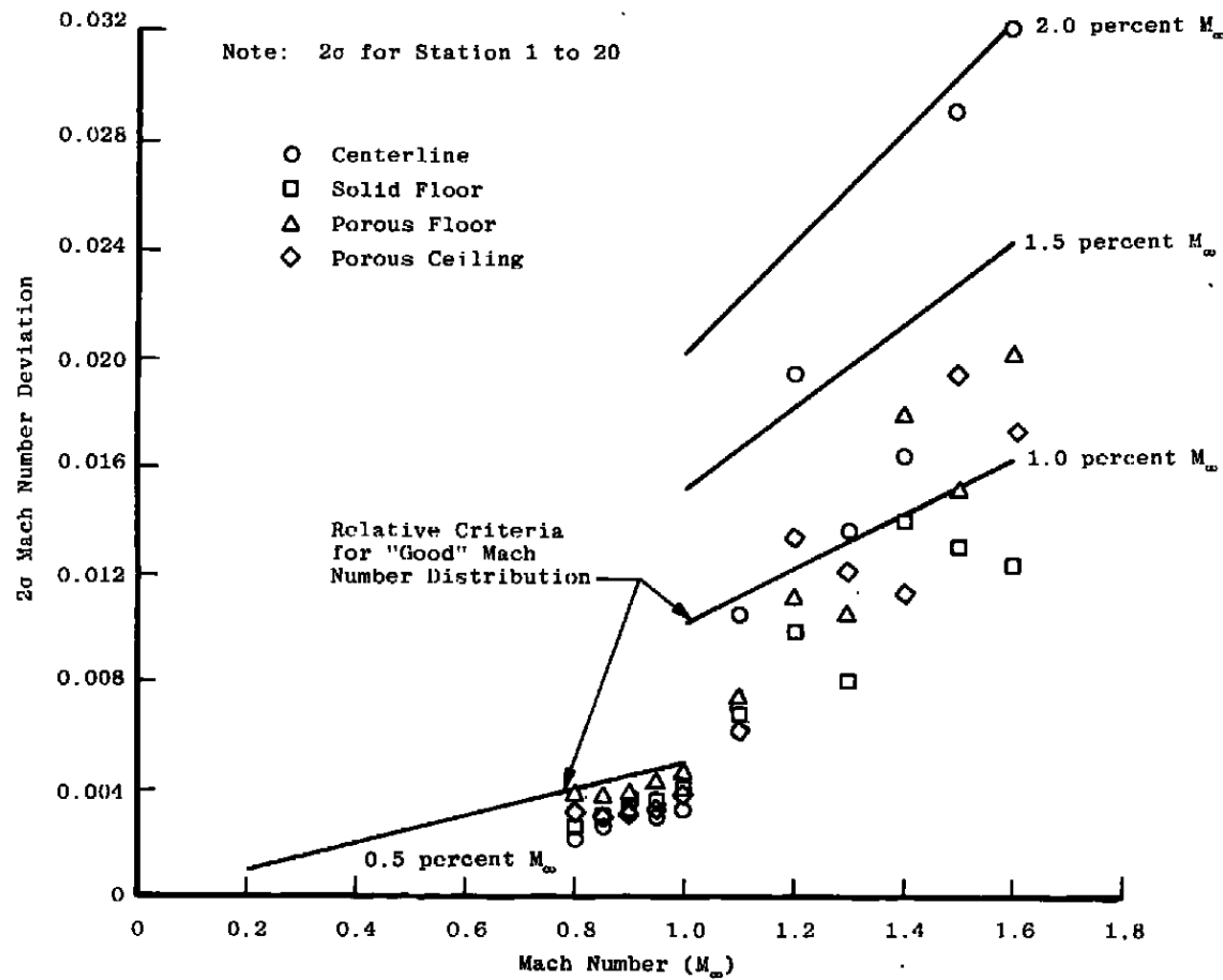
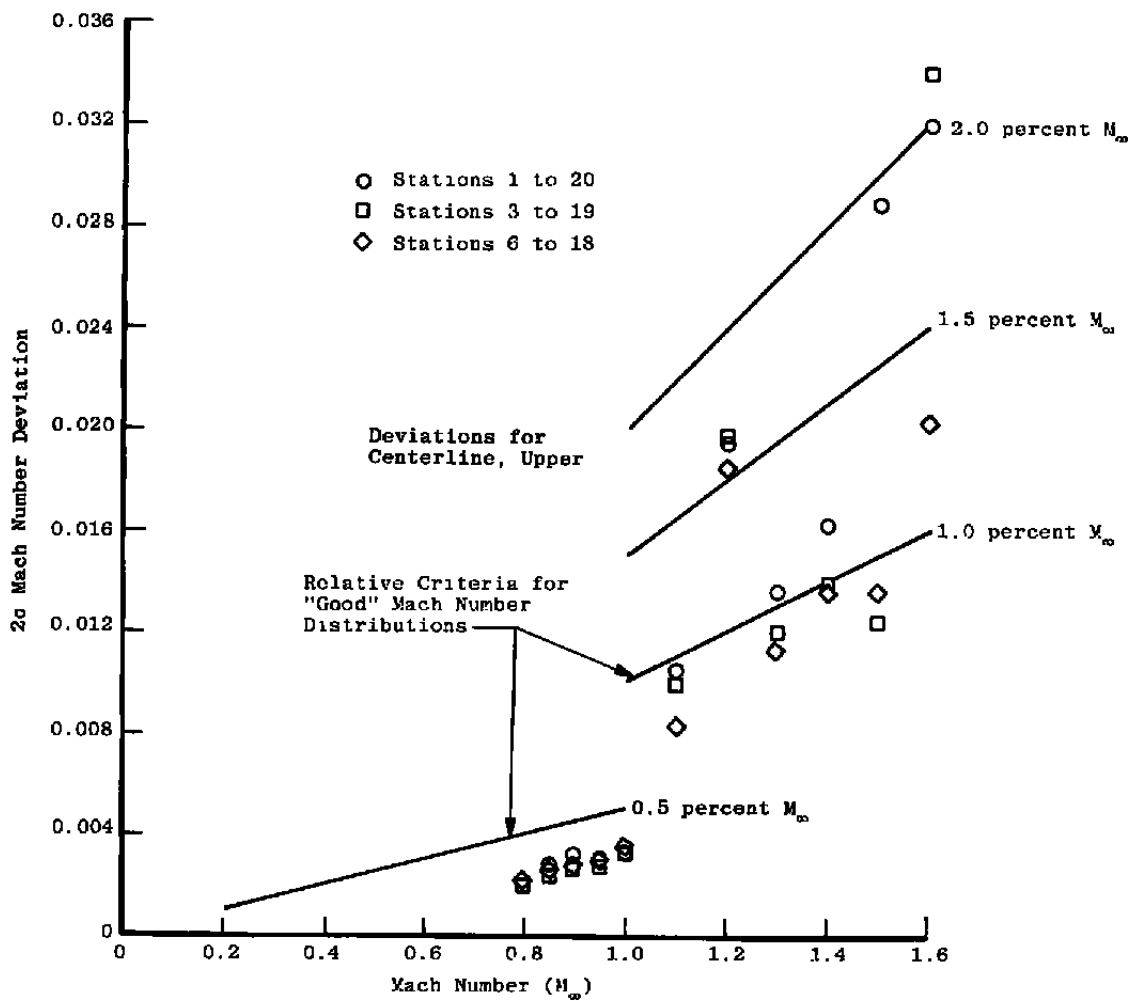


Figure 8. Effect of orifice selection on the Mach number deviations with  $\lambda = \lambda^*$ ,  $\theta = 0$ , and  $P_t = 1,600$  psfa.



**Figure 9. Effect of test region location on the Mach number deviations with  $\lambda = \lambda^*$ ,  $\theta = 0$ , and  $P_t = 1,600$  psfa.**

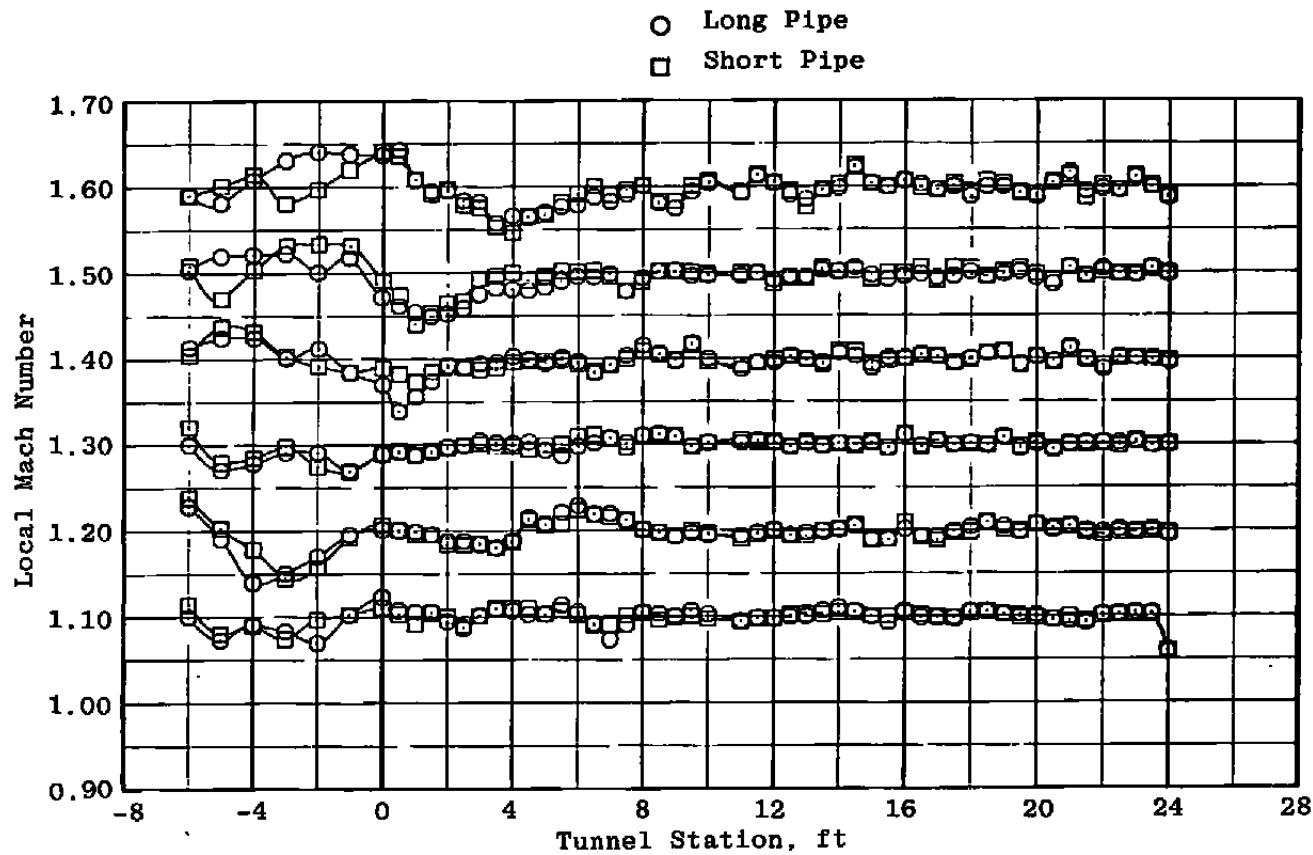


Figure 10. Effect of centerline pipe length on the Mach number distributions from  $M_\infty = 1.1$  to 1.6 with  $\lambda = \lambda^*$ ,  $\theta = 0$ , and  $P_t = 1,600$  psfa.

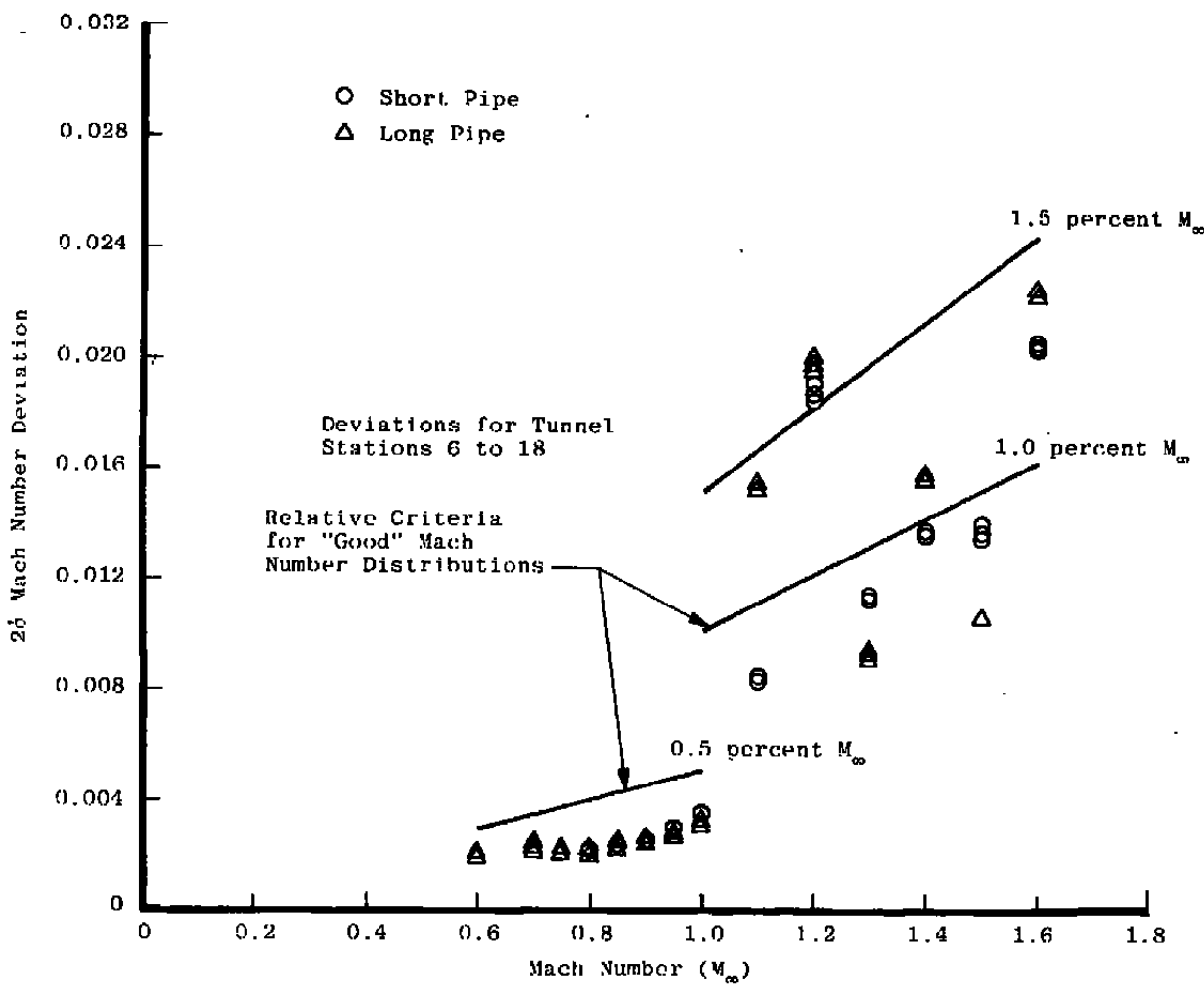


Figure 11. Effect of centerline pipe length on the Mach number deviations with  $\lambda = \lambda^*$ ,  $\theta = 0$ , and  $P_t = 1,600$  psfa.

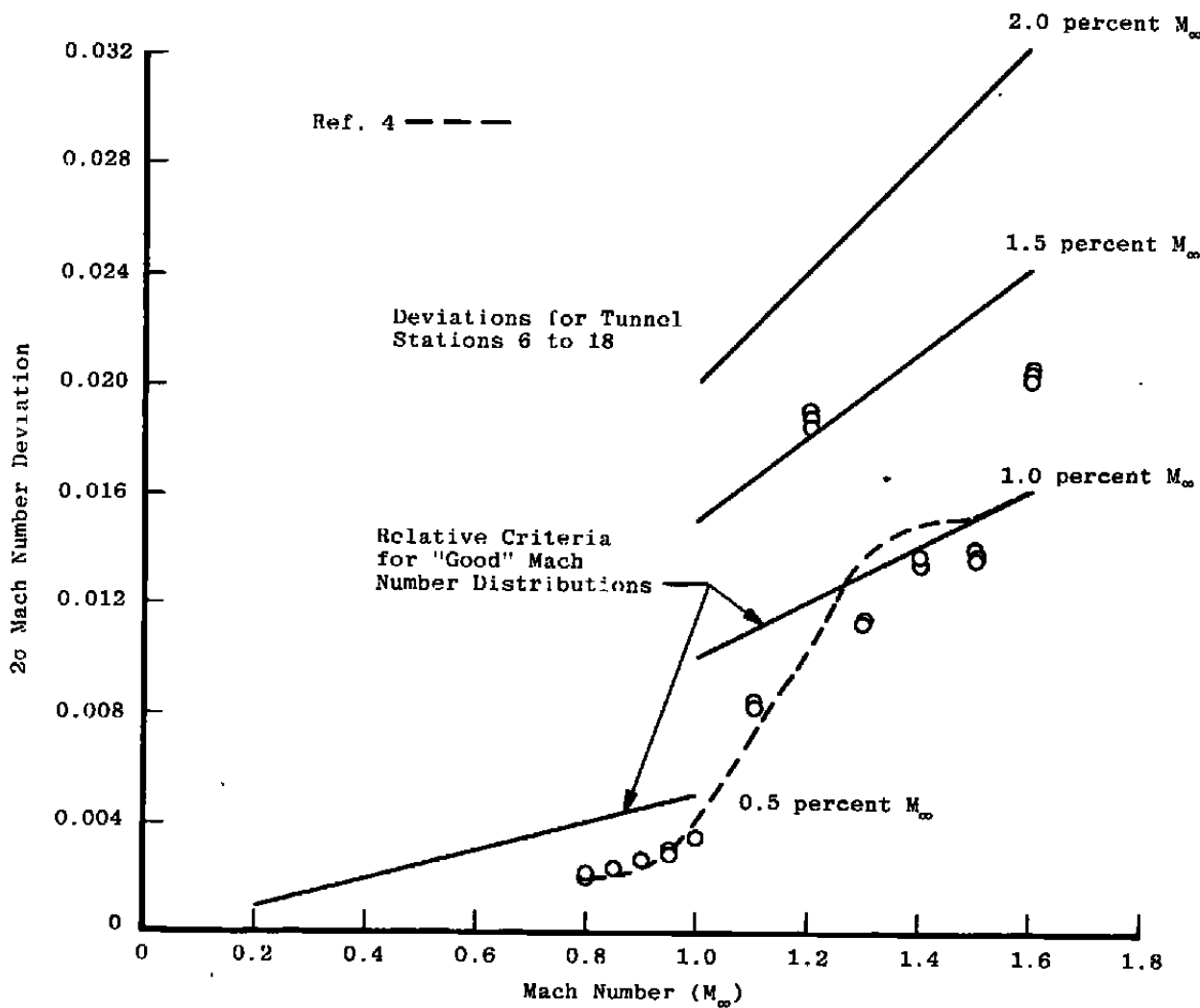
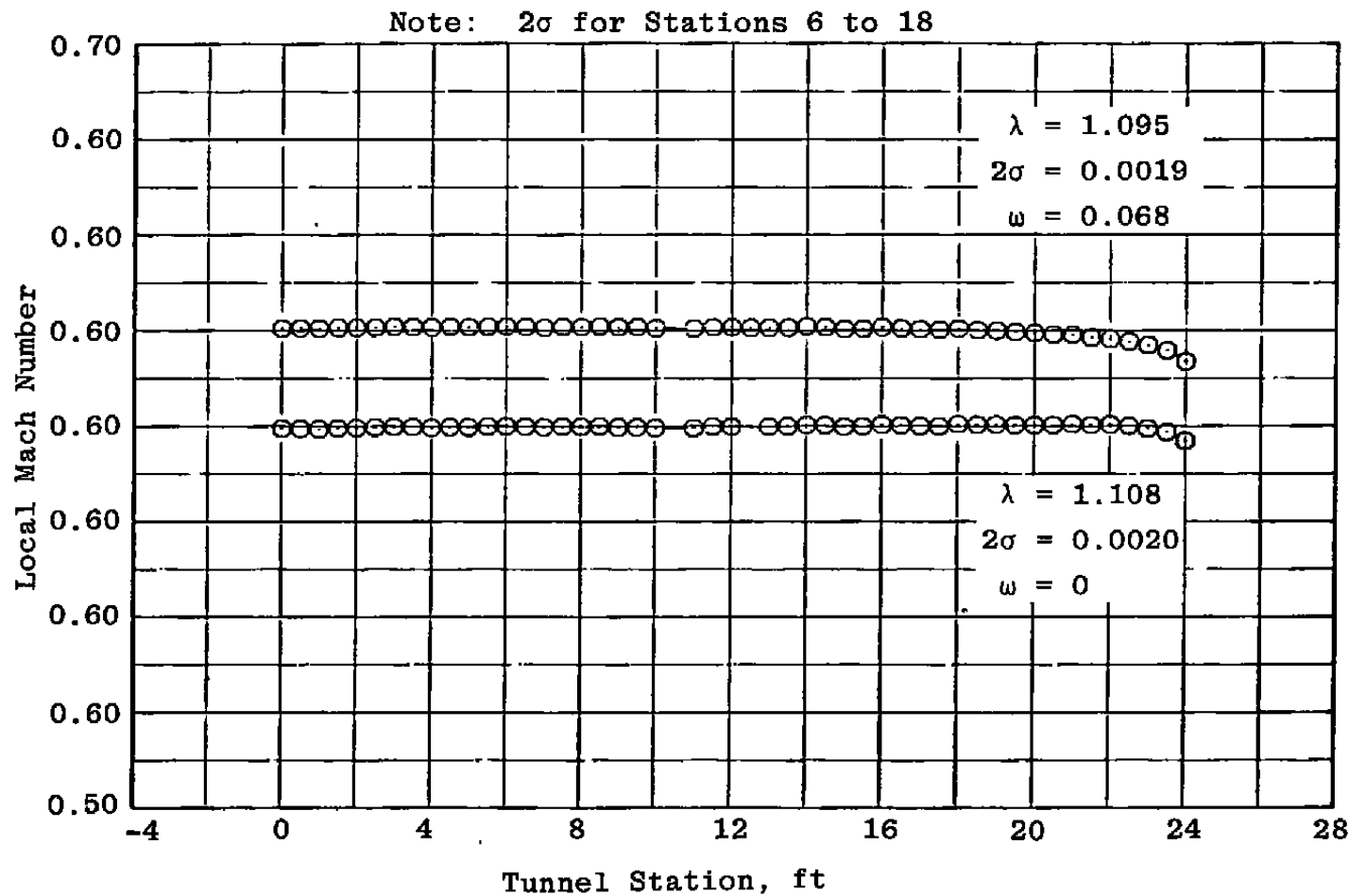
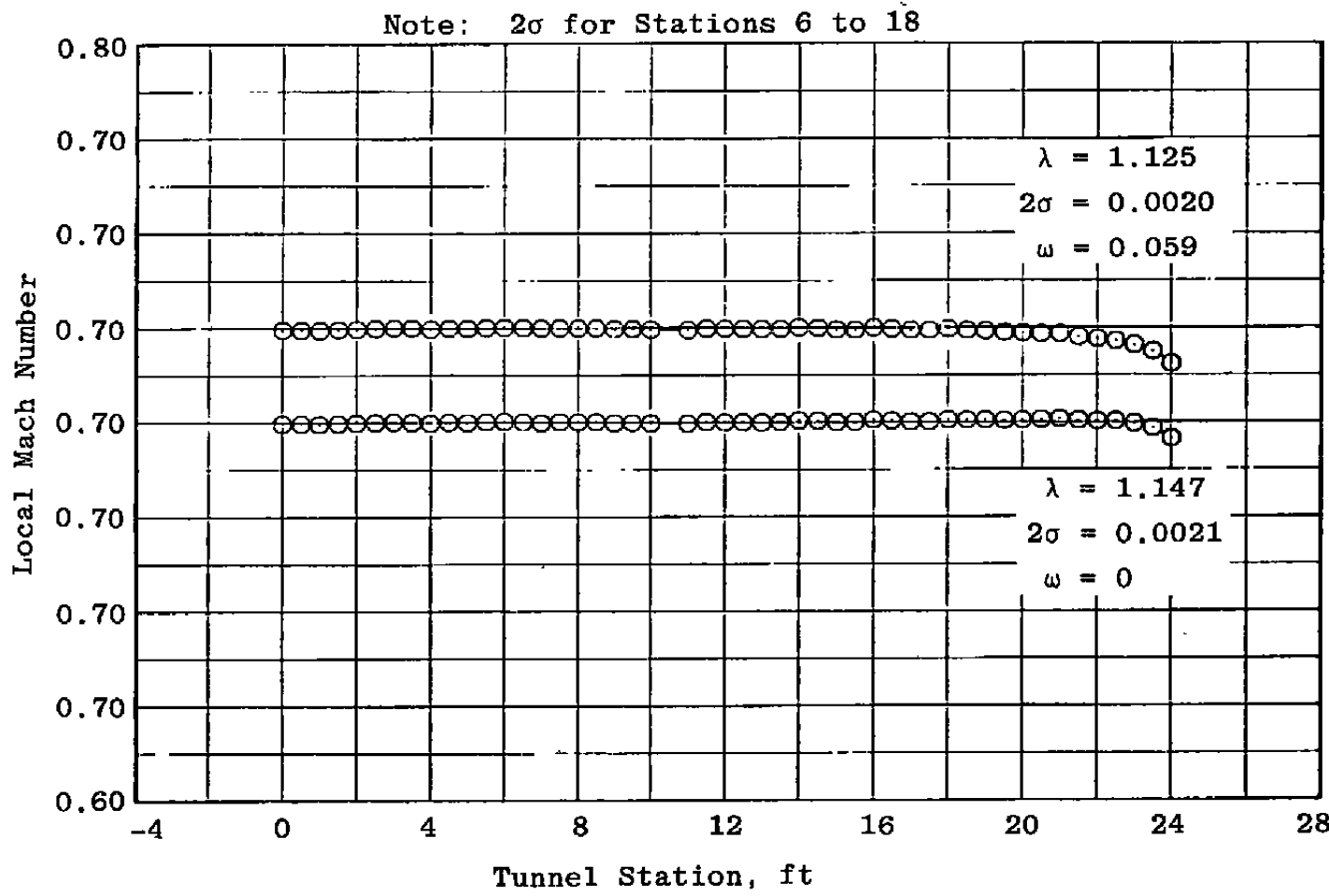


Figure 12. Effect of Mach number on the centerline Mach number deviations with  $\lambda = \lambda^*$ ,  $\theta = 0$ , and  $P_t = 1,600$  psfa.



a.  $M_\infty = 0.6$

Figure 13. Effect of plenum chamber suction on the centerline Mach number distributions at  $P_t = 1,000$  psfa with  $\theta = 0$ .



b.  $M_\infty = 0.7$

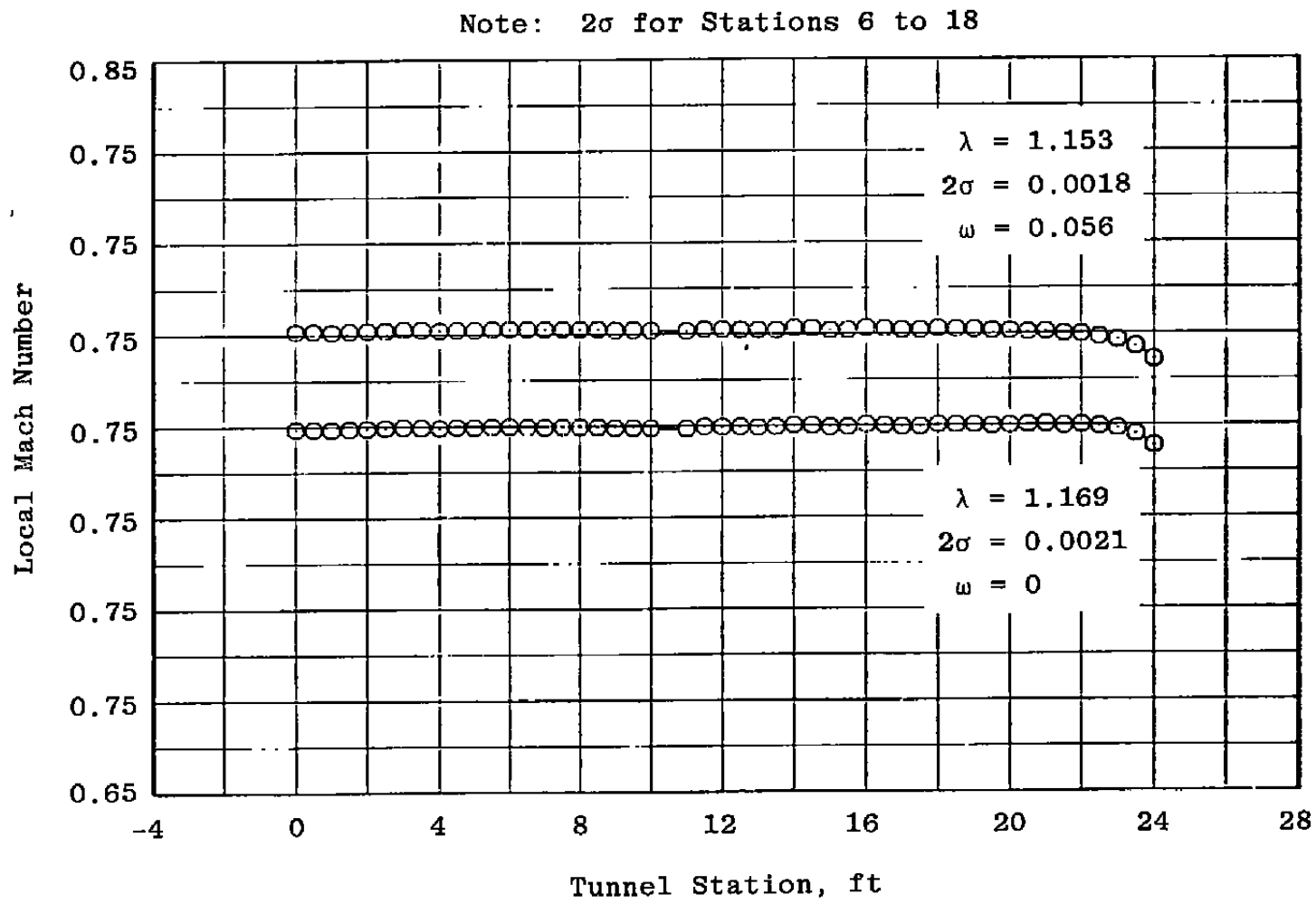
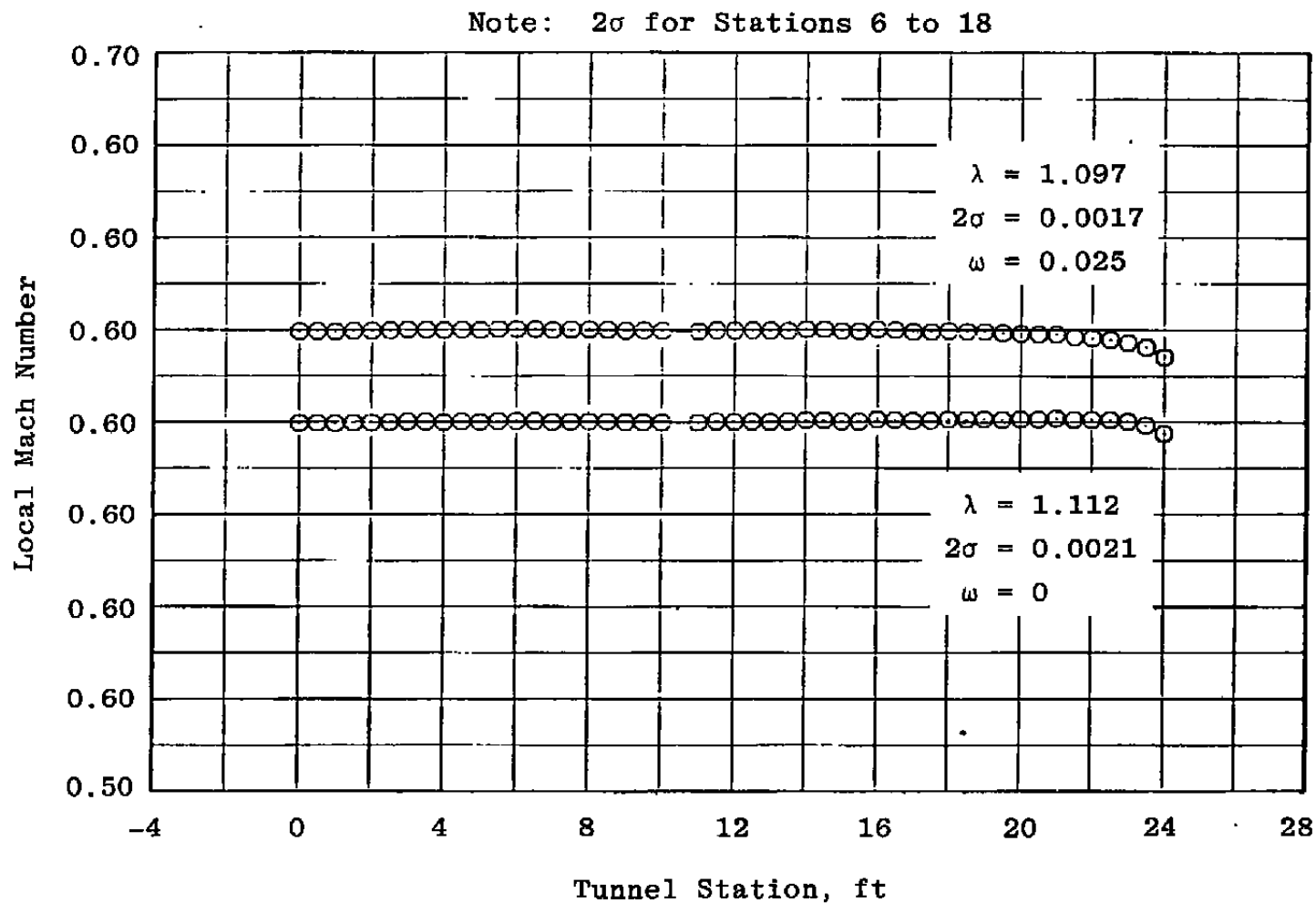
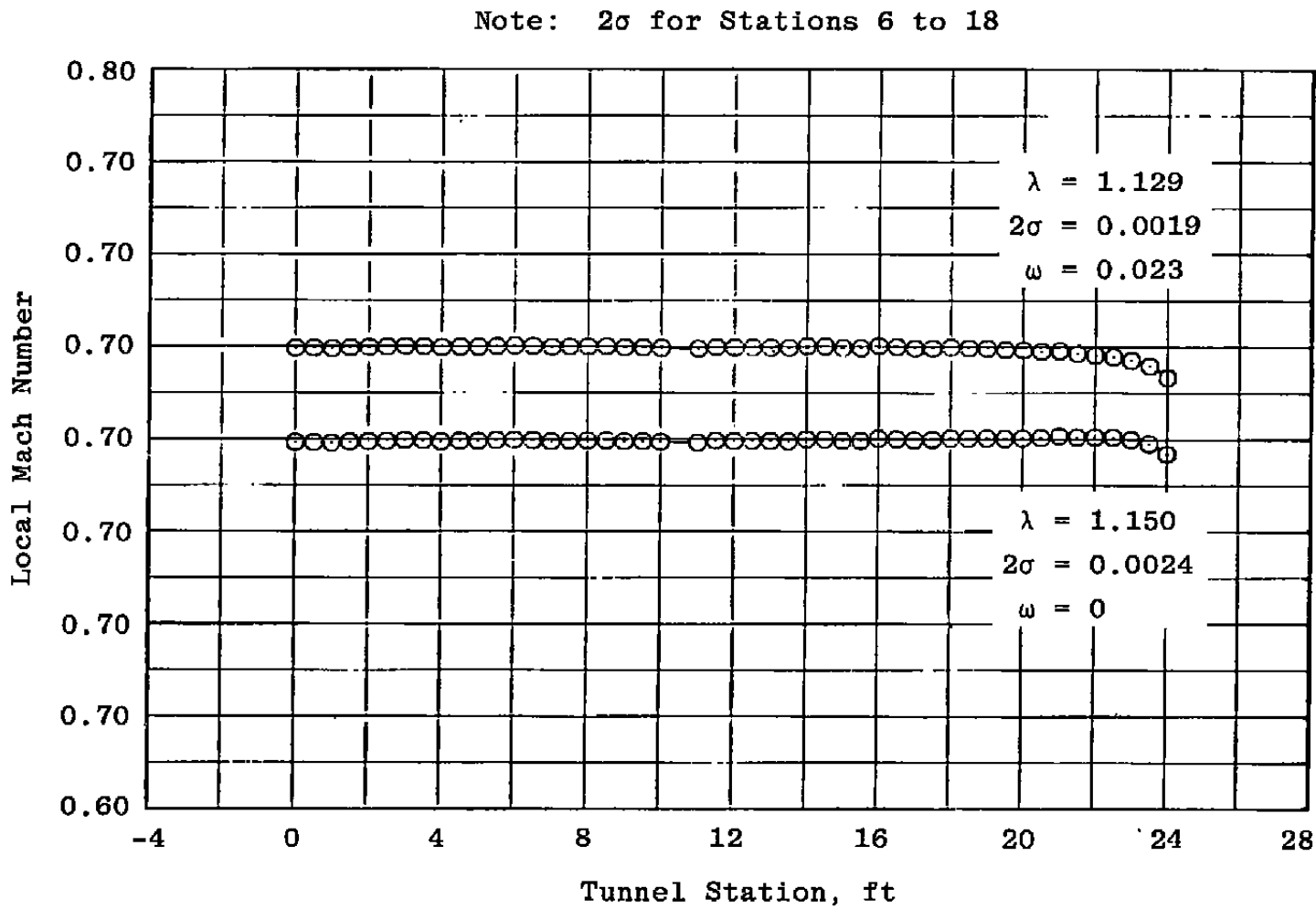


Figure 13. Concluded.



a.  $M_\infty = 0.6$

Figure 14. Effect of plenum chamber suction on the centerline Mach number distributions at  $P_t = 1,600$  psfa with  $\theta = 0$ .



b.  $M_\infty = 0.7$   
Figure 14. Continued.

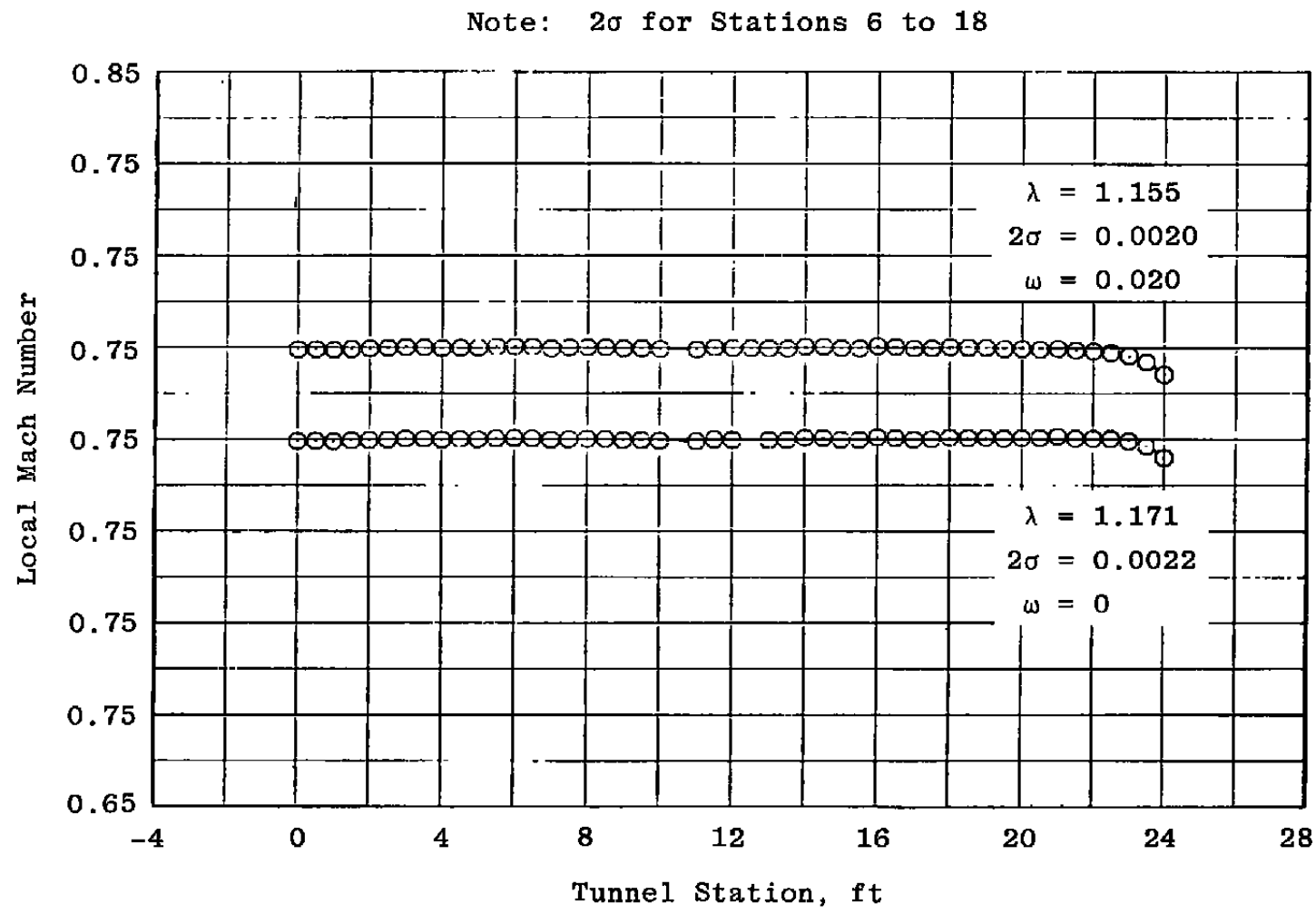


Figure 14. Concluded.

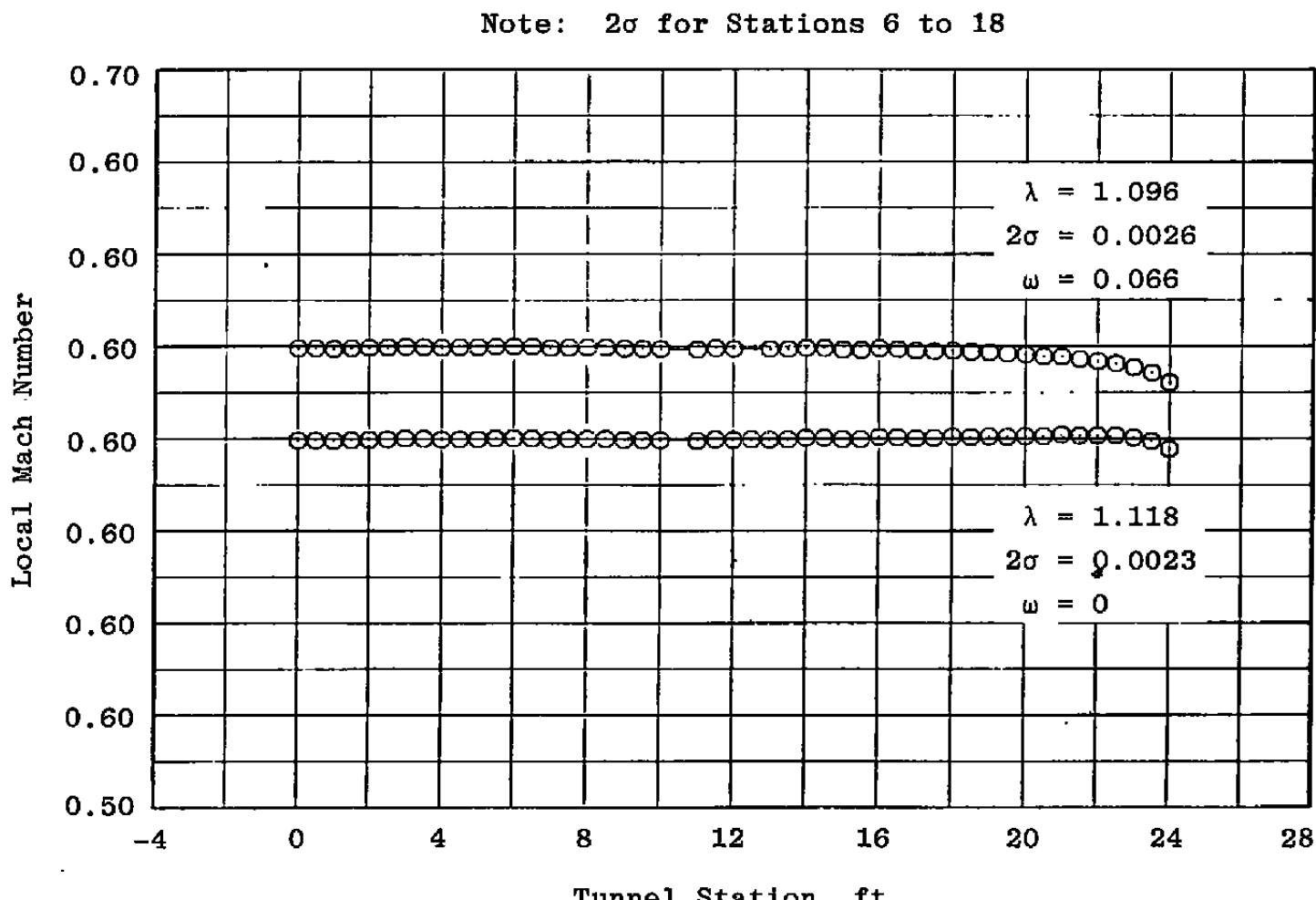
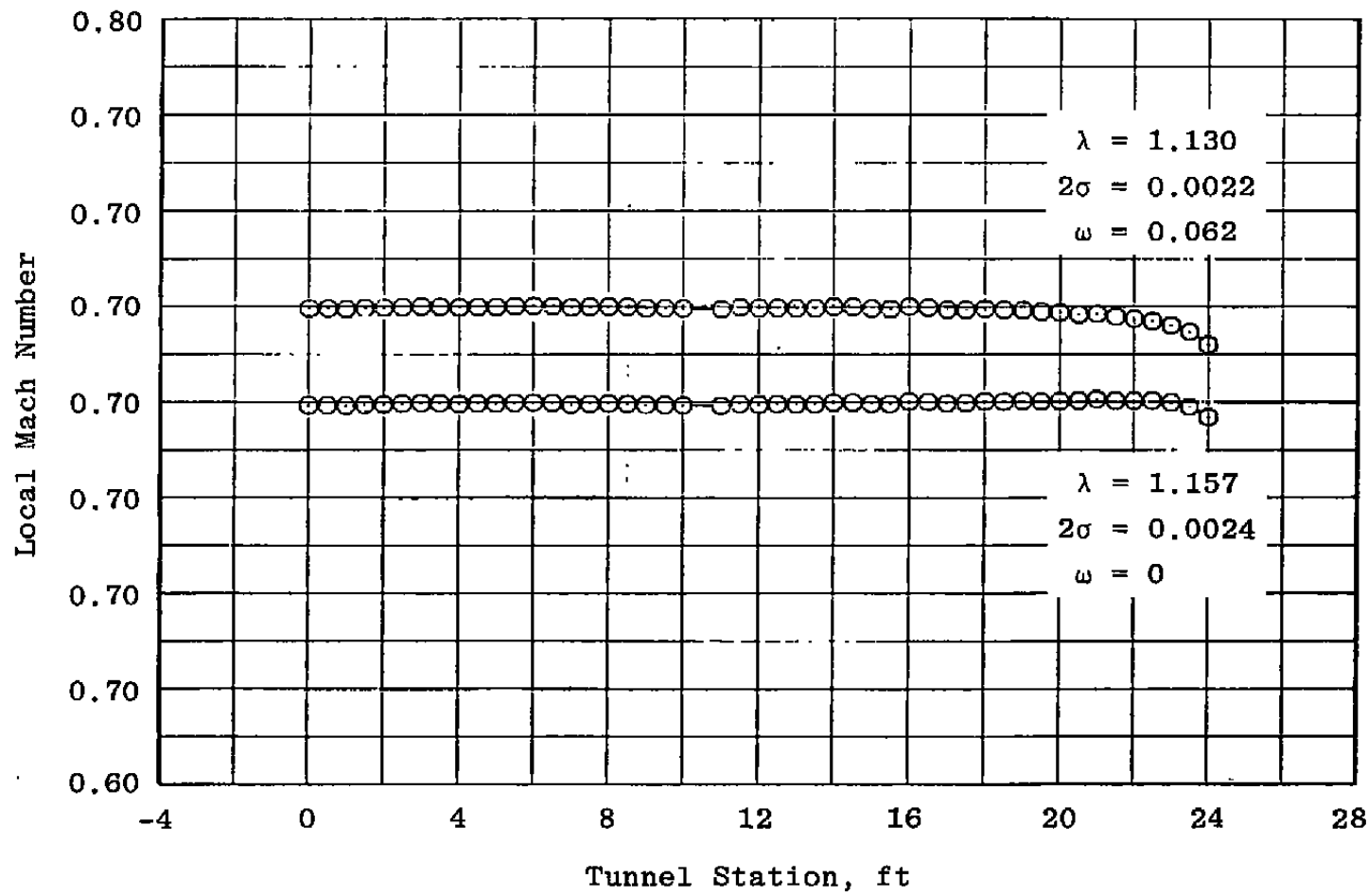
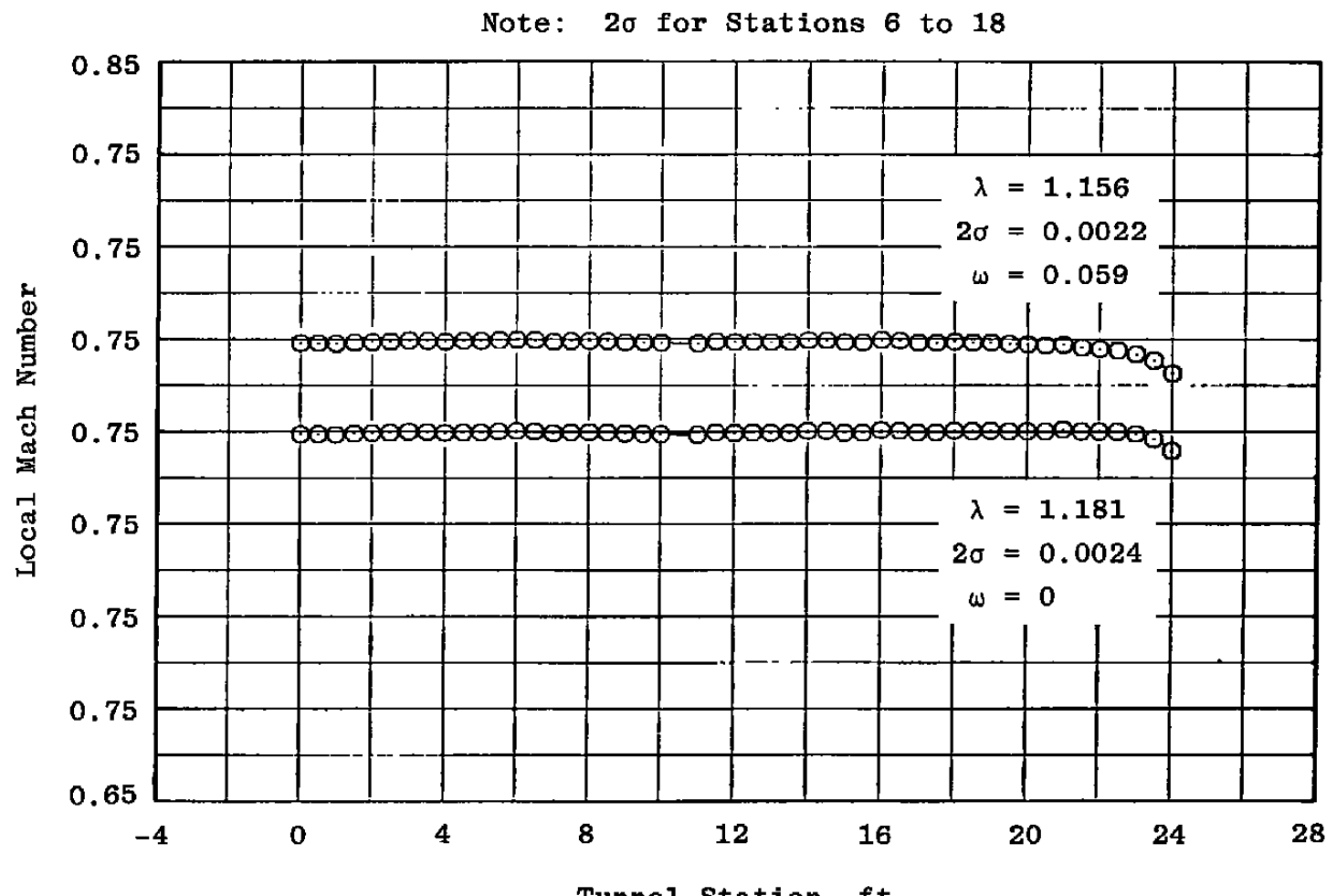


Figure 15. Effect of plenum chamber suction on the centerline Mach number distributions at  $P_t = 2,200$  psfa with  $\theta = 0$ .

Note:  $2\sigma$  for Stations 6 to 18



b.  $M_{\infty} = 0.7$   
Figure 15. Continued.



c.  $M_\infty = 0.75$   
Figure 15. Concluded.

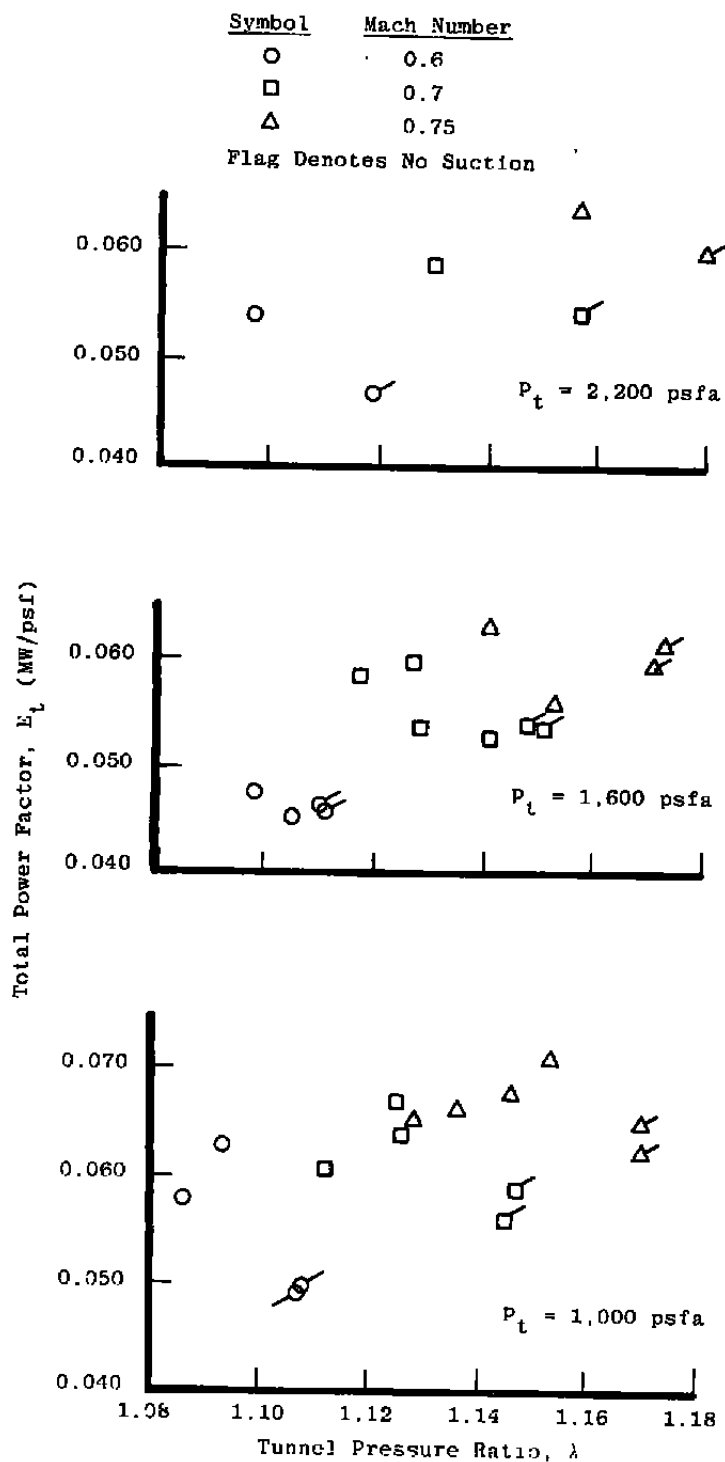
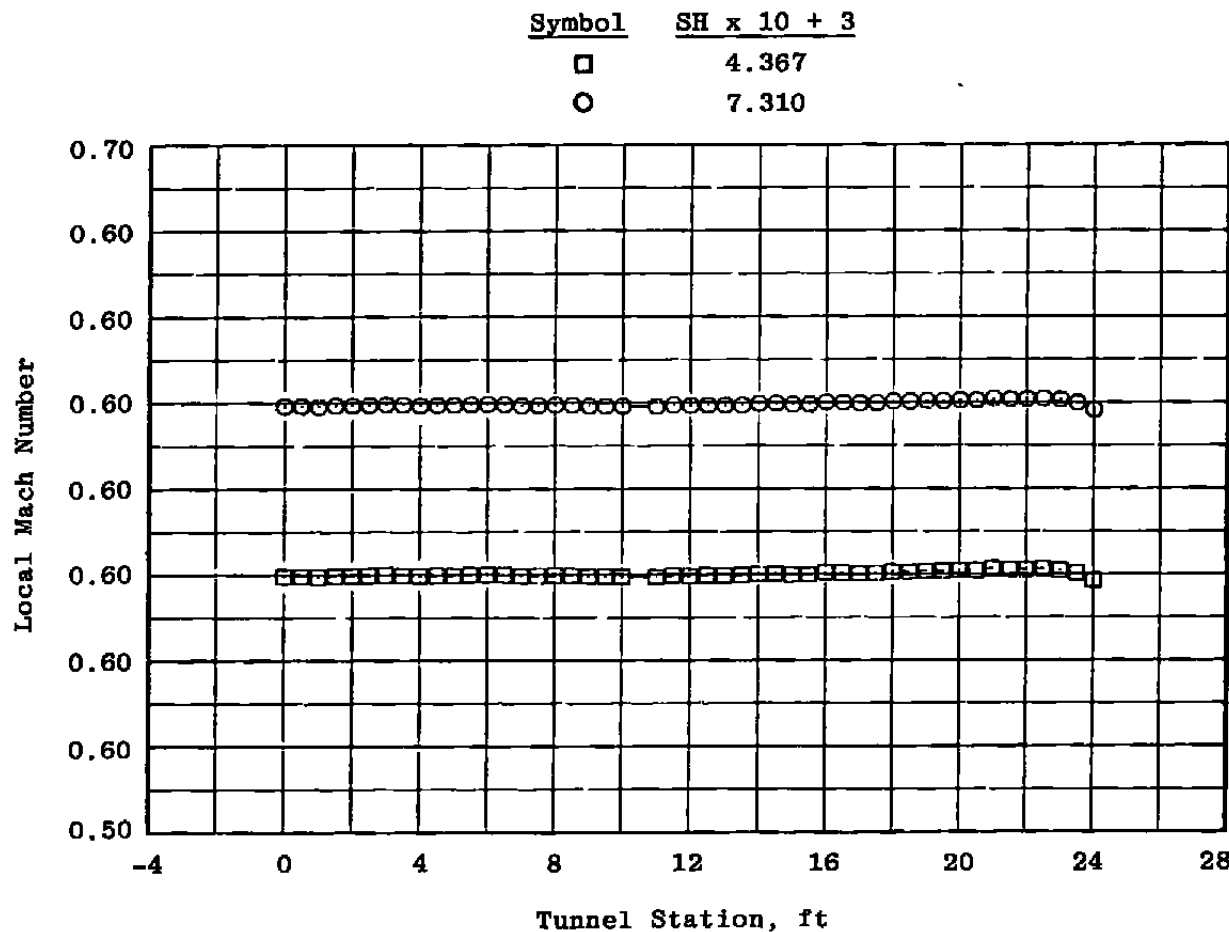
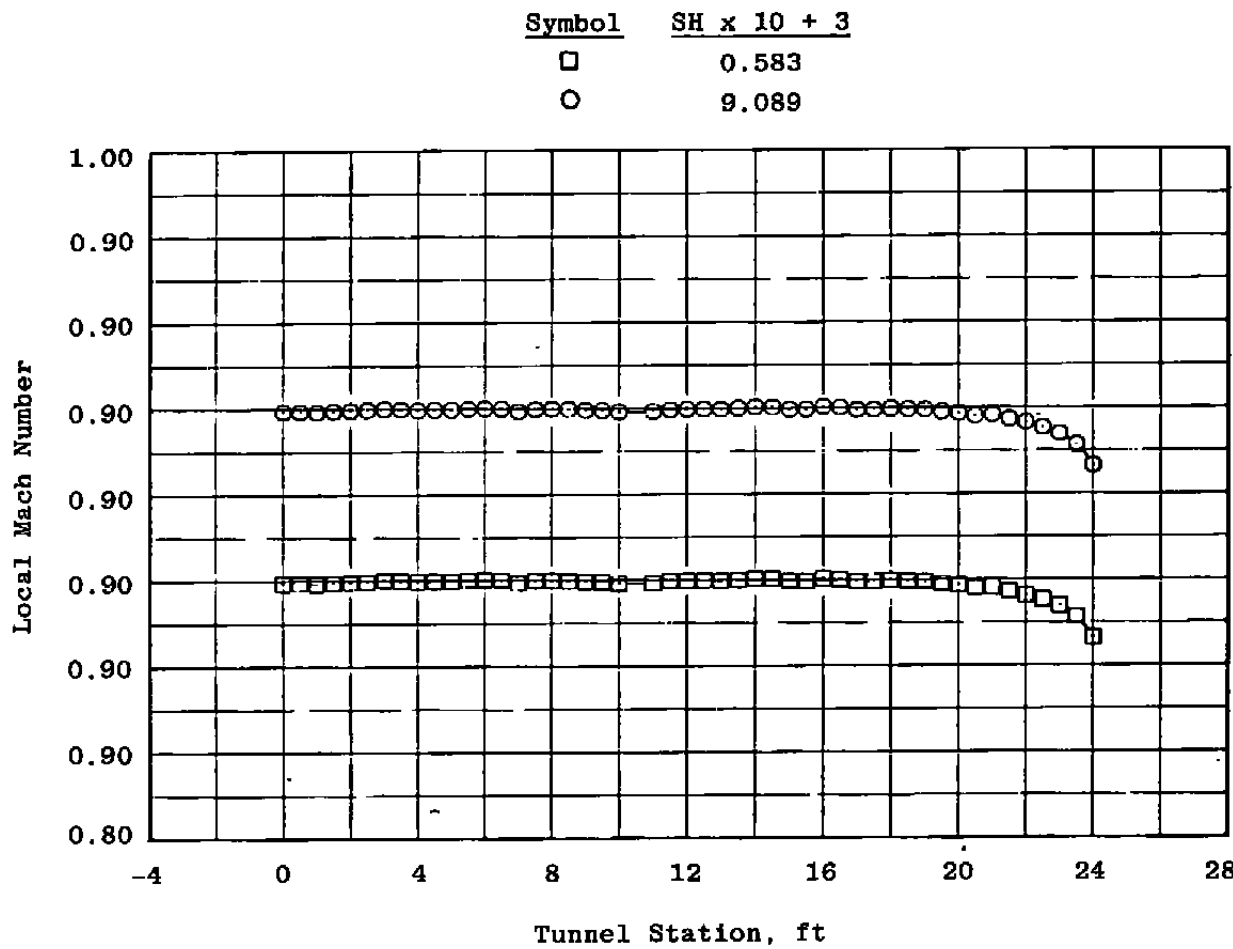


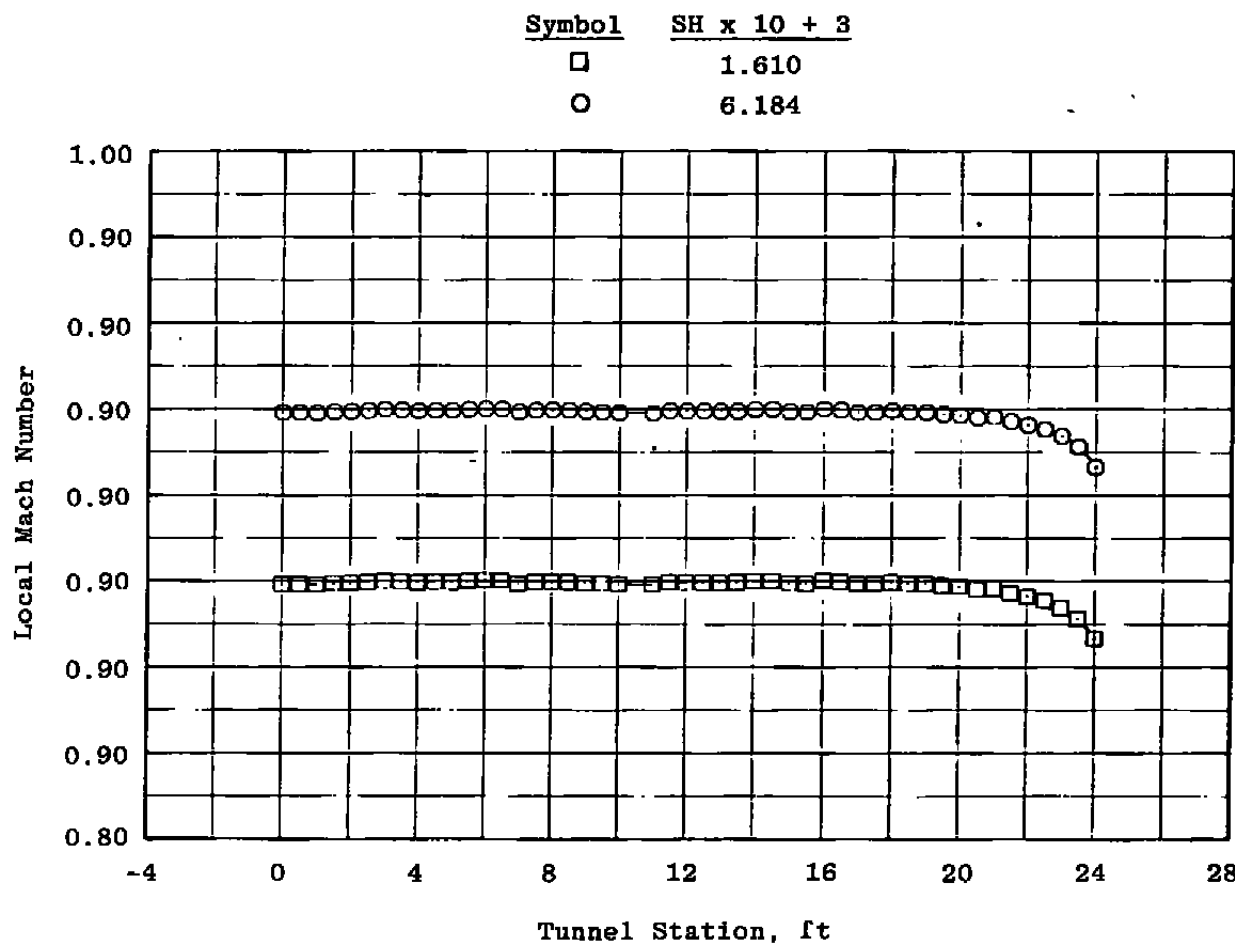
Figure 16. Effect of tunnel pressure ratio on the total power factor at  $M_\infty \leq 0.75$  with  $\theta = 0$ .



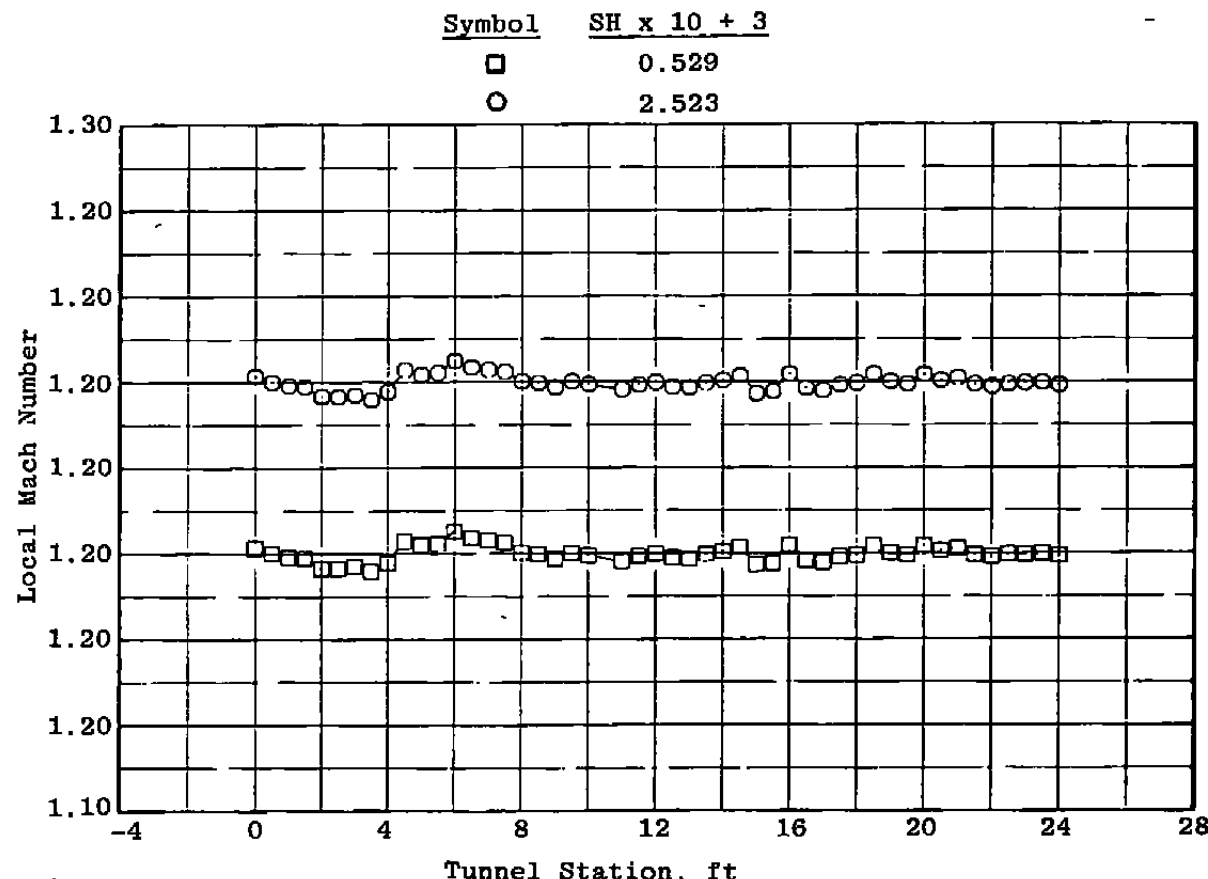
a.  $M_\infty = 0.6$ ,  $P_t = 3,200$  psfa  
Figure 17. Effect of test section humidity on the Mach number distributions with  $\lambda = \lambda^*$  and  $\theta = 0$ .



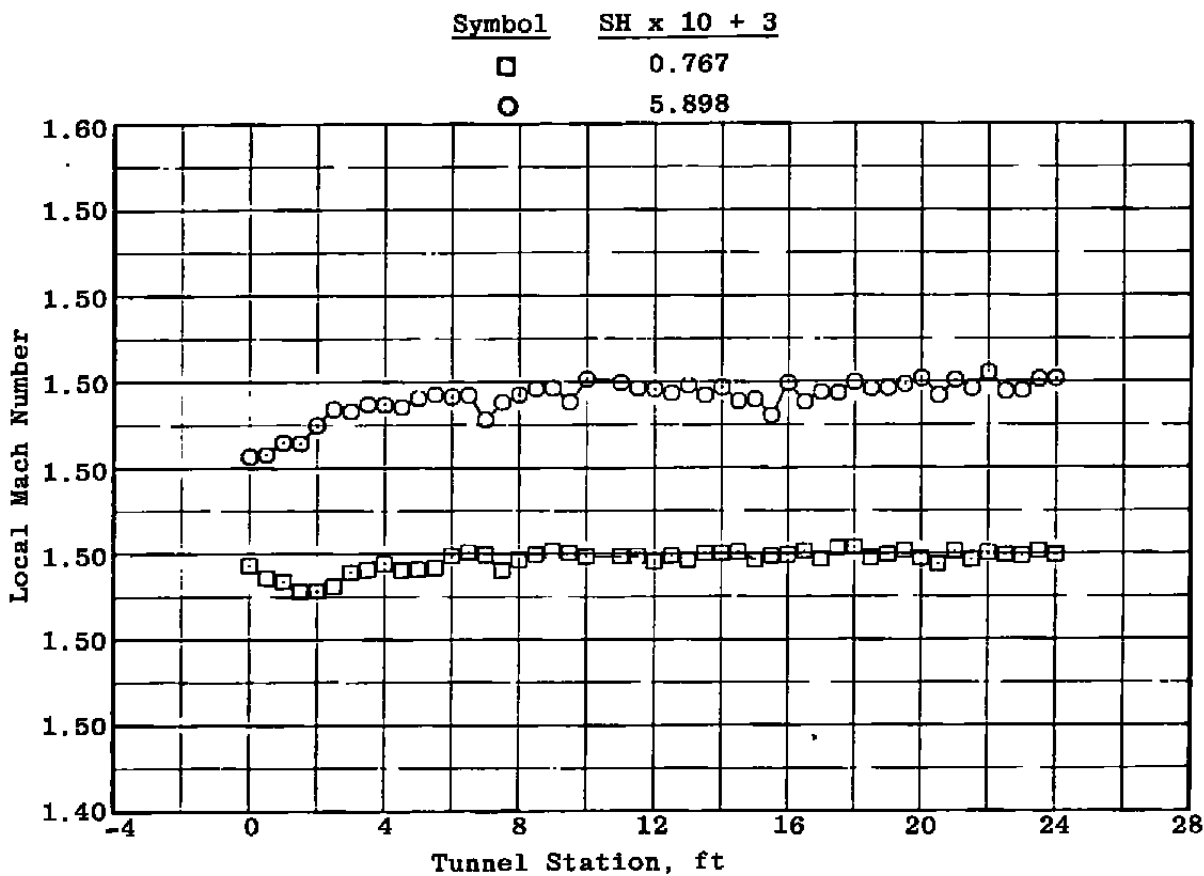
b.  $M_\infty = 0.9$ ,  $P_t = 1,200$  psfa  
 Figure 17. Continued.



c.  $M_\infty = 0.9$ ,  $P_t = 2,400$  psfa  
Figure 17. Continued.



d.  $M_\infty = 1.2$ ,  $P_t = 1,600$  psfa  
Figure 17. Continued.



e.  $M_\infty = 1.5, P_t = 1,600 \text{ psfa}$   
Figure 17. Concluded.

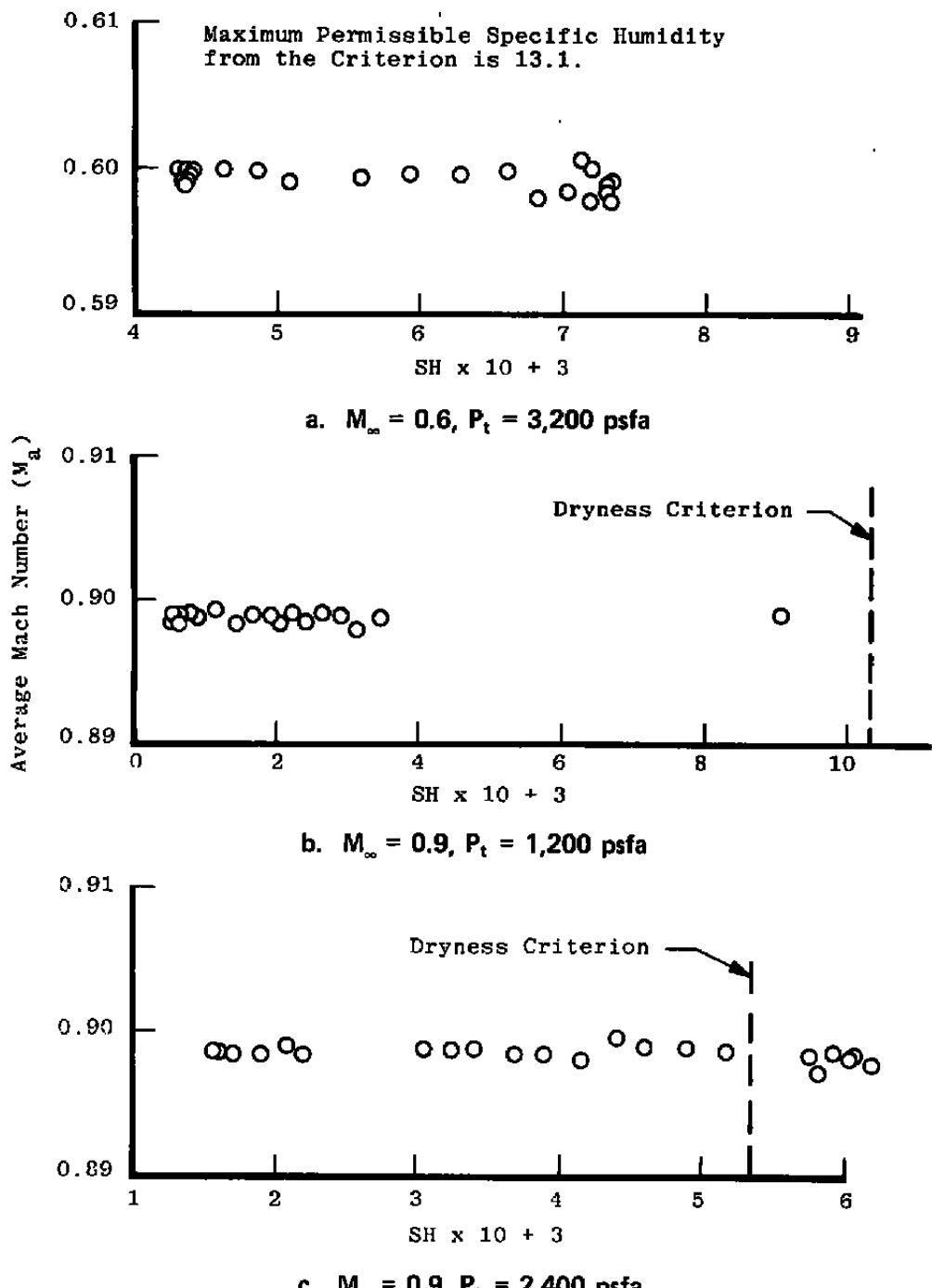
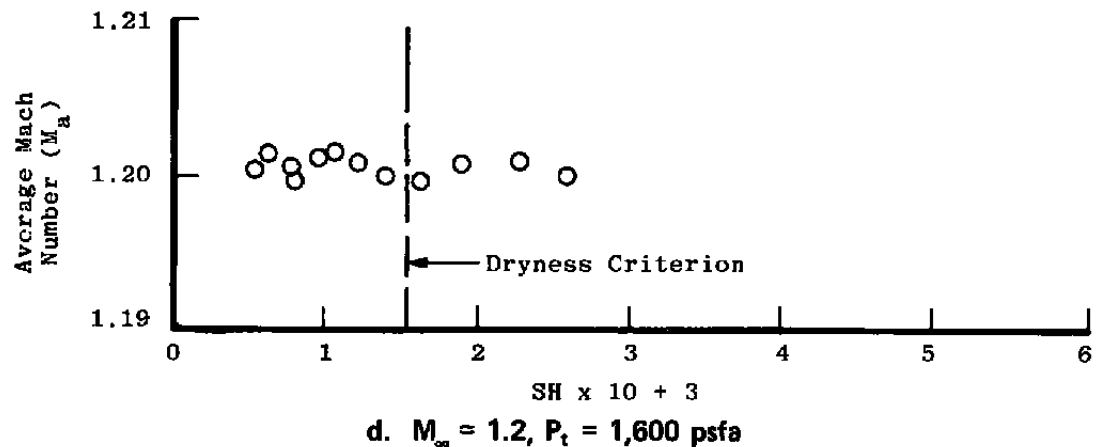
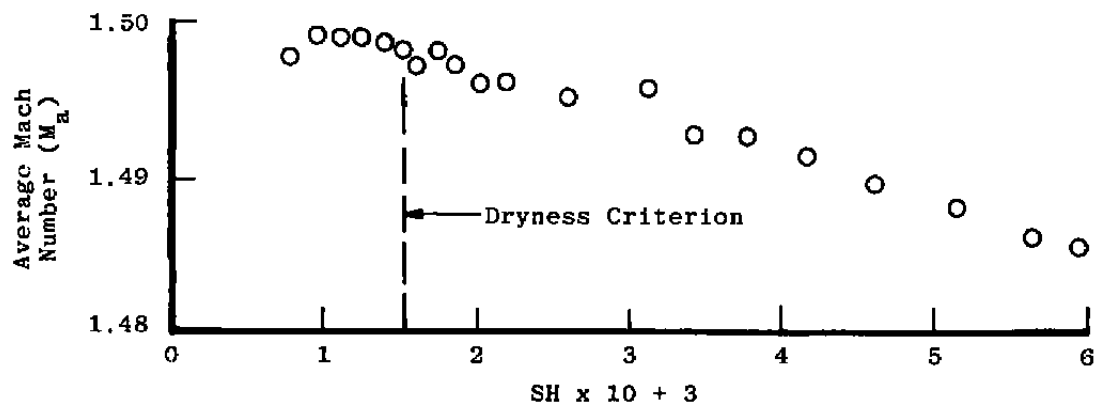


Figure 18. Effect of test section humidity on the average Mach number with  $\lambda = \lambda^*$  and  $\theta = 0$ .

d.  $M_{\infty} = 1.2, P_t = 1,600 \text{ psfa}$ e.  $M_{\infty} = 1.5, P_t = 1,600 \text{ psfa}$   
Figure 18. Concluded.

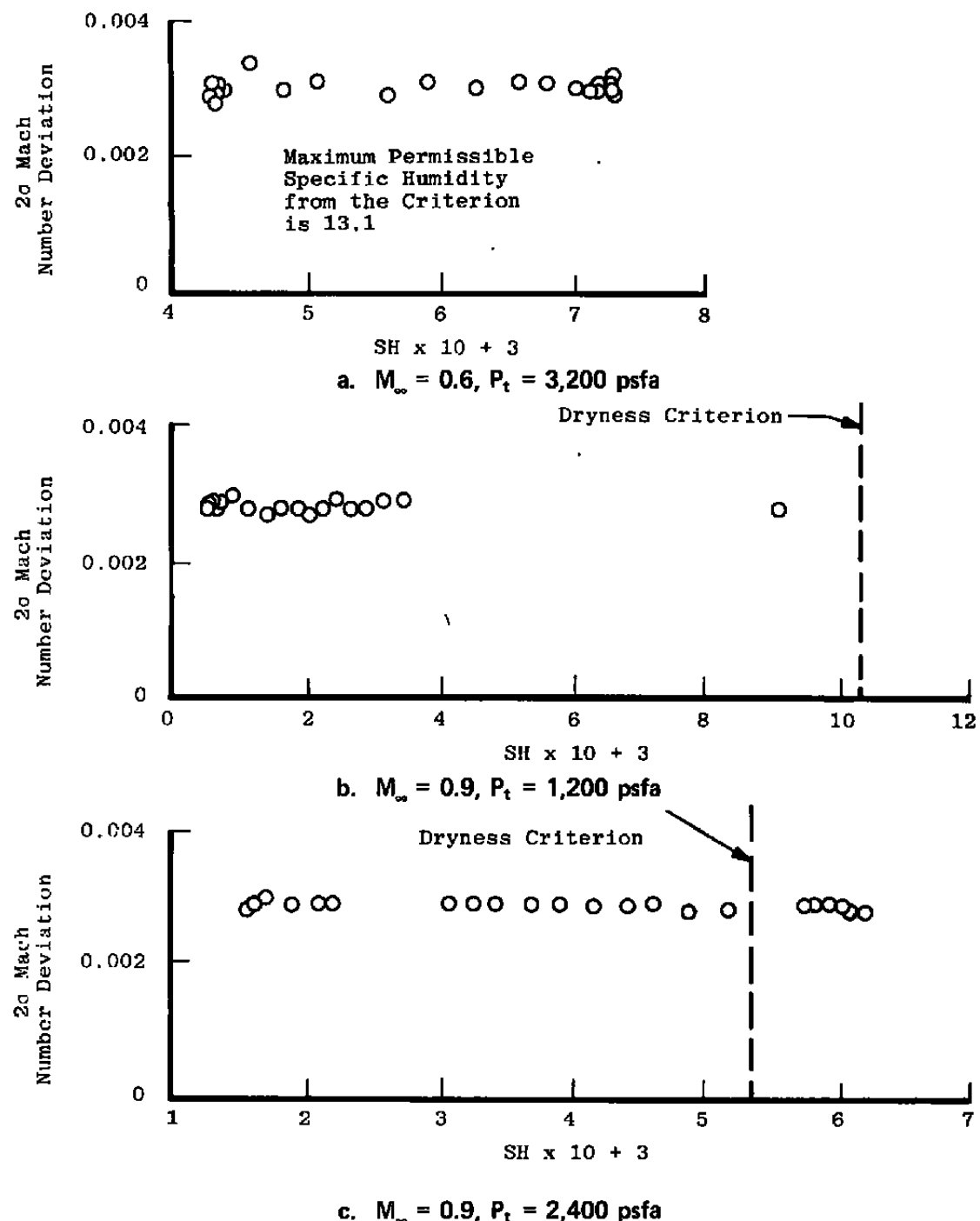


Figure 19. Effect of test section humidity of the  $2\sigma$  Mach number deviations with  $\lambda = \lambda^*$  and  $\theta = 0$ .

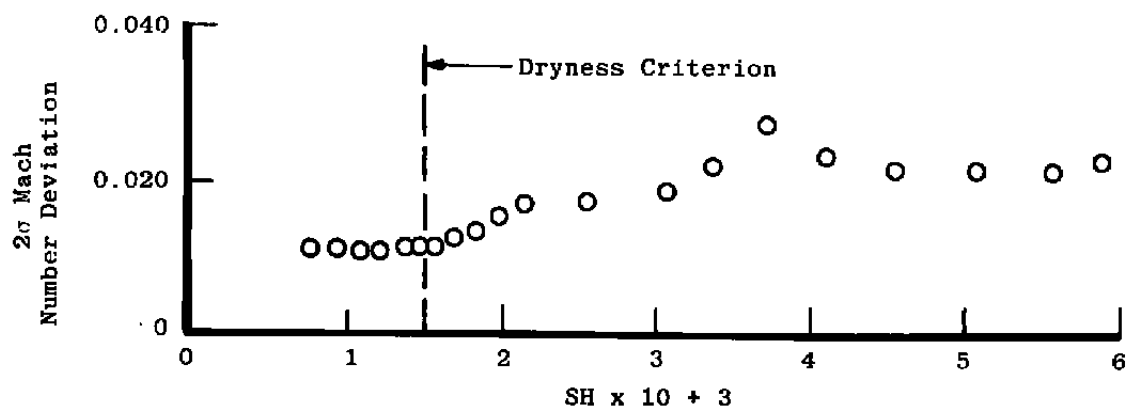
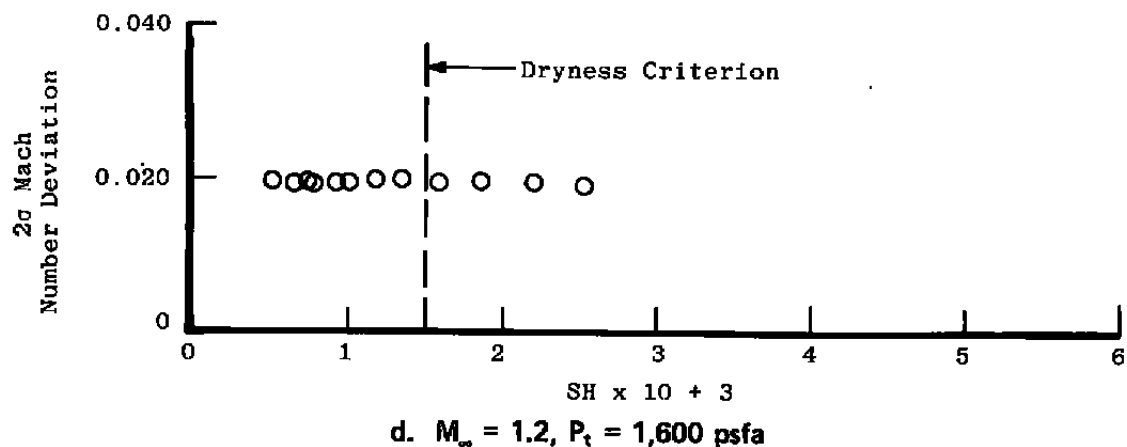


Figure 19. Concluded.

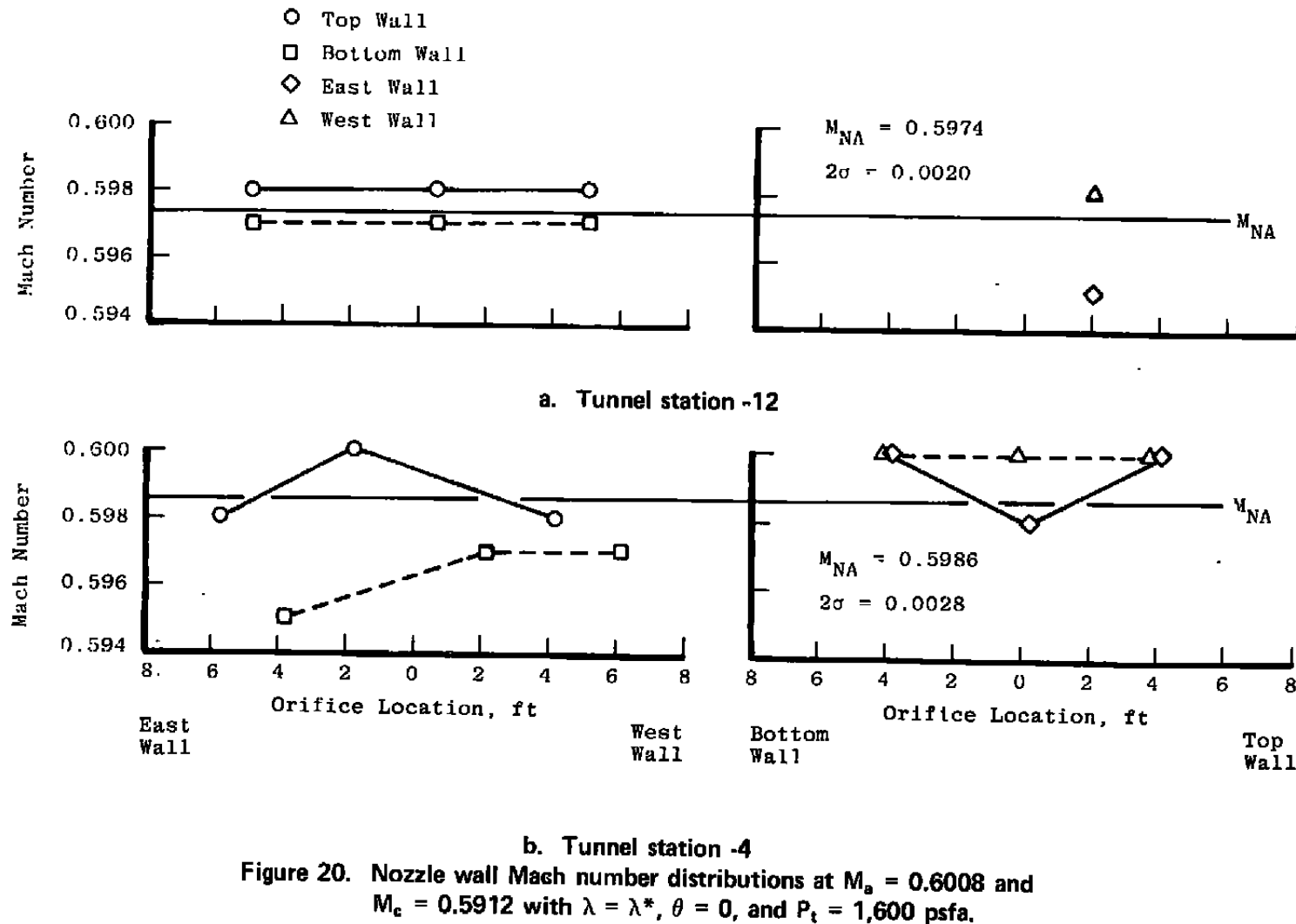


Figure 20. Nozzle wall Mach number distributions at  $M_a = 0.6008$  and  $M_e = 0.5912$  with  $\lambda = \lambda^*$ ,  $\theta = 0$ , and  $P_t = 1,600$  psfa.

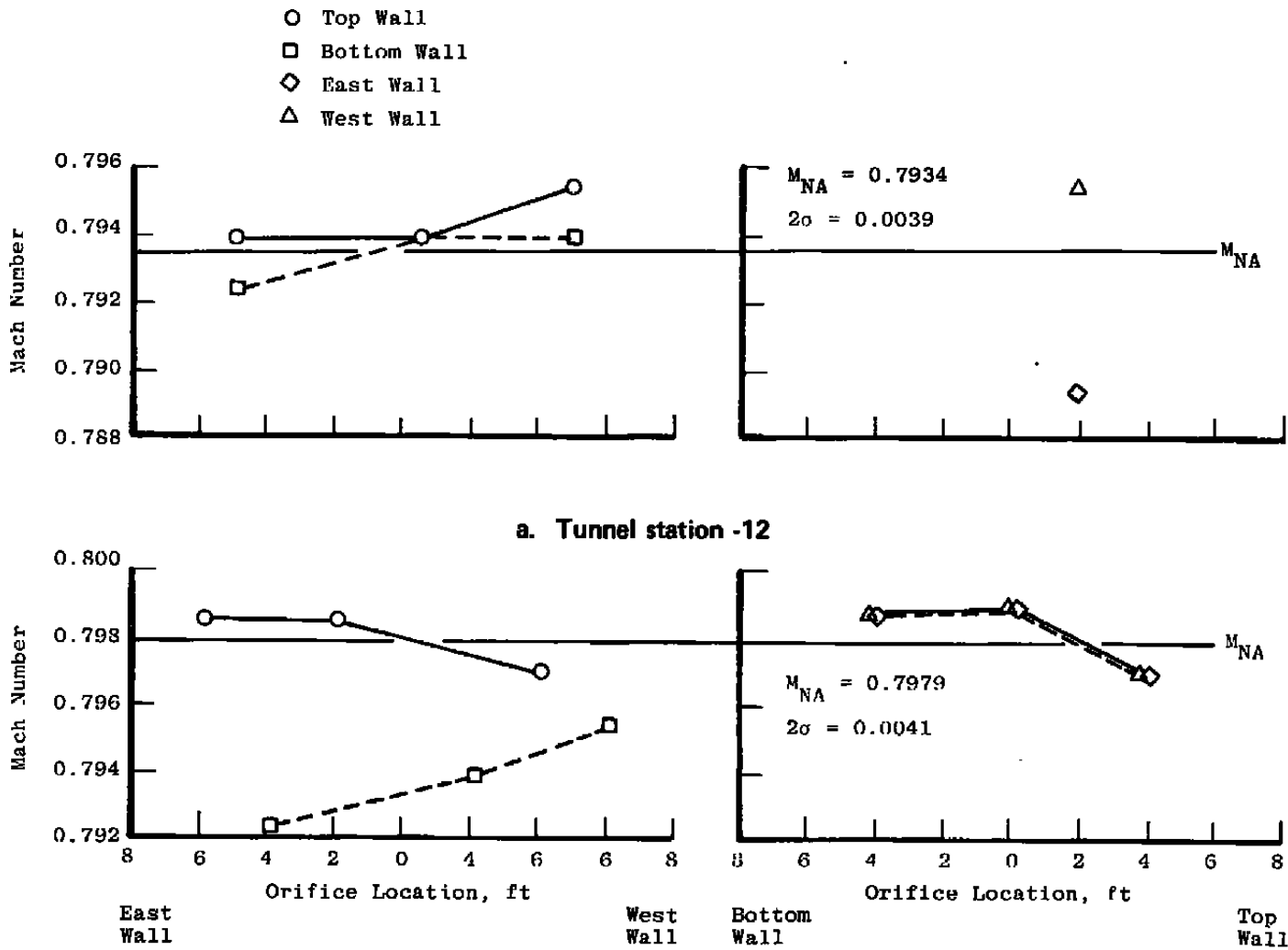
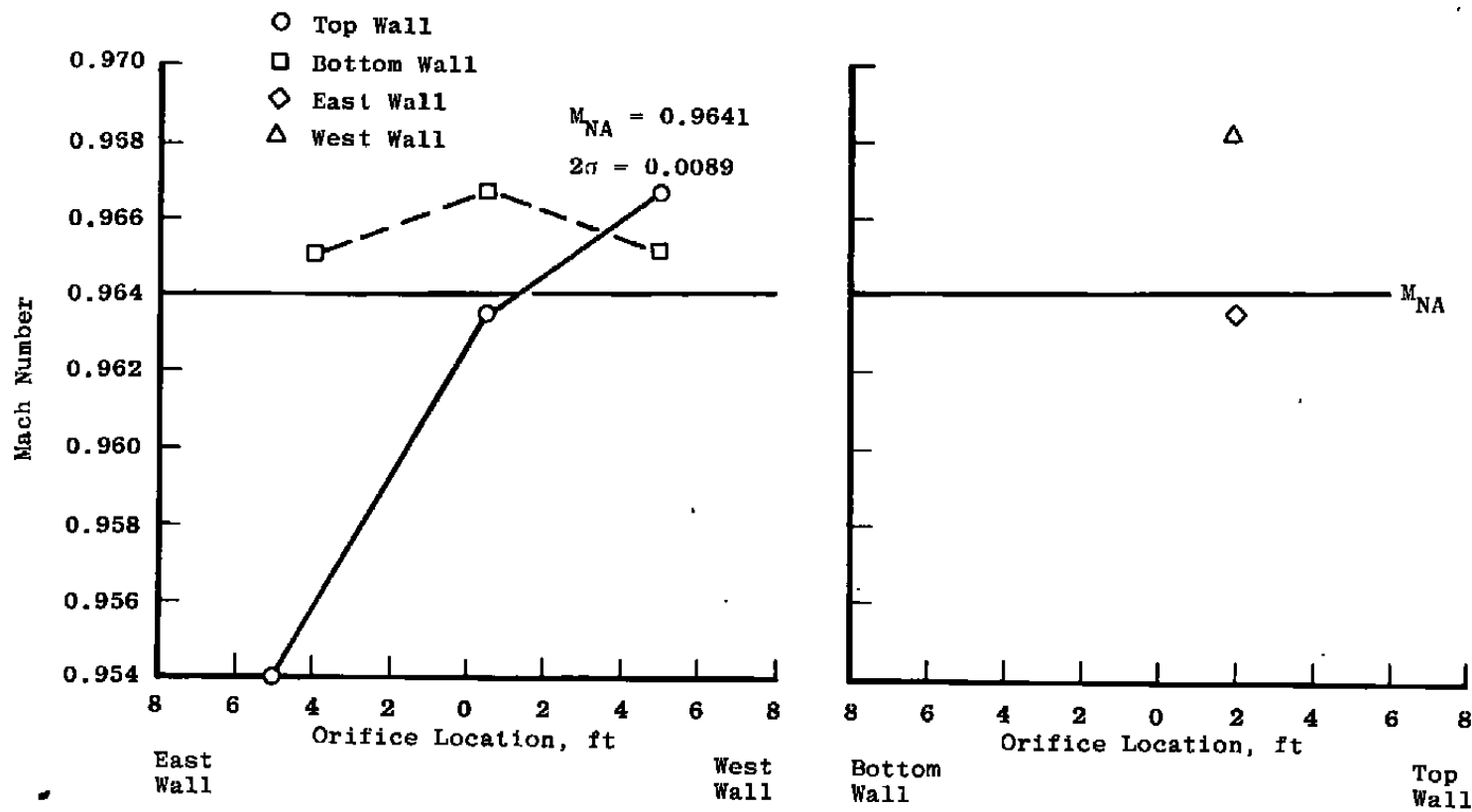
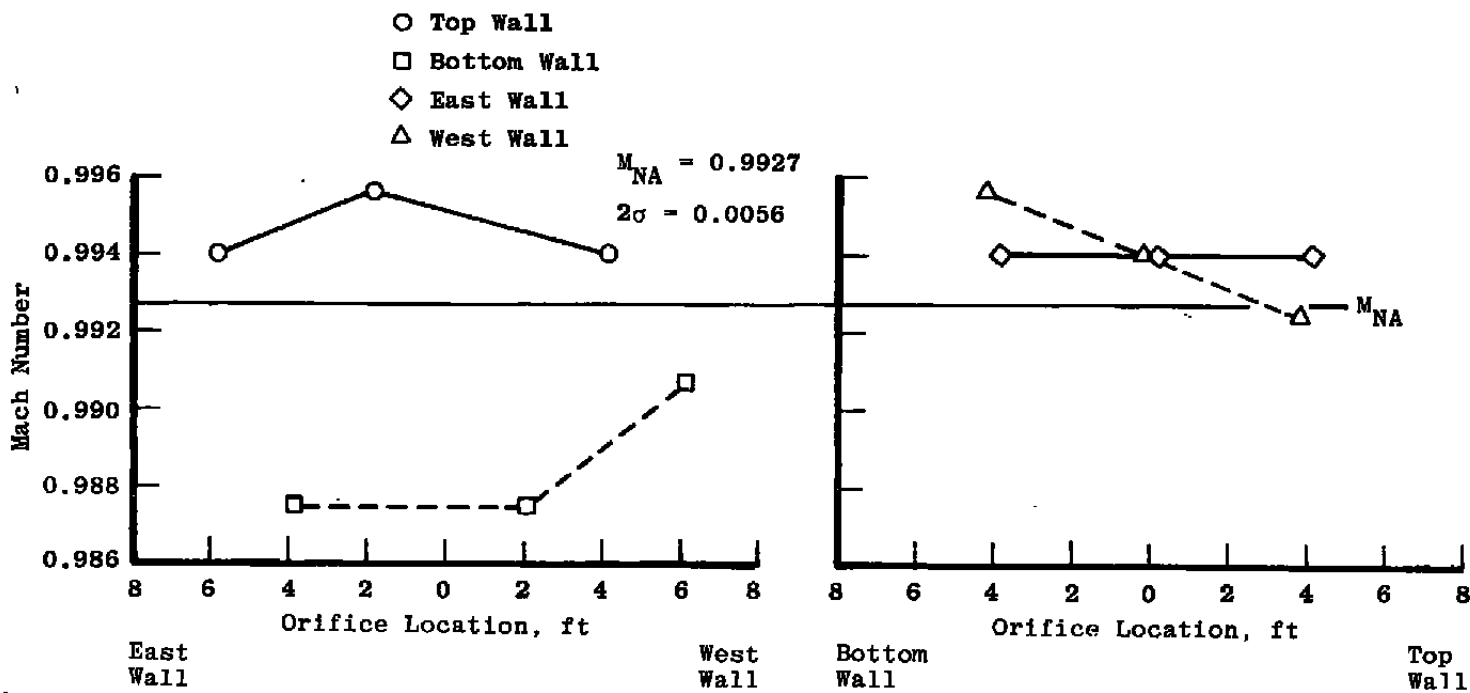


Figure 21. Nozzle wall Mach number distributions at  $M_a = 0.7996$  and  $M_c = 0.7890$  with  $\lambda = \lambda^*$ ,  $\theta = 0$ , and  $P_t = 1,600$  psfa.

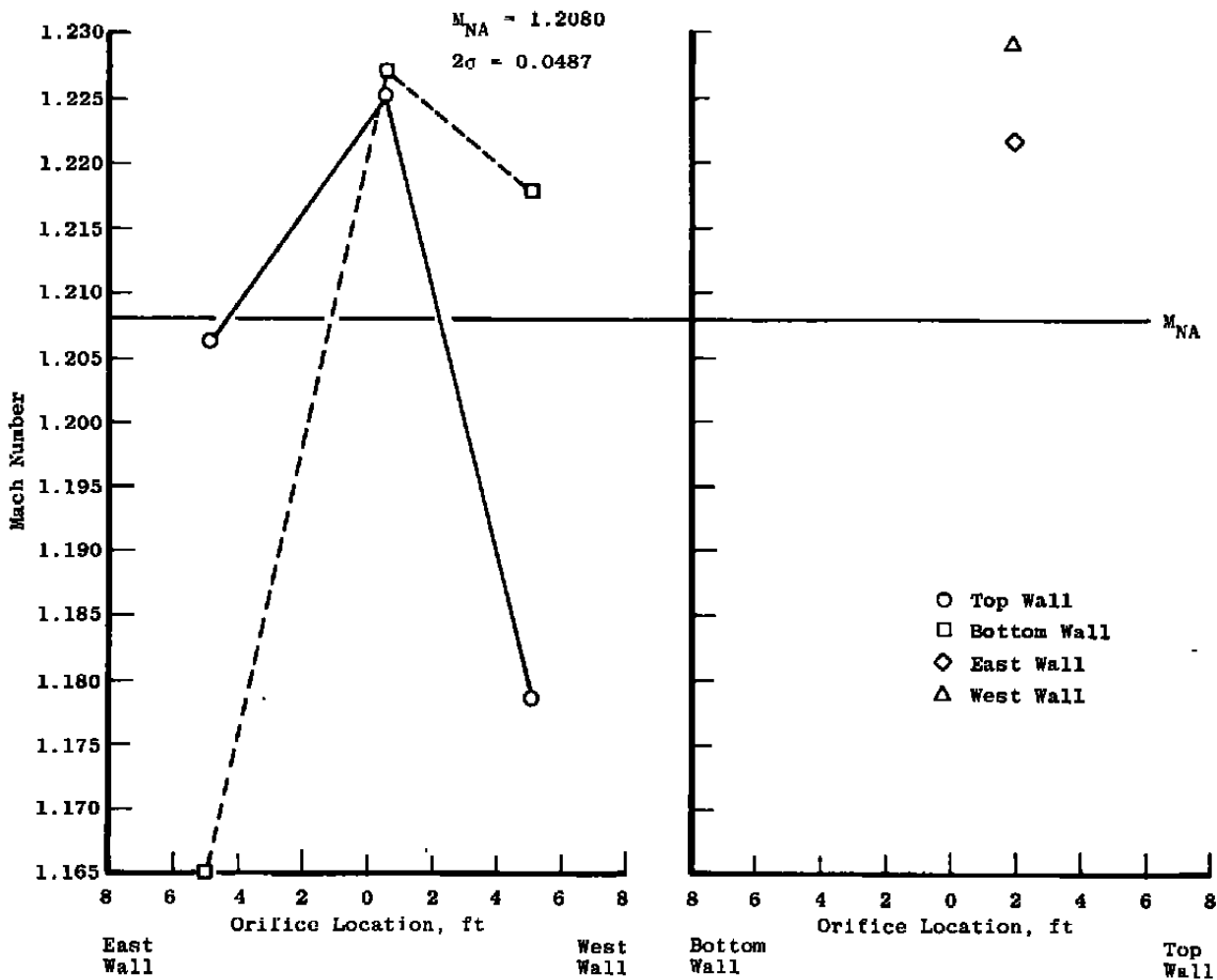


a. Tunnel station -12

Figure 22. Nozzle wall Mach number distributions at  $M_a = 0.9979$  and  $M_c = 0.9859$  with  $\lambda = \lambda^*$ ,  $\theta = 0$ , and  $P_t = 1,600$  psfa.

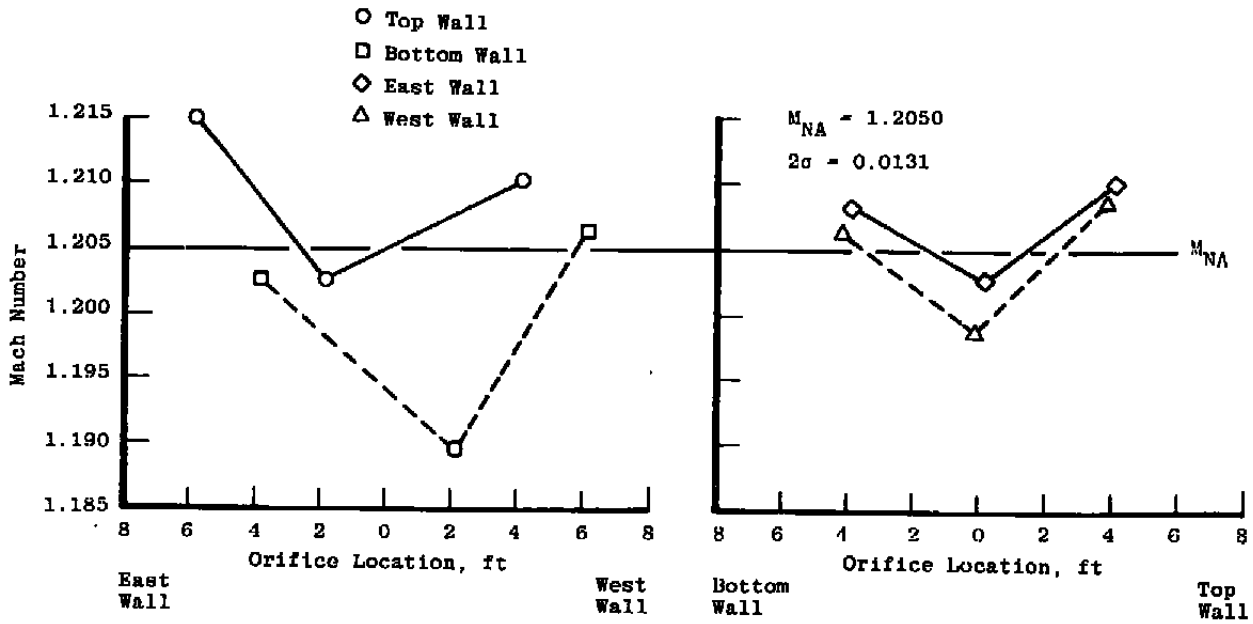


b. Tunnel station -4  
Figure 22. Concluded.

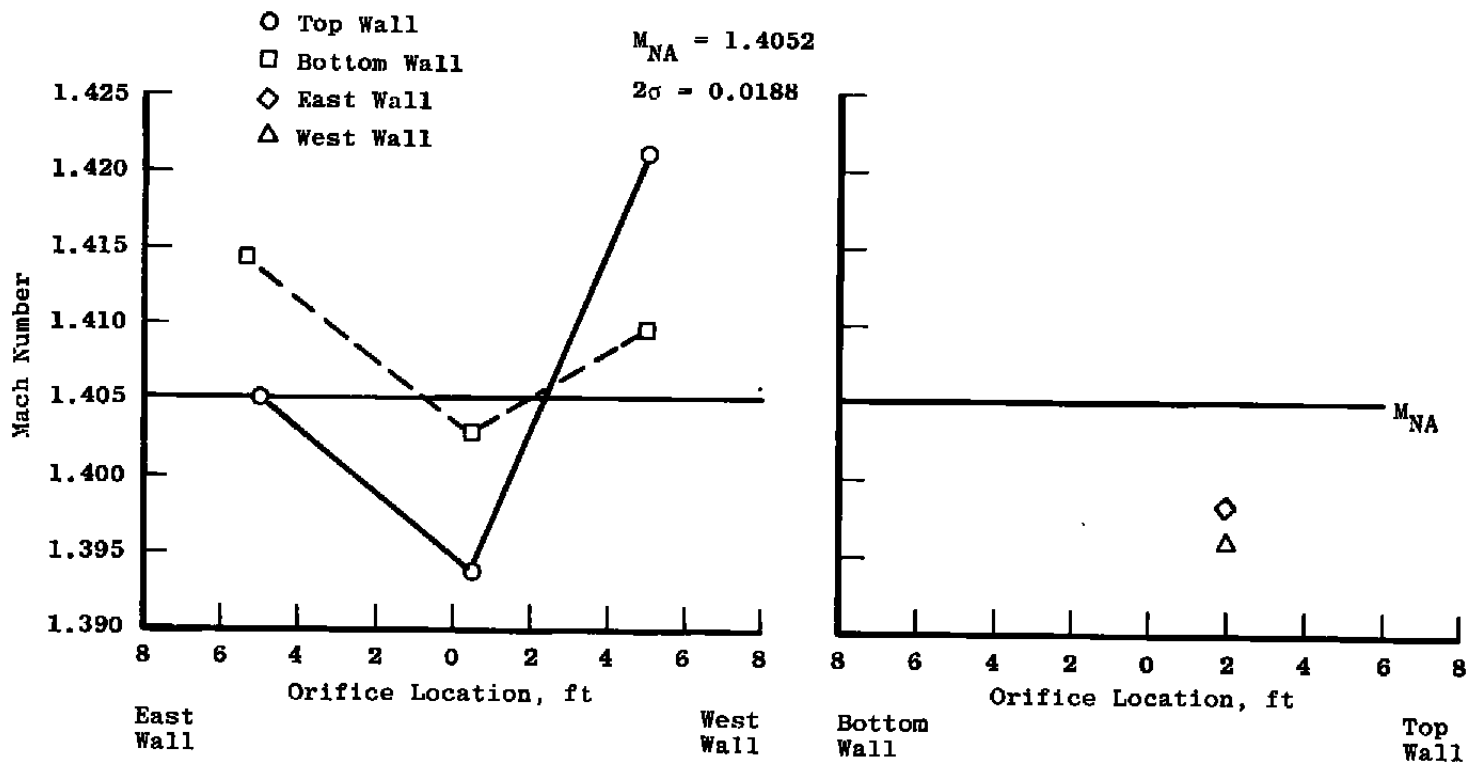


a. Tunnel station -12

**Figure 23.** Nozzle wall Mach number distributions at  $M_a = 1.2023$  and  $M_c = 1.1868$  with  $\lambda = \lambda^*$ ,  $\theta = 0$ , and  $P_1 = 1,600$  psfa.

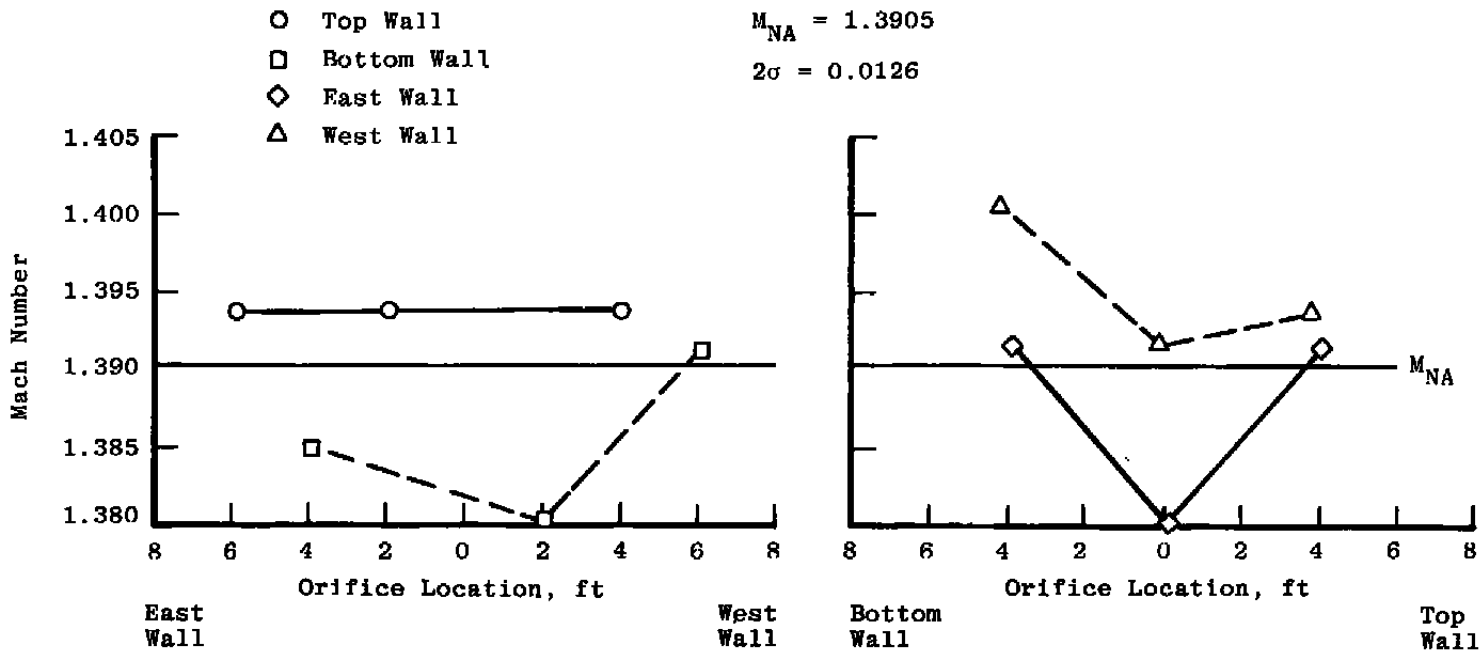


**b. Tunnel station -4**  
**Figure 23. Concluded.**

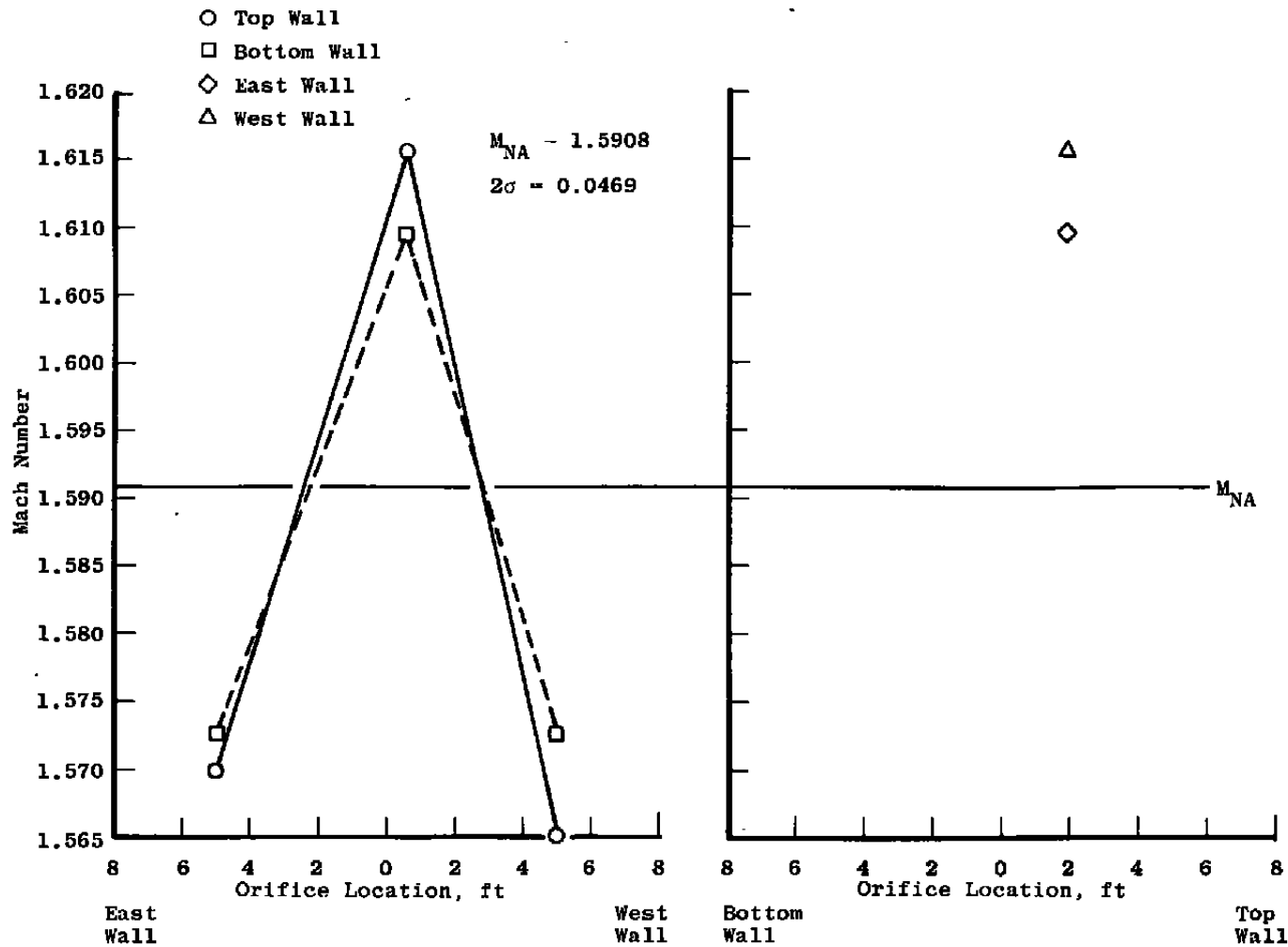


a. Tunnel station -12

Figure 24. Nozzle wall Mach number distributions at  $M_a = 1.3994$  and  $M_c = 1.3853$  with  $\lambda = \lambda^*$ ,  $\theta = 0$ , and  $P_t = 1,600$  psfa.

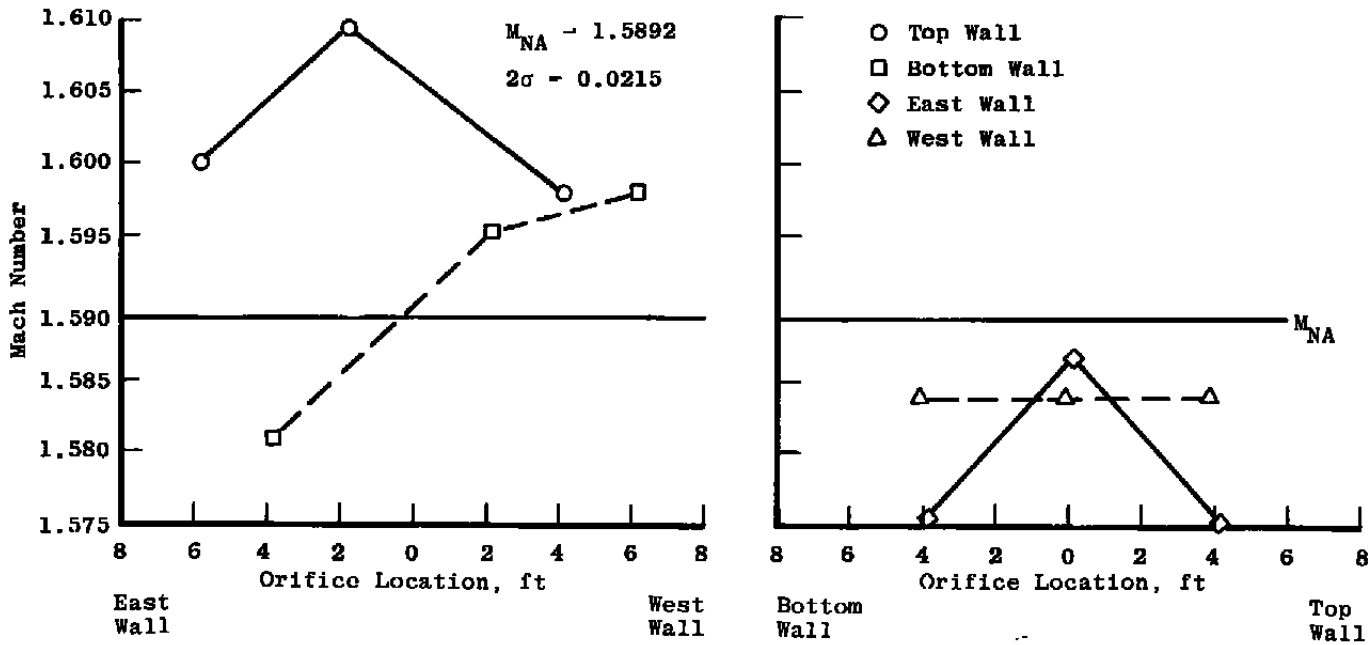


b. Tunnel station -4  
Figure 24. Concluded.



a. Tunnel station -12

Figure 25. Nozzle wall Mach number distributions at  $M_e = 1.5985$  and  $M_c = 1.5847$  with  $\lambda = \lambda^*$ ,  $\theta = 0$ , and  $P_t = 1,600$  psfa.



b. Tunnel station 4  
Figure 25. Concluded.

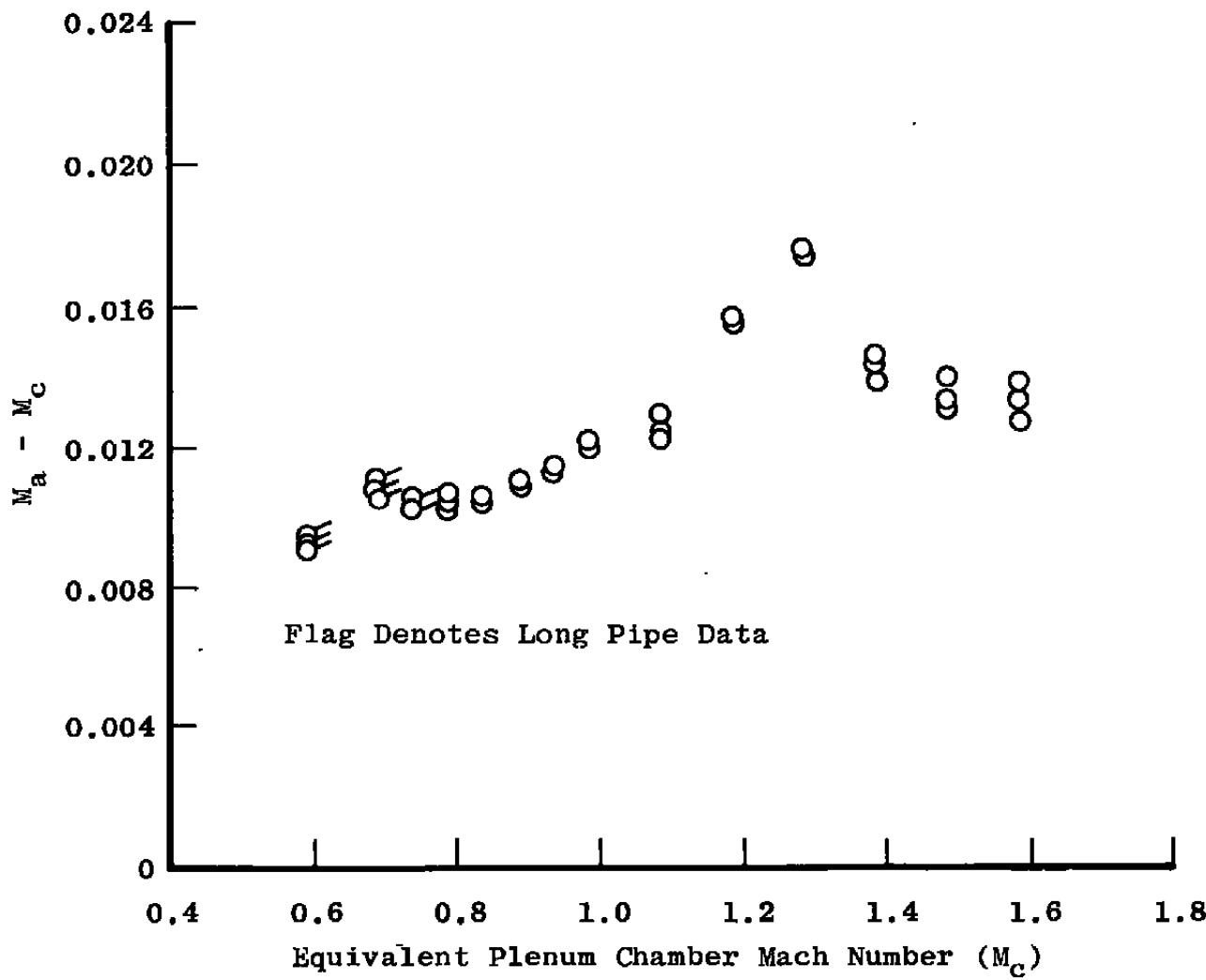
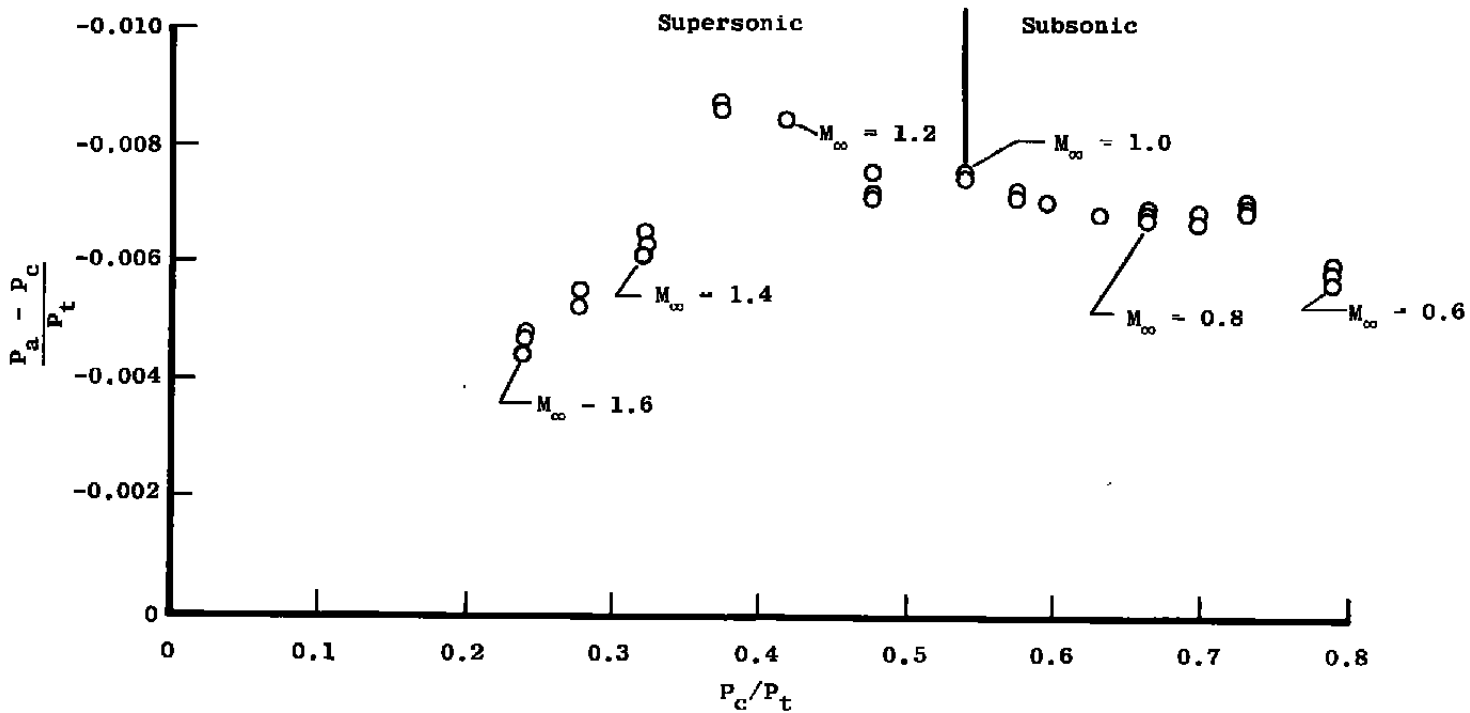
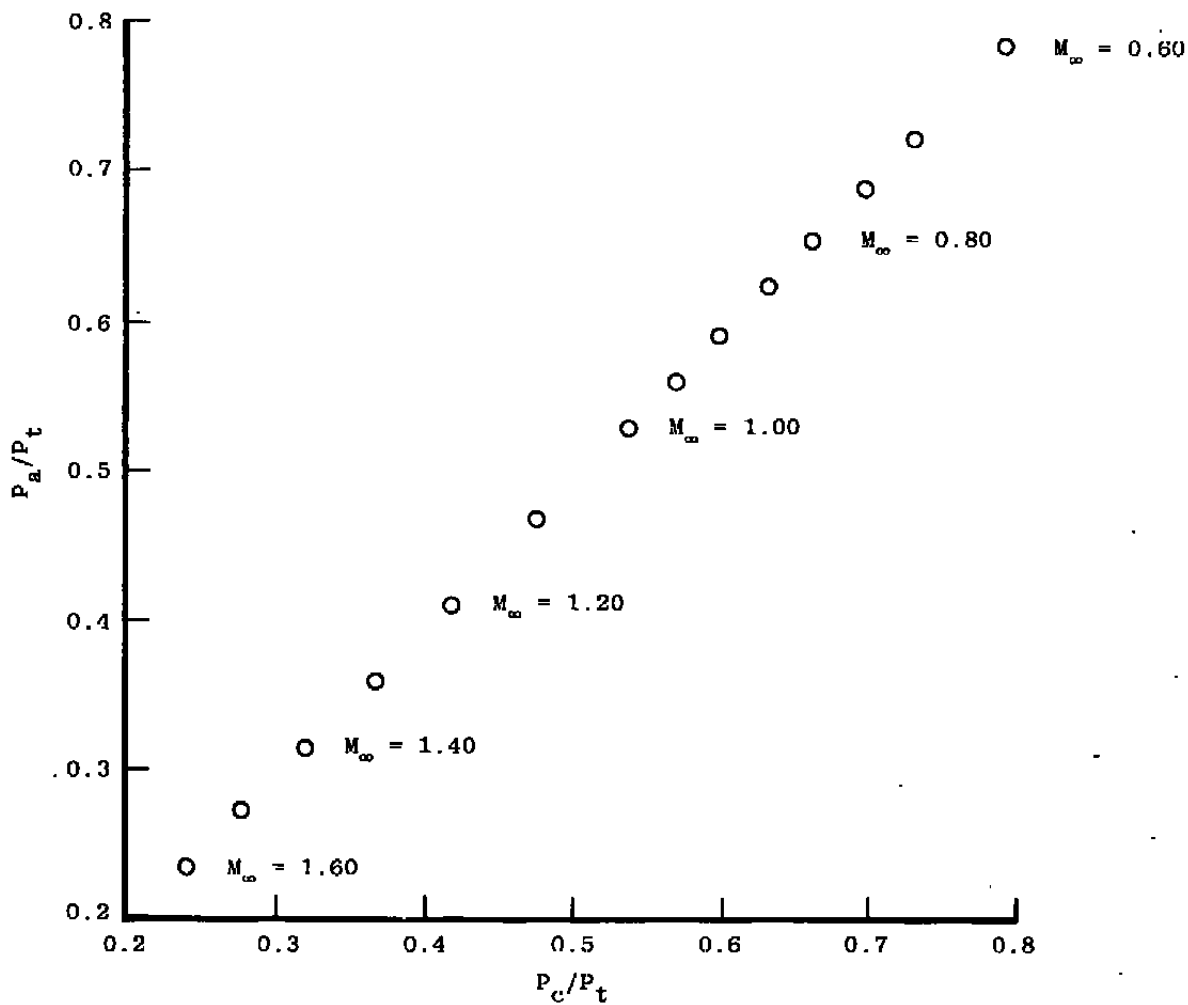


Figure 26. Tunnel 16T Mach number calibration with  $\lambda = \lambda^*$ ,  $\theta = 0$ , and  $P_t = 1,600$  psfa.

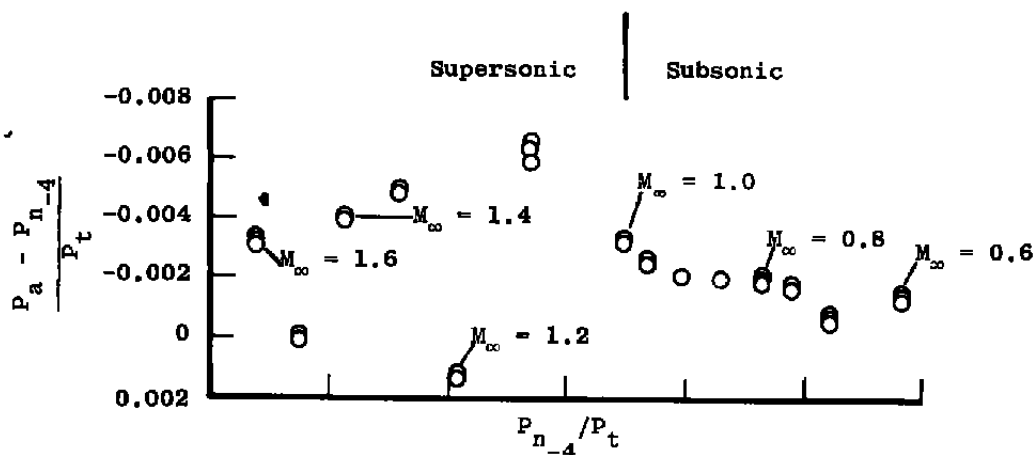


a. Test section and plenum static pressure difference

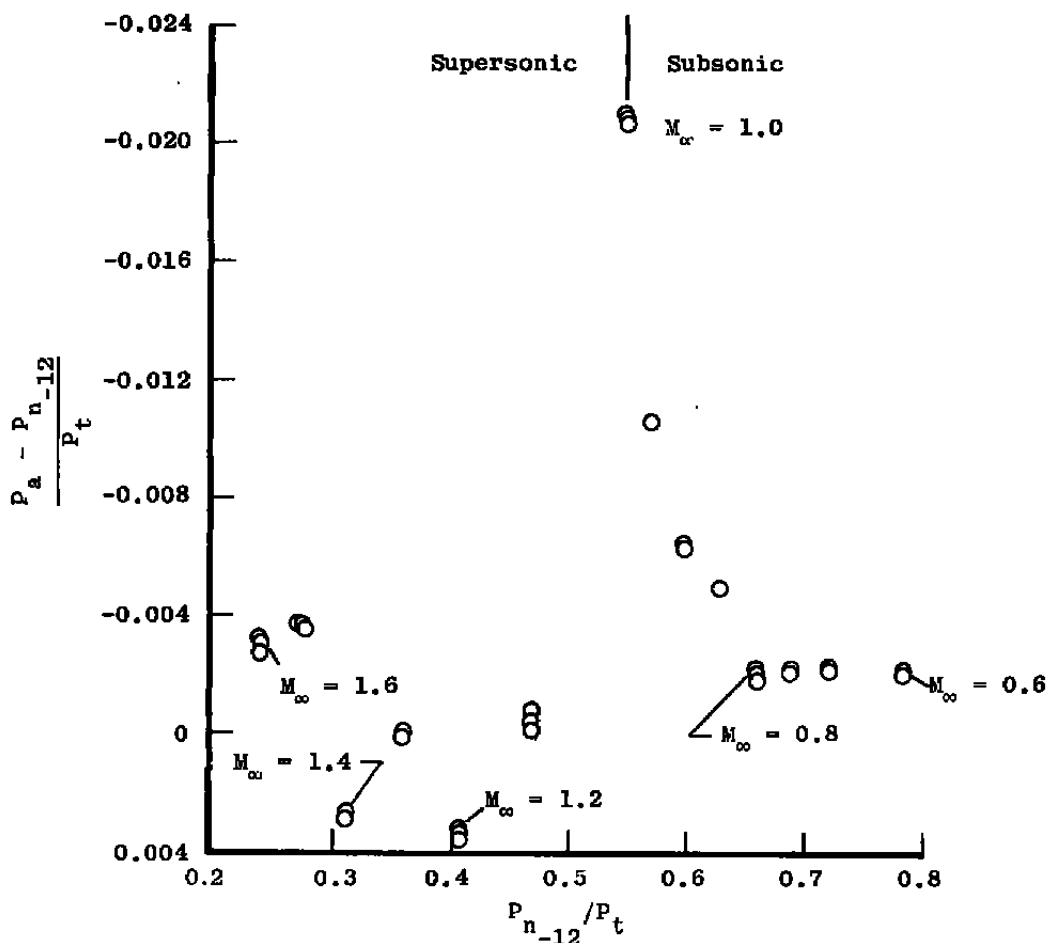
Figure 27. Tunnel 16T pressure calibrations from  $M_\infty = 0.6$  to 1.6  
with  $\lambda = \lambda^*$ ,  $\theta = 0$ , and  $P_t = 1,600$  psfa.



b. Test section static pressure only  
Figure 27. Continued.



c. Test section and nozzle static pressure difference at station -4

d. Test section and nozzle static pressure difference at station -12  
Figure 27. Concluded.

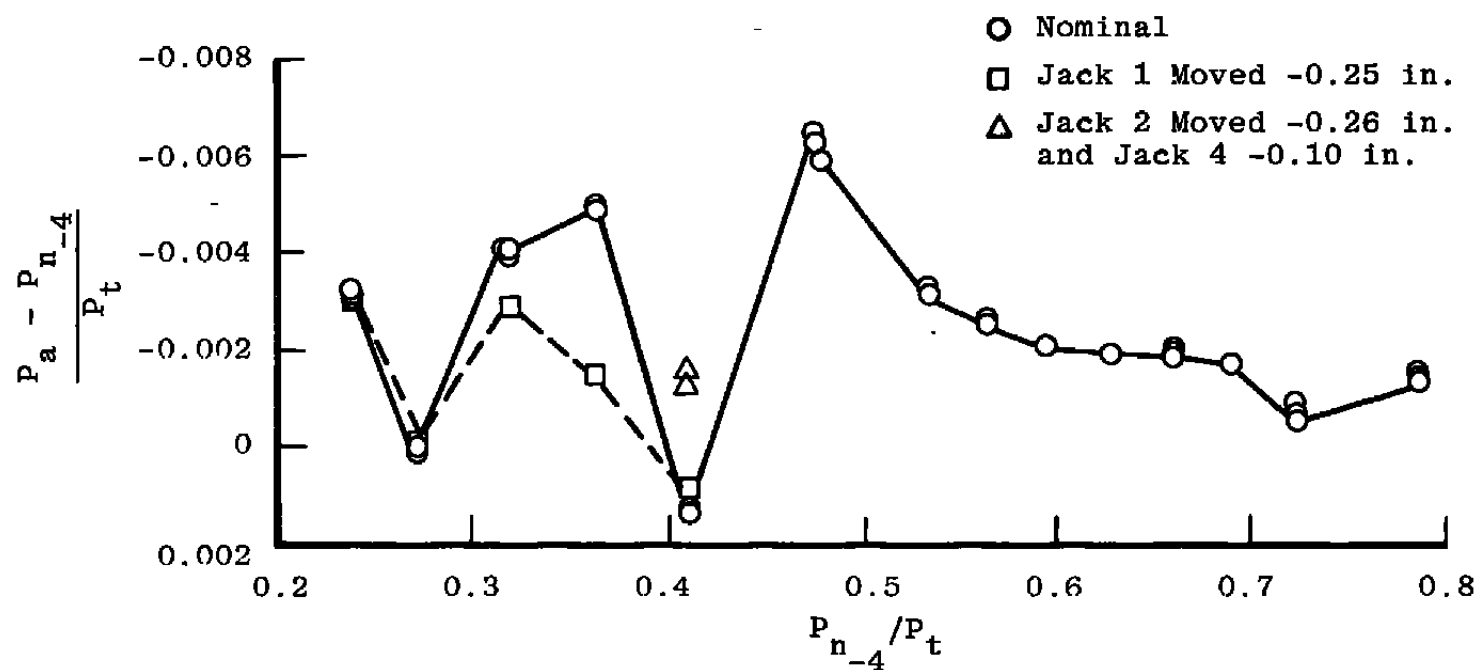
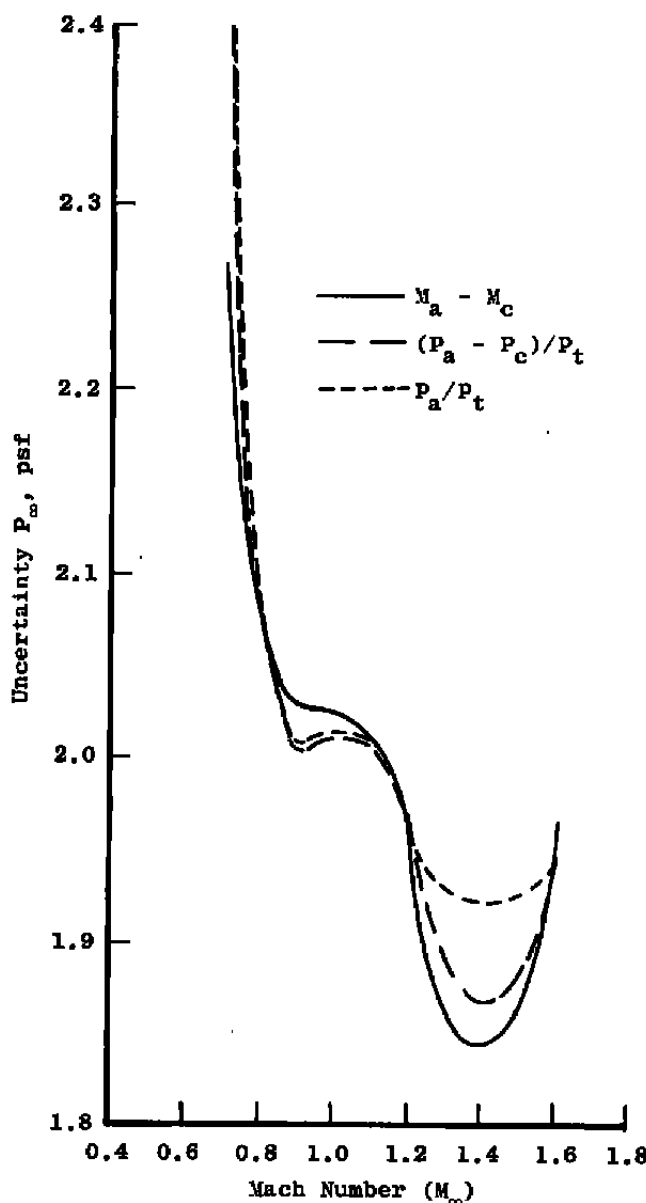
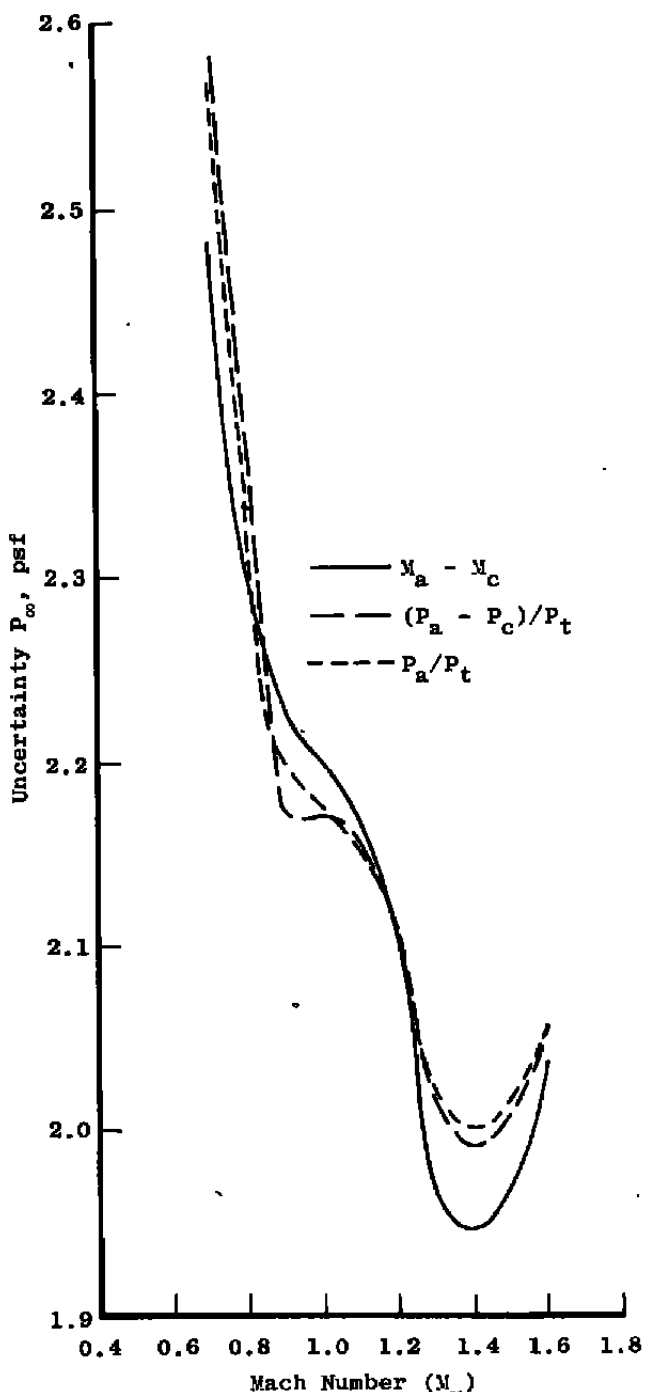


Figure 28. Effect of nozzle jack perturbations on the nozzle-test section calibration with  $\lambda = \lambda^*$ ,  $\theta = 0$ , and  $P_t = 1,600$  psfa.

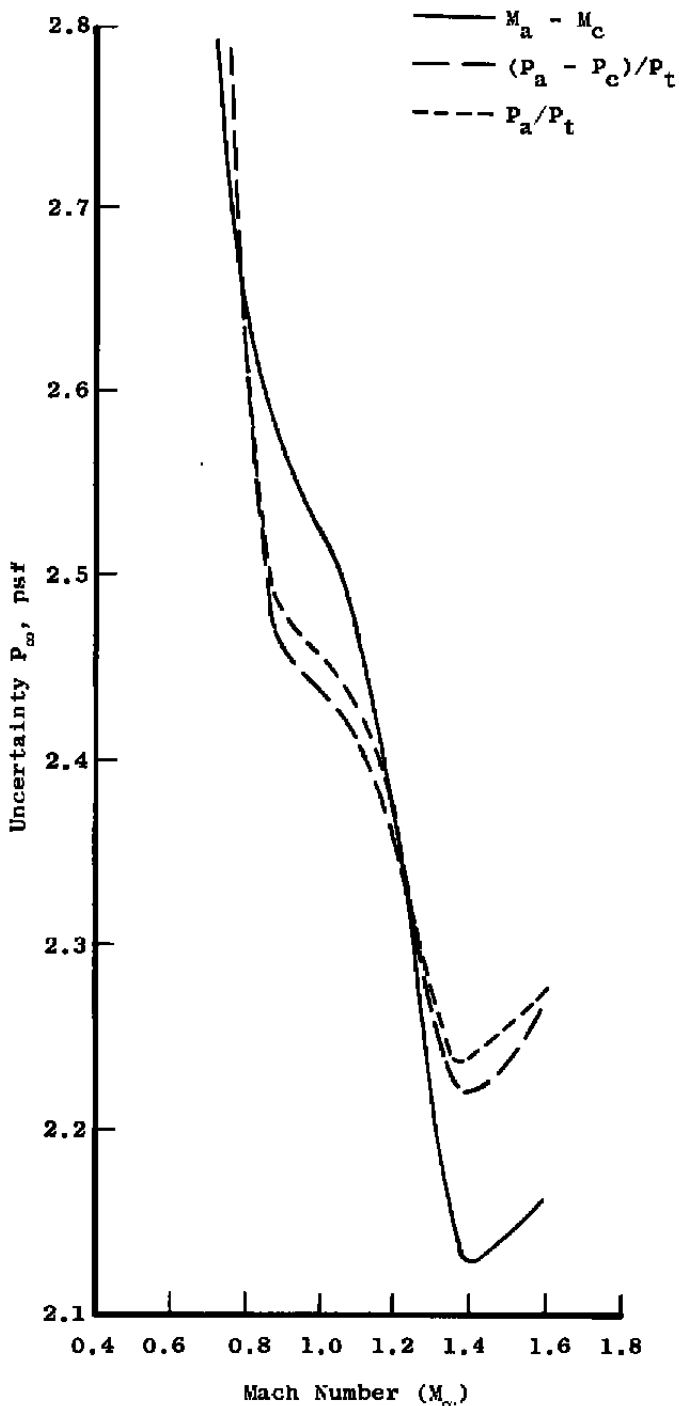


a.  $P_t = 1,000$  psfa

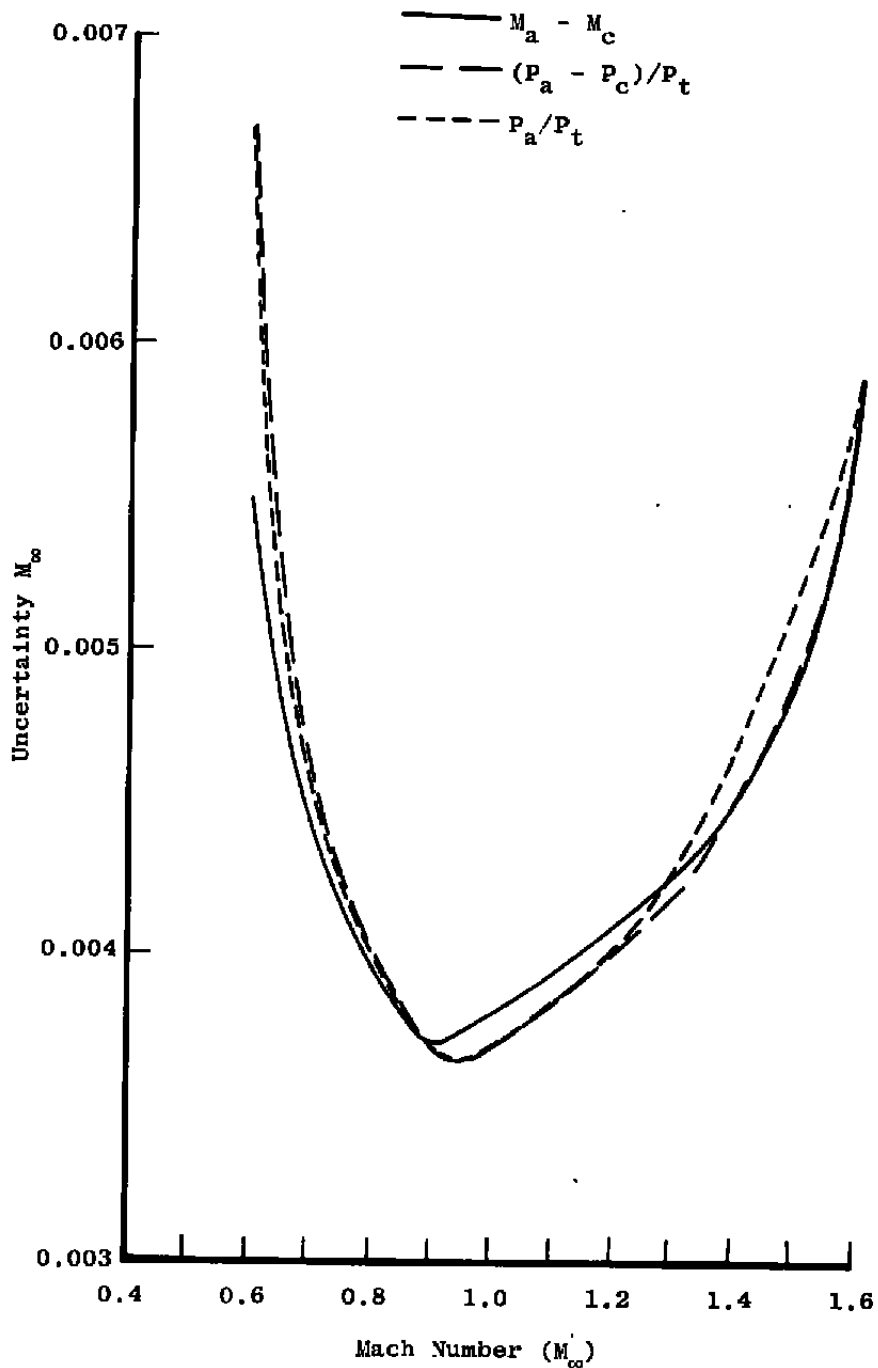
Figure 29. Effect of the calibration method on the uncertainty of the calibrated free-stream static pressure with  $\theta = 0$ .



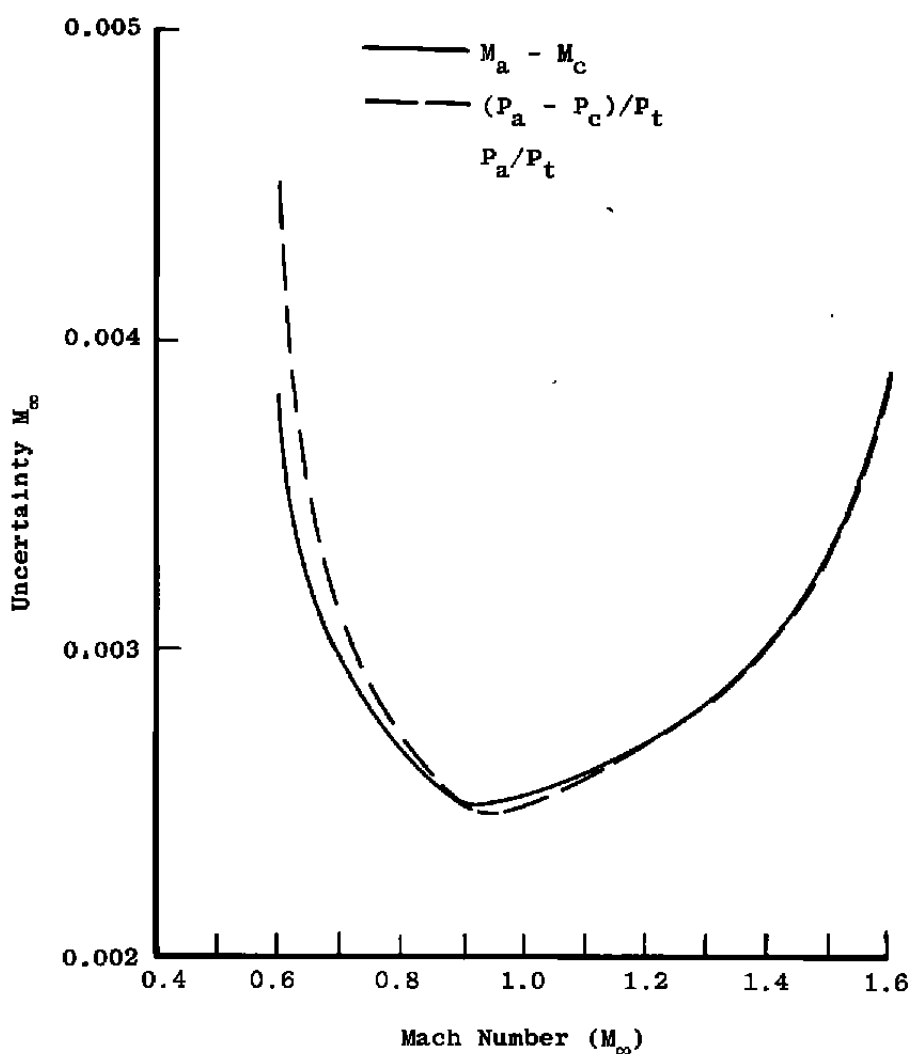
b.  $P_t = 1,600$  psfa  
Figure 29. Continued.



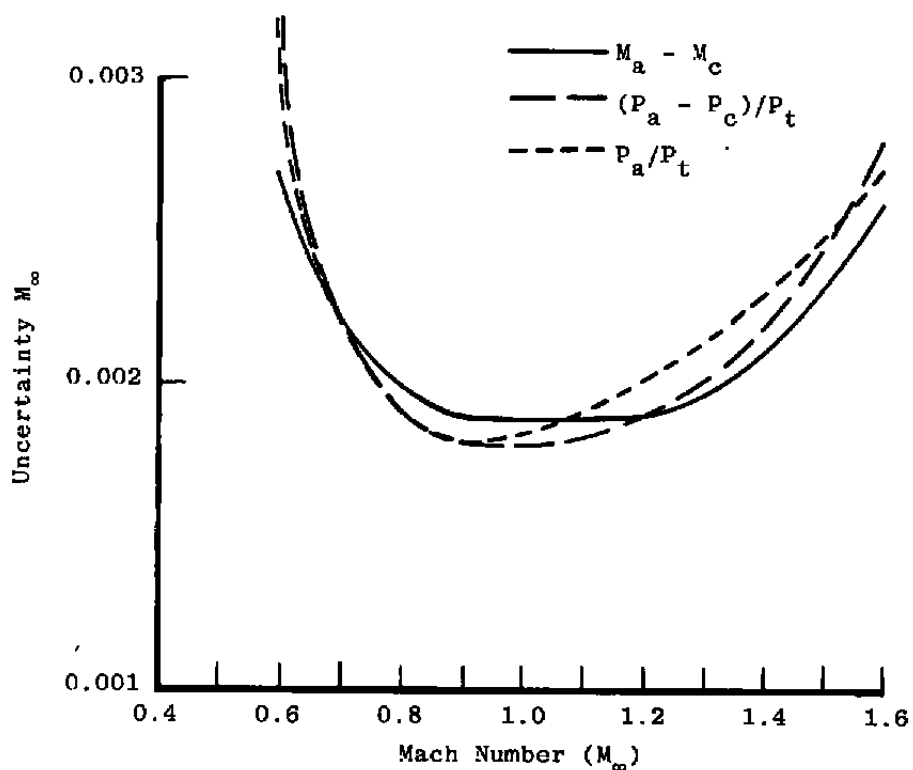
c.  $P_t = 2,500$  psfa  
Figure 29. Concluded.



a.  $P_t = 1,000$  psfa  
**Figure 30. Effect of the calibration method on the uncertainty of the calibrated free-stream Mach number with  $\theta = 0$ .**



b.  $P_t = 1,600$  psfa  
Figure 30. Continued.



c.  $P_t = 2,500$  psfa  
Figure 30. Concluded.

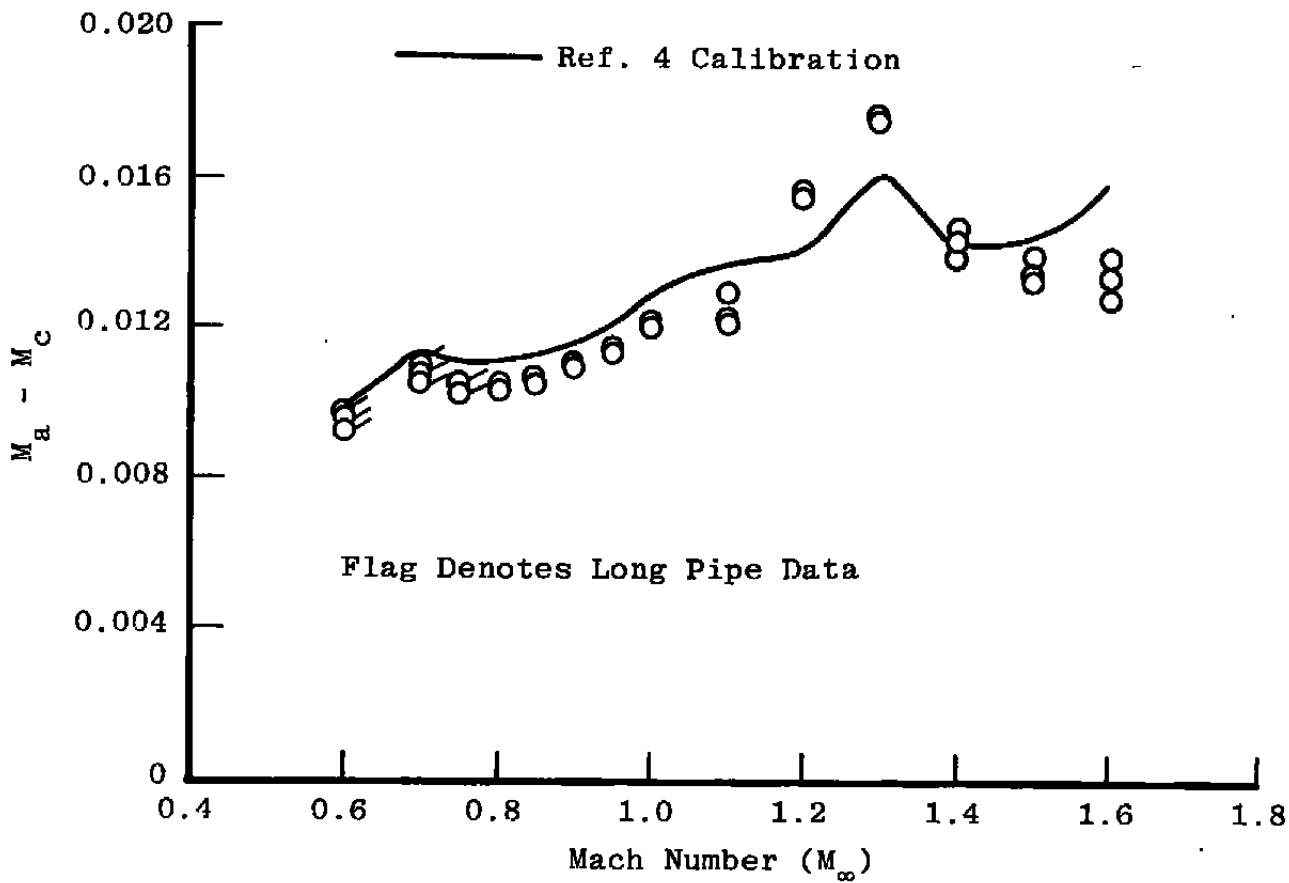


Figure 31. Effect of Mach number on the calibration with  $\lambda = \lambda^*$ ,  $\theta = 0$ , and  $P_t = 1,600$  psfa.

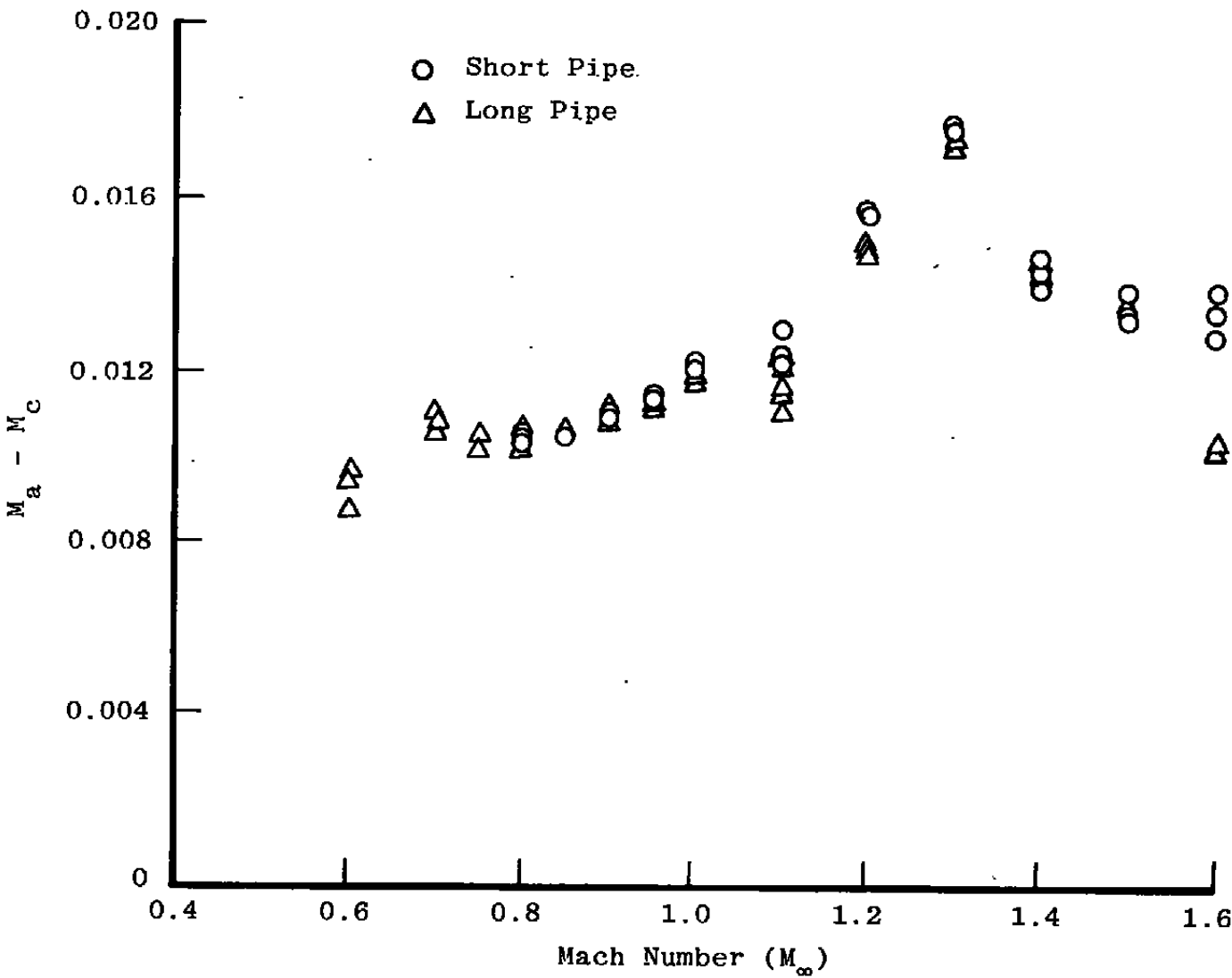


Figure 32. Effect of the centerline pipe length on the calibration with  $\lambda = \lambda^*$ ,  $\theta = 0$ , and  $P_t = 1,600$  psfa.

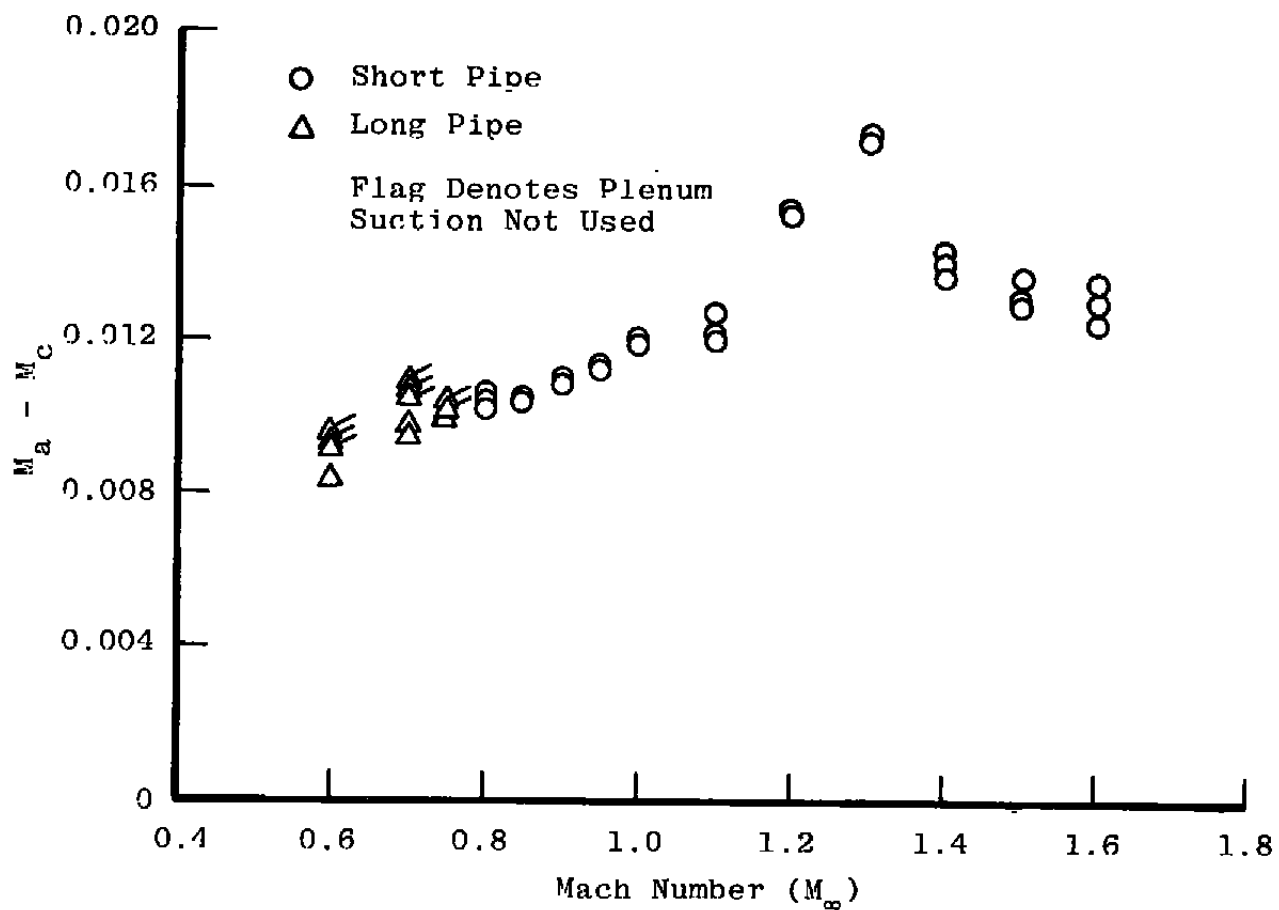
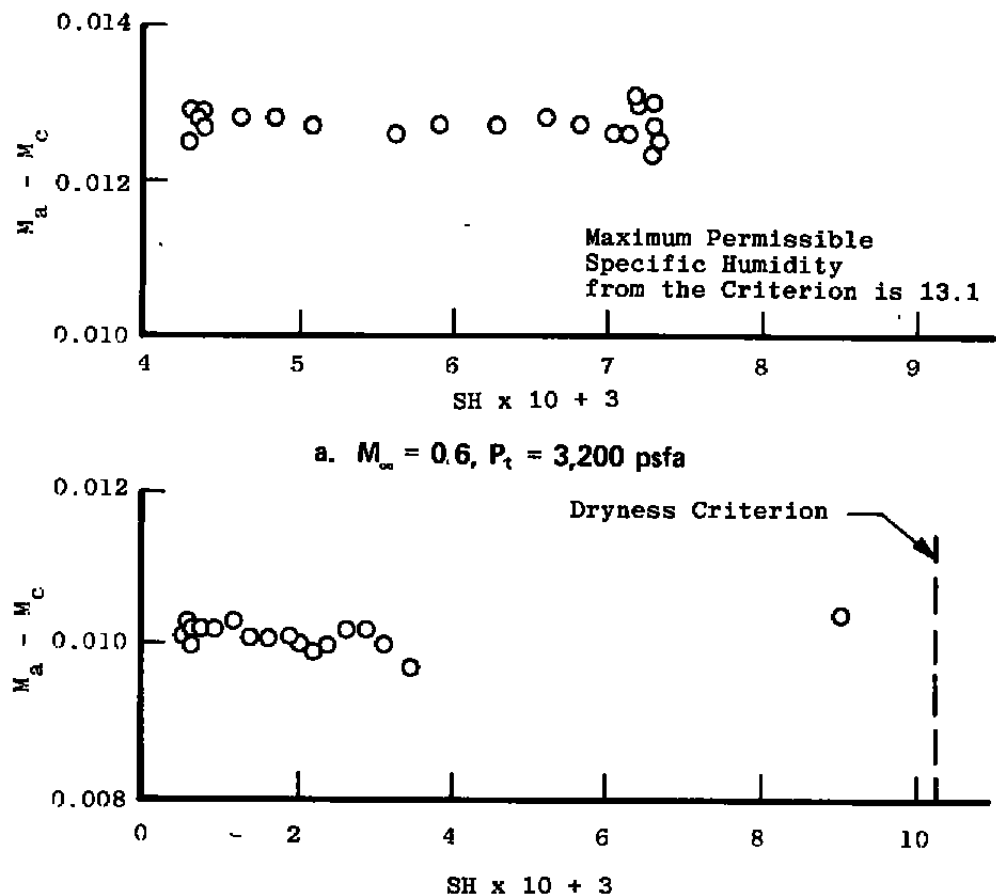
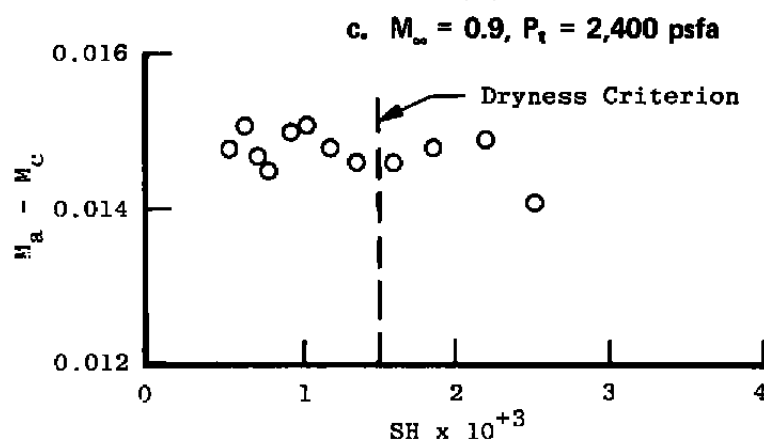
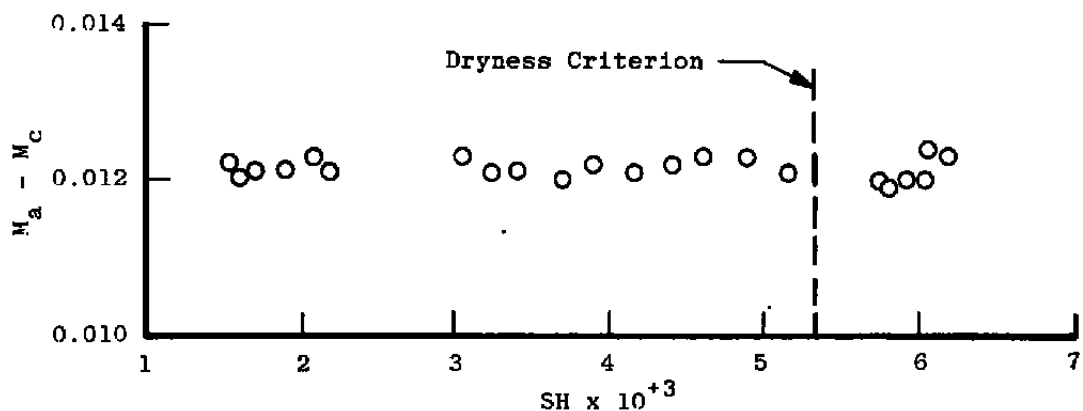


Figure 33. Effect of plenum chamber suction on the calibration at  $M_\infty \leq 0.75$  with  $\lambda = \lambda^*$ ,  $\theta = 0$ , and  $P_t = 1,600$  psfa.



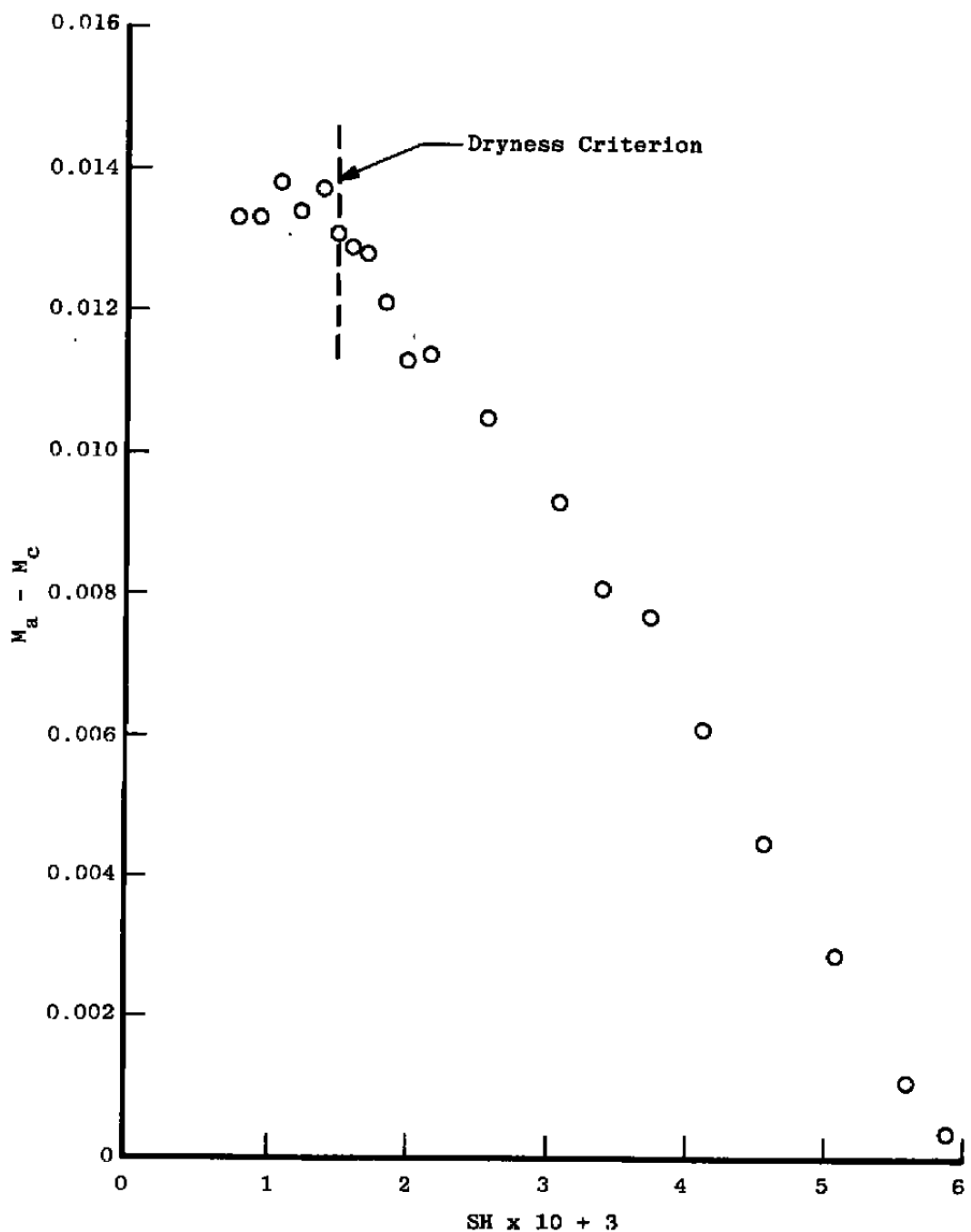
b.  $M_{\infty} = 0.9$ ,  $P_t = 1,200$  psfa  
**Figure 34. Effect of test section humidity on the Mach number calibration with  $\lambda = \lambda^*$ ,  $\theta = 0$ .**



c.  $M_\infty = 0.9, P_t = 2,400$  psfa

d.  $M_\infty = 1.2, P_t = 1,600$  psfa

Figure 34. Continued.



e.  $M_\infty = 1.5$ ,  $P_t = 1,600$  psfa  
Figure 34. Concluded.

## APPENDIX A

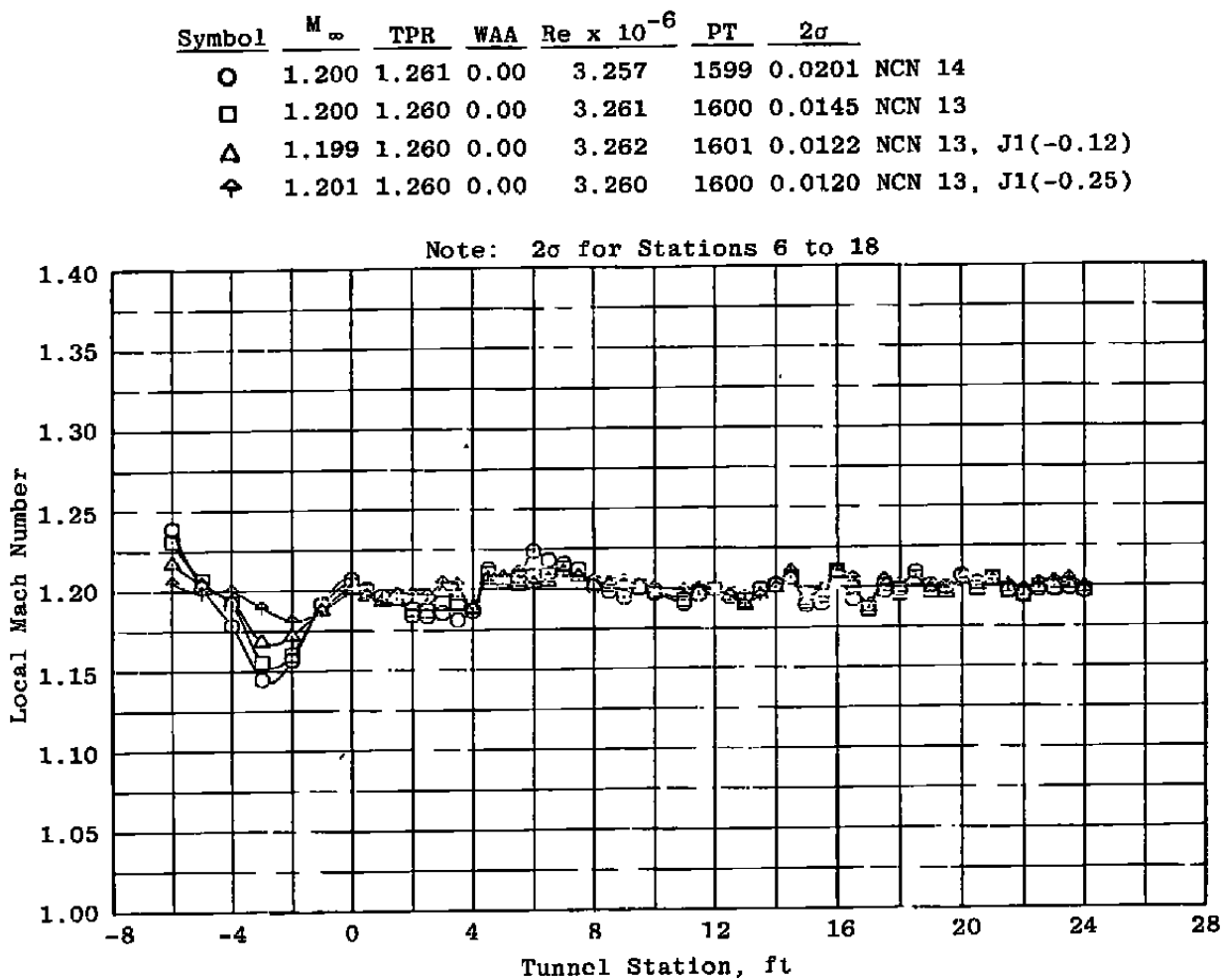
### NOZZLE JACK PERTURBATIONS

The Tunnel 16T nozzle design contours were modified by utilizing off-design contours or by perturbing various combinations of nozzle jacks 1, 2, 4, 5, and 6 to improve the centerline Mach number distributions. The disturbance at tunnel station 4 at  $M_{\infty} = 1.2$  reported in Ref. 4 was a special concern, especially since it had become larger (Fig. 7a) and extended to tunnel station 8. Since extending the calibration pipe did not remove the disturbance, a nozzle irregularity was assumed to cause the disturbance. The effects of perturbing the nozzle on the Mach distributions at  $M_{\infty} = 1.2$  are presented in Fig. A1. The disturbance at tunnel station 4 was not removed, but the flow acceleration at tunnel station 5 was decreased. In general, the Mach number distribution was improved and the  $2\sigma$  deviations decreased as the nozzle was perturbed. The fact that the nozzle perturbations did not remove the disturbance at station 4 reinforces the possibility of the disturbance originating at the test section-nozzle interface (STATION 0), as indicated by Mach lines traced from tunnel station 0 which intersect the calibration pipe in the vicinity of tunnel station 4 presented in Ref. 4. This hypothesis should be investigated during a subsequent calibration.

The effects of the nozzle perturbations at  $M_{\infty} = 1.0, 1.3, 1.4, 1.5$ , and  $1.6$  are presented in Figs. A2 through A6. The Mach number distributions were also improved at  $M_{\infty} = 1.4, 1.5$ , and  $1.6$ . The Mach number distributions were not changed at  $M_{\infty} = 1.0$  and became worse at  $M_{\infty} = 1.3$ . The disturbances in the Mach distributions downstream of tunnel station 16 were not affected by changes in the nozzle contours. These disturbances may be attributed to surface irregularities on the calibration pipe, orifice imperfection, or waves originating test section walls.

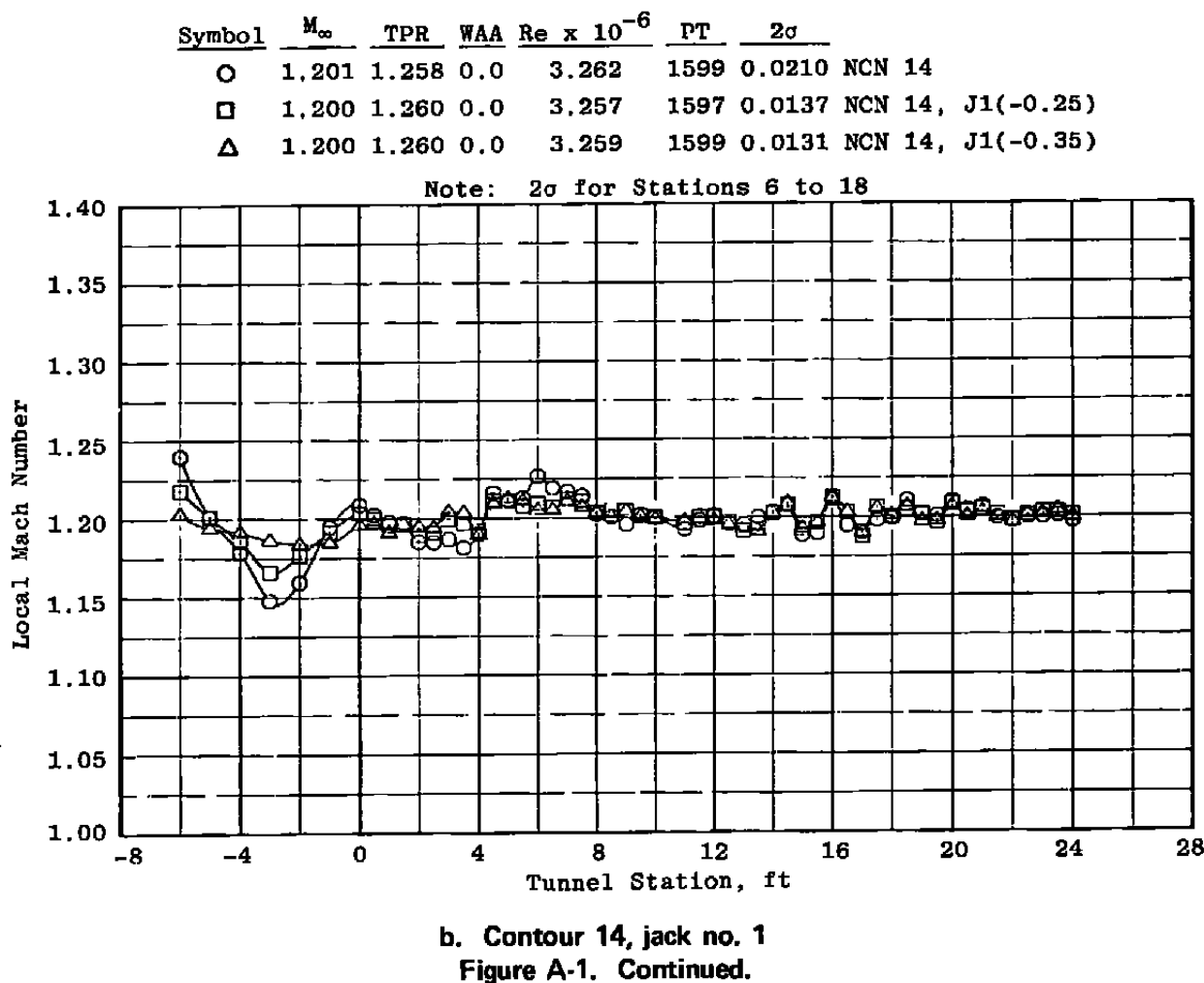
The data presented in Fig. A7 show the perturbations that had the most influence in making the calibration parameter ( $M_a - M_c$ ) equal the Ref. 4 data. The other perturbations had a smaller influence on the calibration or increased the difference between the current and Ref. 4 data. This indicates the possibility that the nozzle has changed between the current and Ref. 4 calibration test.

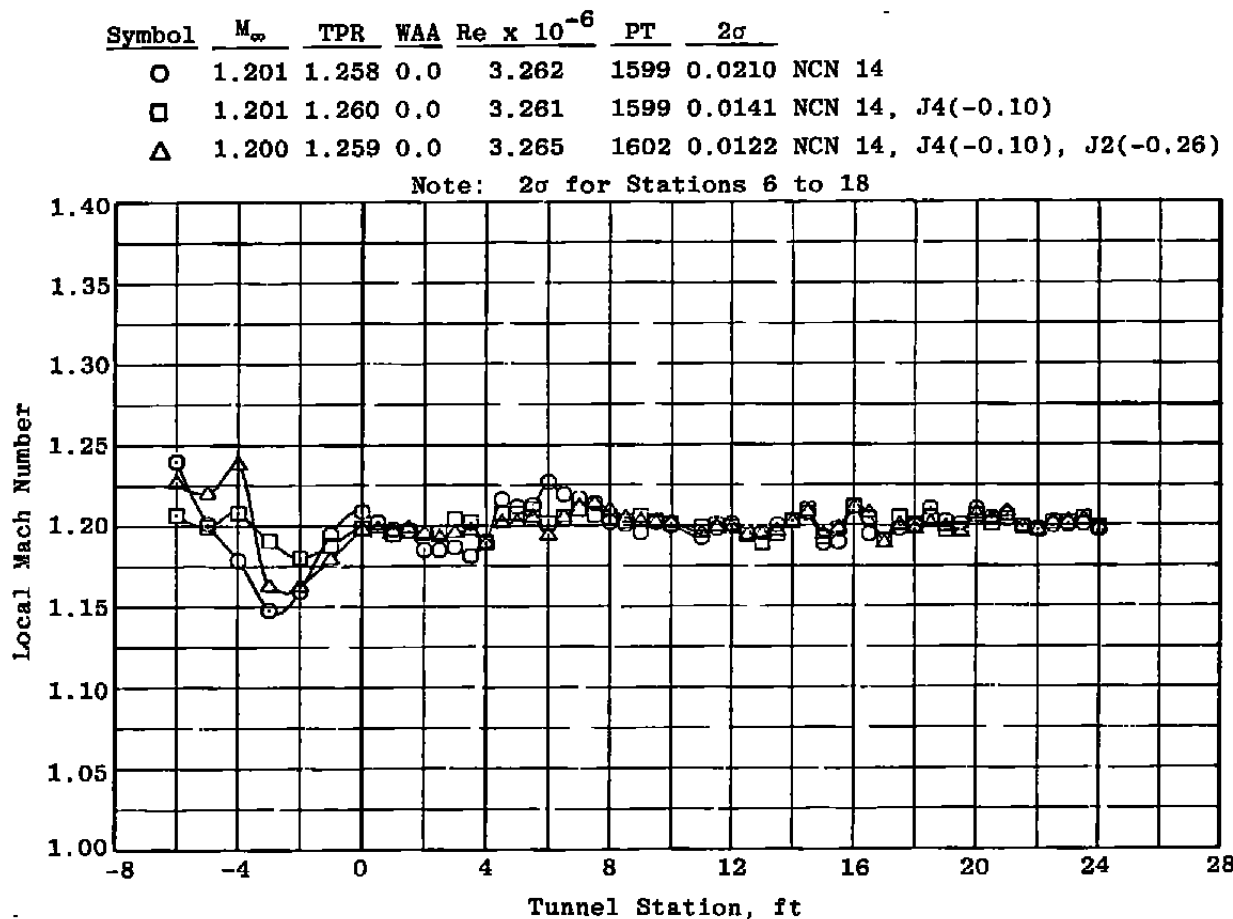
The data presented in Figs. A1 through A6 indicate that the centerline Mach distributions can be improved and the  $2\sigma$  deviations reduced. As a result of these data and nozzle contour measurements which indicated some nozzle jacks were out of tolerance, the nozzle and nozzle positioning system are being investigated. Additional discussion is beyond the scope of this report.



a. Contour 13, jack no. 1

Figure A-1. Effects of nozzle jack perturbations on the centerline distributions at  $M_\infty = 1.2$ .





c. Contour 14, jack nos. 2 and 4  
Figure A-1. Concluded.

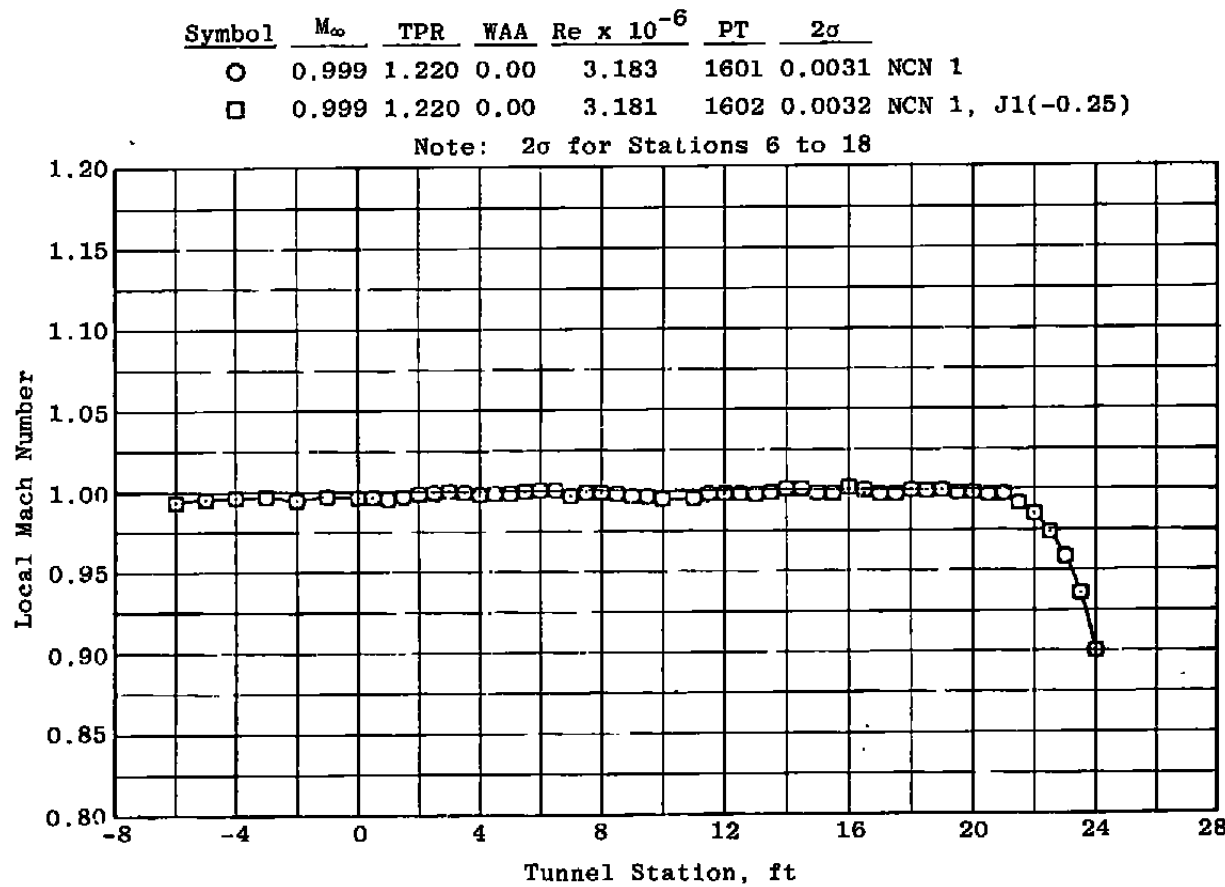
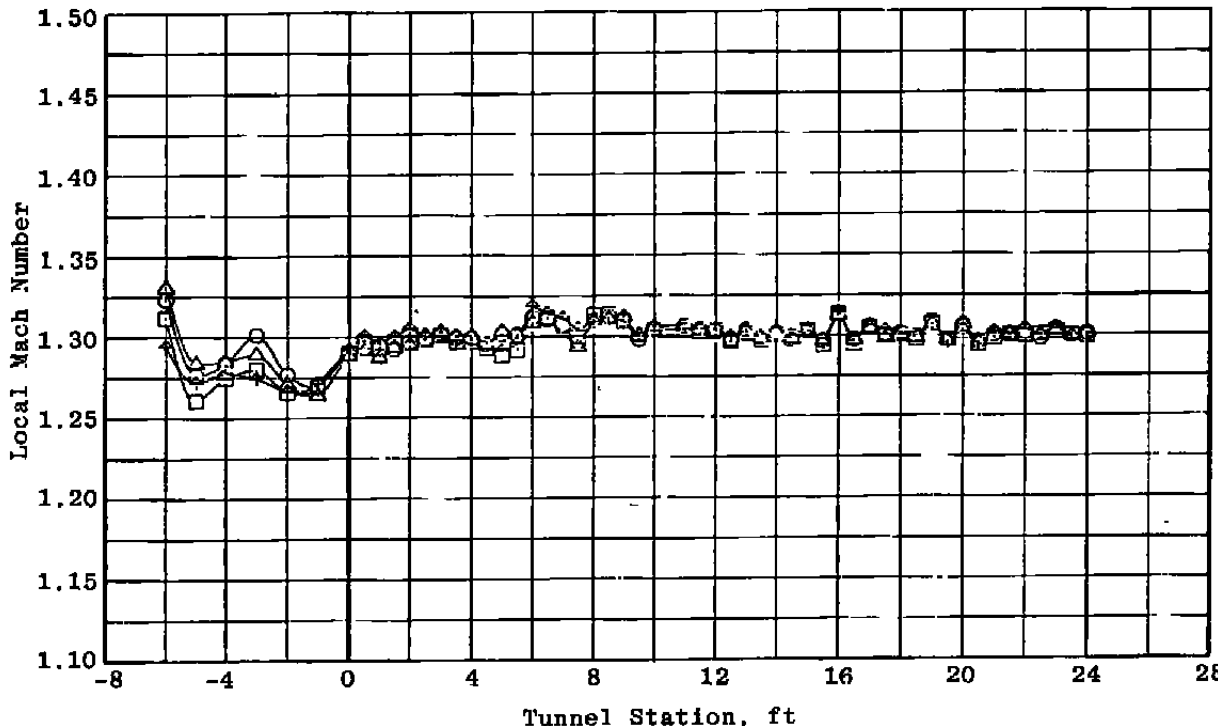


Figure A-2. Effect of perturbing nozzle jack no. 1 on the centerline distribution at  $M_\infty = 1.0$ .

Symbol	$M_\infty$	TPR	WAA	$Re \times 10^{-6}$	PT	$2\sigma$
○	1.300	1.281	0.0	3.253	1601	0.0113 NCN 20
□	1.300	1.281	0.0	3.253	1600	0.0123 NCN 20, J6(-0.27)
△	1.300	1.281	0.0	3.253	1600	0.0113 NCN 20, J6(-0.27), J5(-0.25)
▲	1.300	1.281	0.0	3.252	1599	0.0126 NCN 20, J6(-0.27), J5(-0.25), J1(-0.25)

Note:  $2\sigma$  for Stations 6 to 18

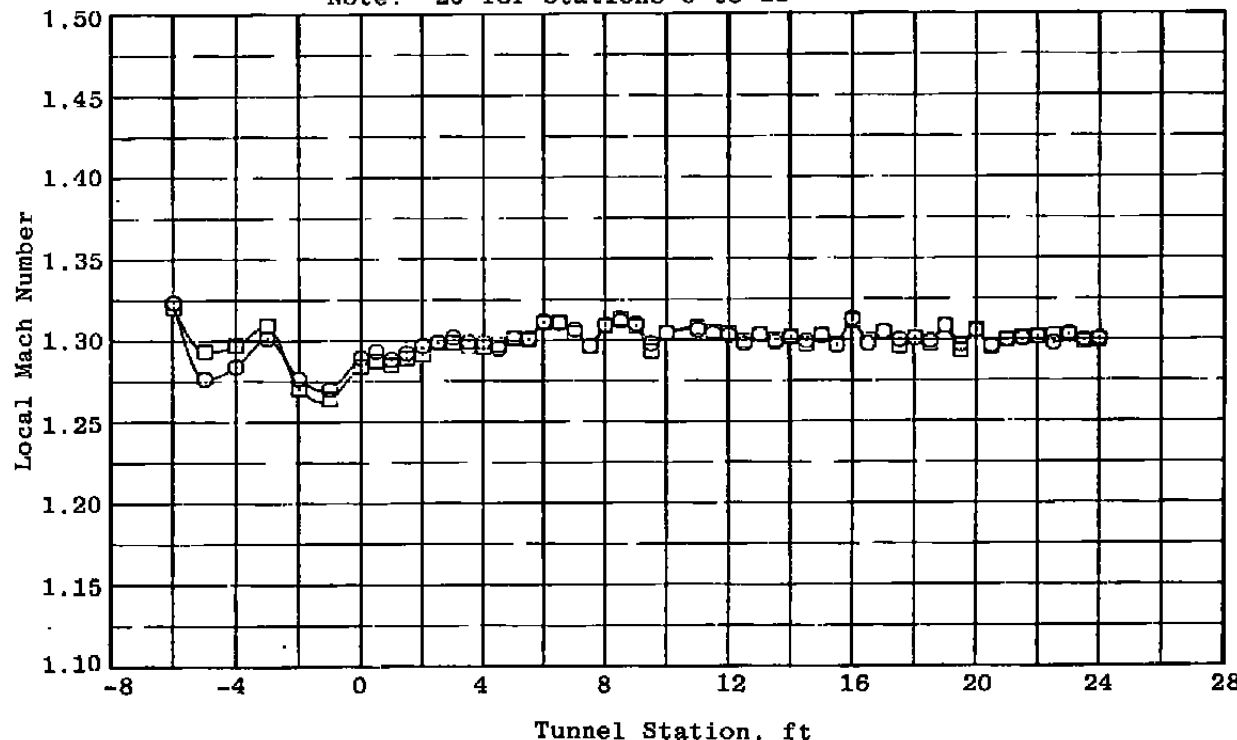


a. Contour 20, jack nos. 1, 5, 6

Figure A-3. Effects of nozzle jack perturbations on the centerline distributions at  $M_\infty = 1.3$ .

Symbol	$M_\infty$	TPR	WAA	$Re \times 10^{-6}$	PT	$2\sigma$
○	1,300	1.281	0.0	3.253	1601	0.0113 NCN 20
□	1,300	1.280	0.0	3.260	1603	0.0131 NCN 19

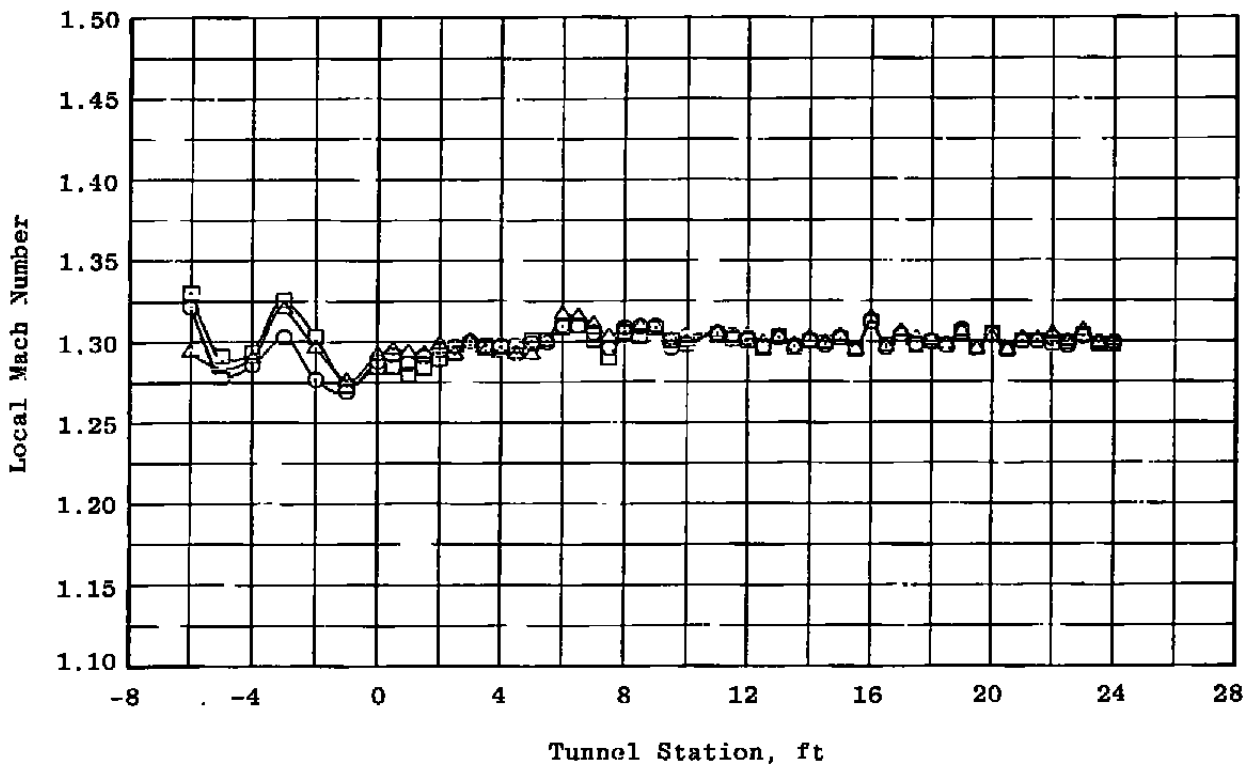
Note:  $2\sigma$  for Stations 6 to 18



b. Contours 19 and 20  
Figure A-3. Continued.

Symbol	$M_\infty$	TPR	WAA	$Re \times 10^{-6}$	PT	$2\sigma$
○	1.300	1.281	0.0	3.252	1600	0.0117 NCN 20
□	1.300	1.283	0.0	3.252	1601	0.0131 NCN 20, J6(+0.25)
△	1.300	1.283	0.0	3.251	1599	0.0131 NCN 20, J6(+0.25), J1(-0.25)

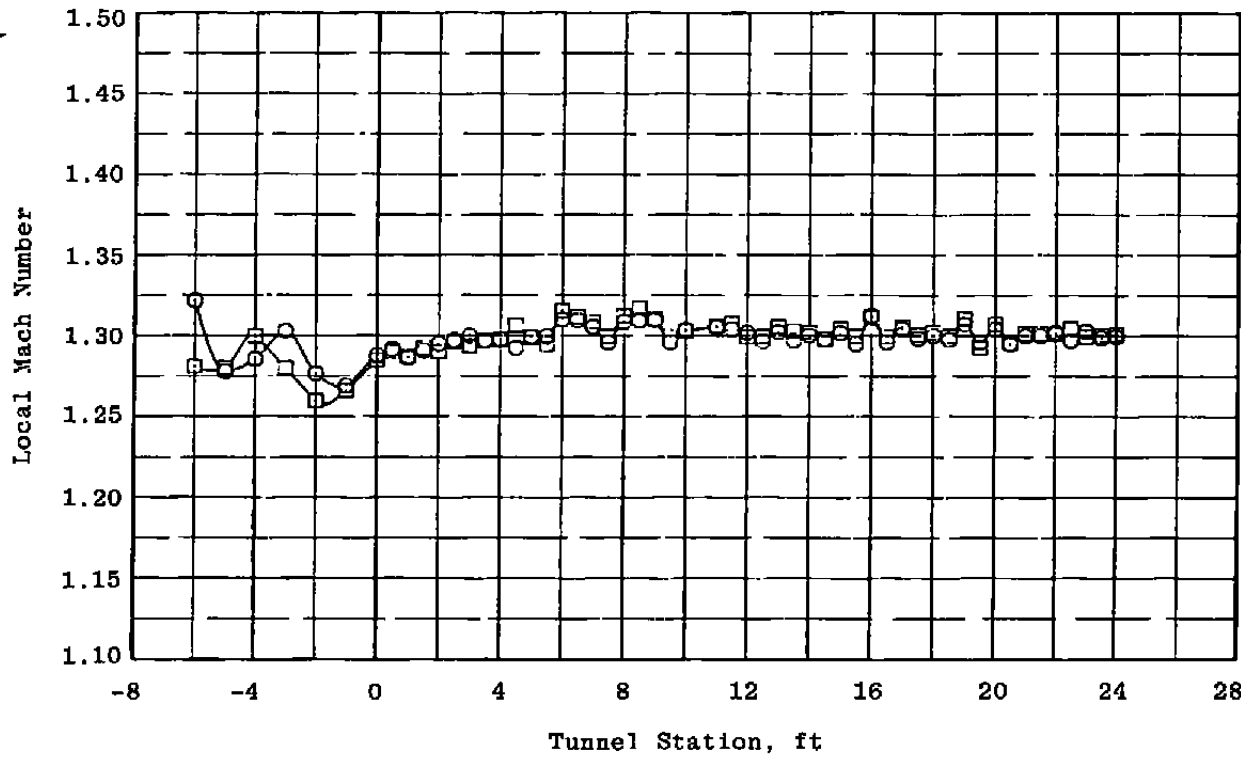
Note:  $2\sigma$  for Stations 6 to 18



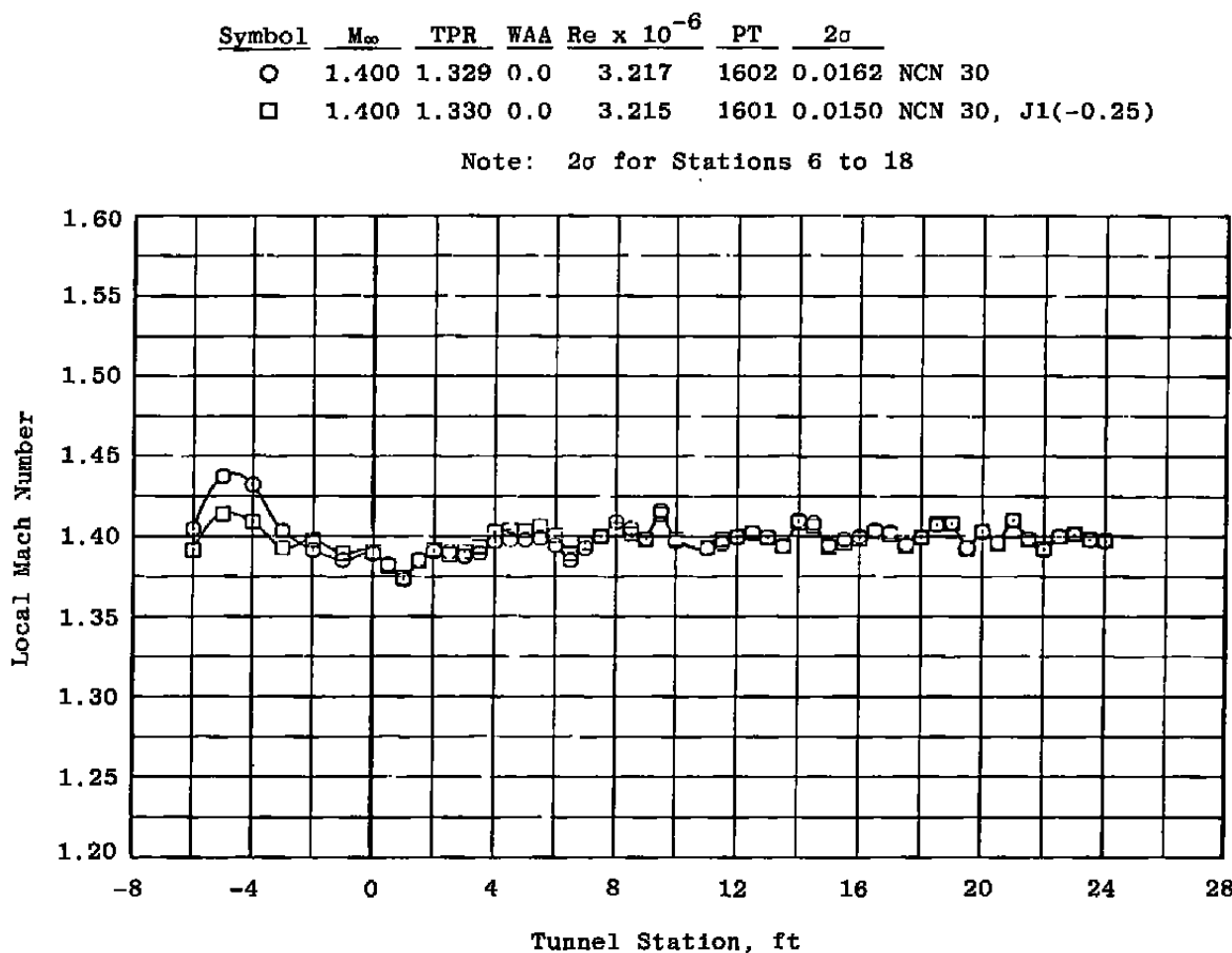
c. Contour 20, jack nos. 1 and 6  
Figure A-3. Continued.

Symbol	$M_\infty$	TPR	WAA	$Re \times 10^{-6}$	PT	$2\sigma$
○	1.300	1.281	0.0	3.252	1600	0.0117 NCN 20
□	1.300	1.275	0.0	3.255	1601	0.0141 NCN 18

Note:  $2\sigma$  for Stations 6 to 18

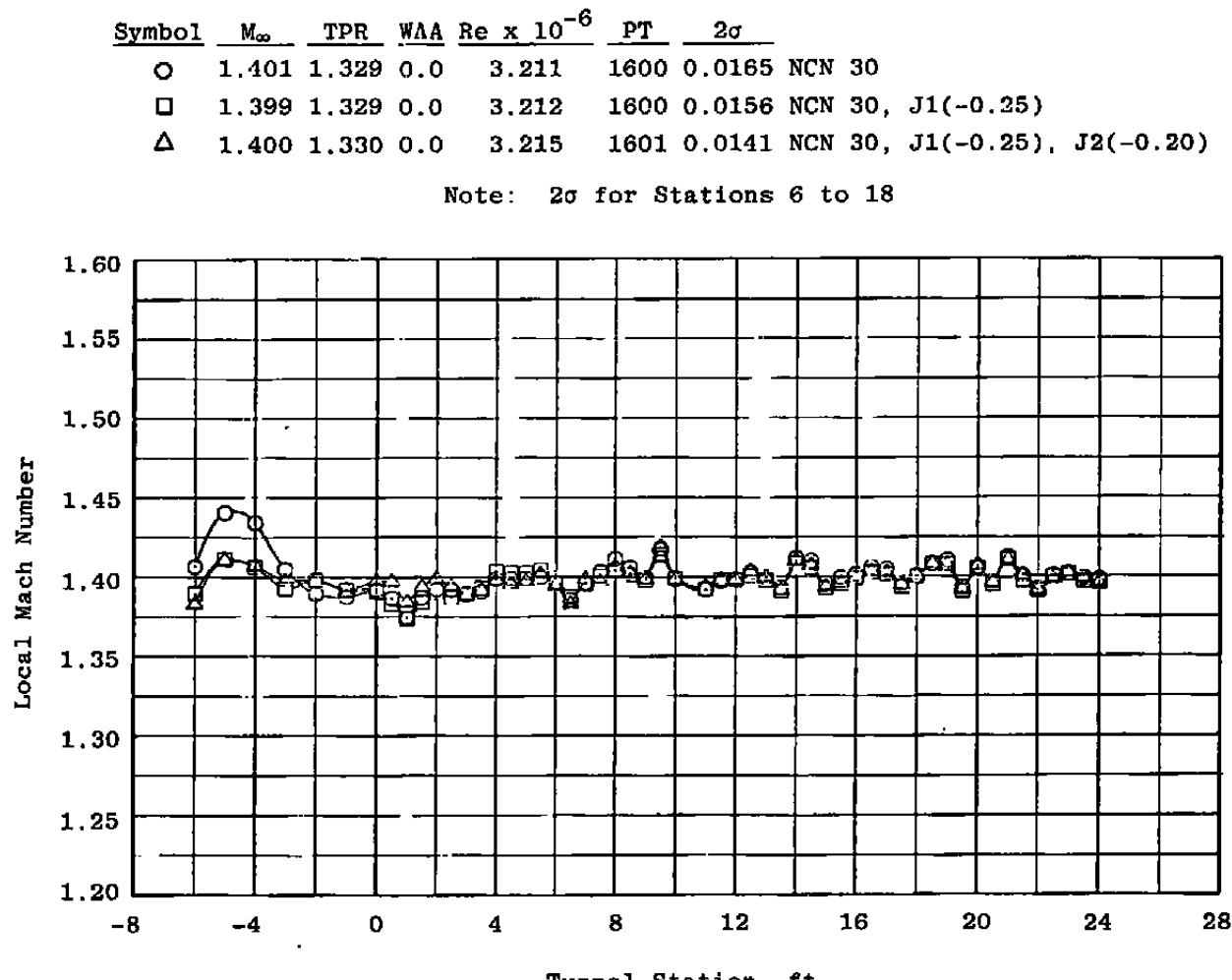


d. Contours 18 and 20  
Figure A-3. Concluded.



a, Contour 30, jack no. 1

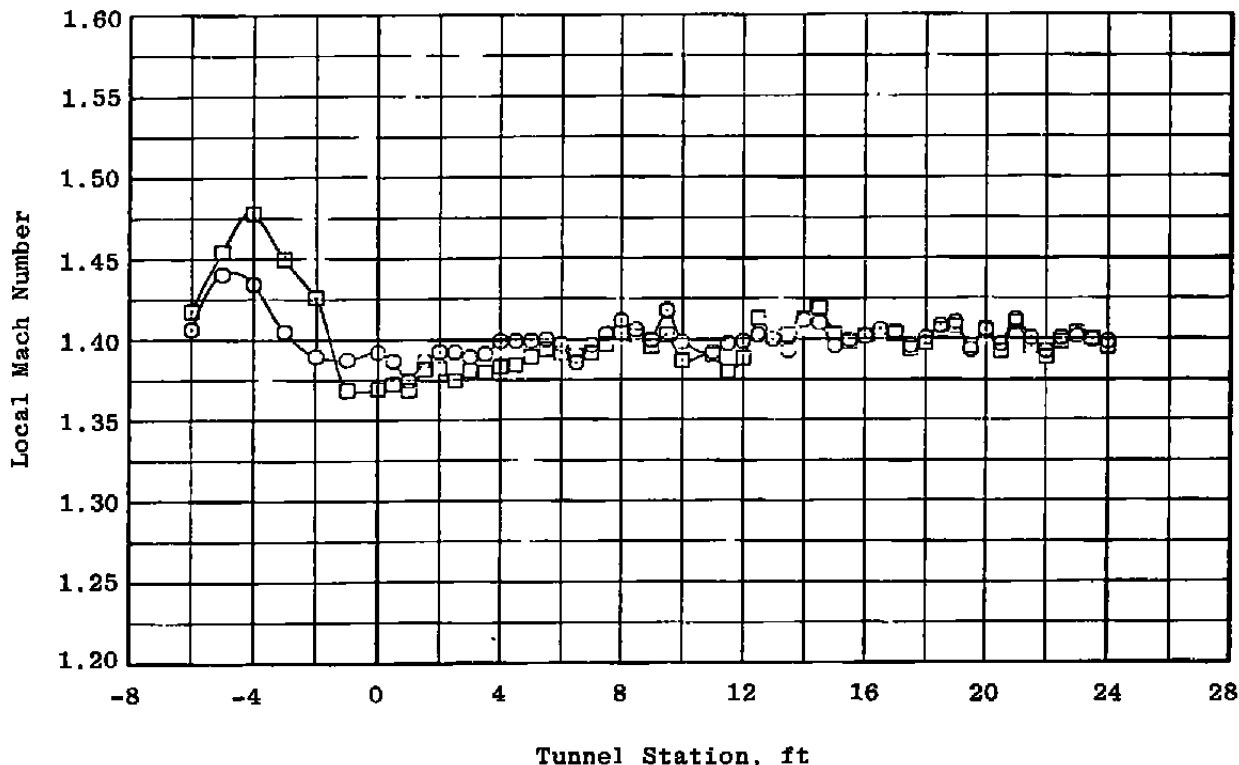
Figure A-4. Effects of nozzle jack perturbations on the centerline distributions at  $M_\infty = 1.4$ .



b. Contour 30, jack nos. 1 and 2  
Figure A-4. Continued.

Symbol	$M_\infty$	TPR	WAA	$Re \times 10^{-6}$	PT	$2\sigma$
○	1.401	1.329	0.0	3.211	1600	0.0165 NCN 30
□	1.400	1.331	0.0	3.219	1603	0.0235 NCN 33

Note:  $2\sigma$  for Stations 6 to 18



c. Contours 30 and 33  
Figure A-4. Concluded.

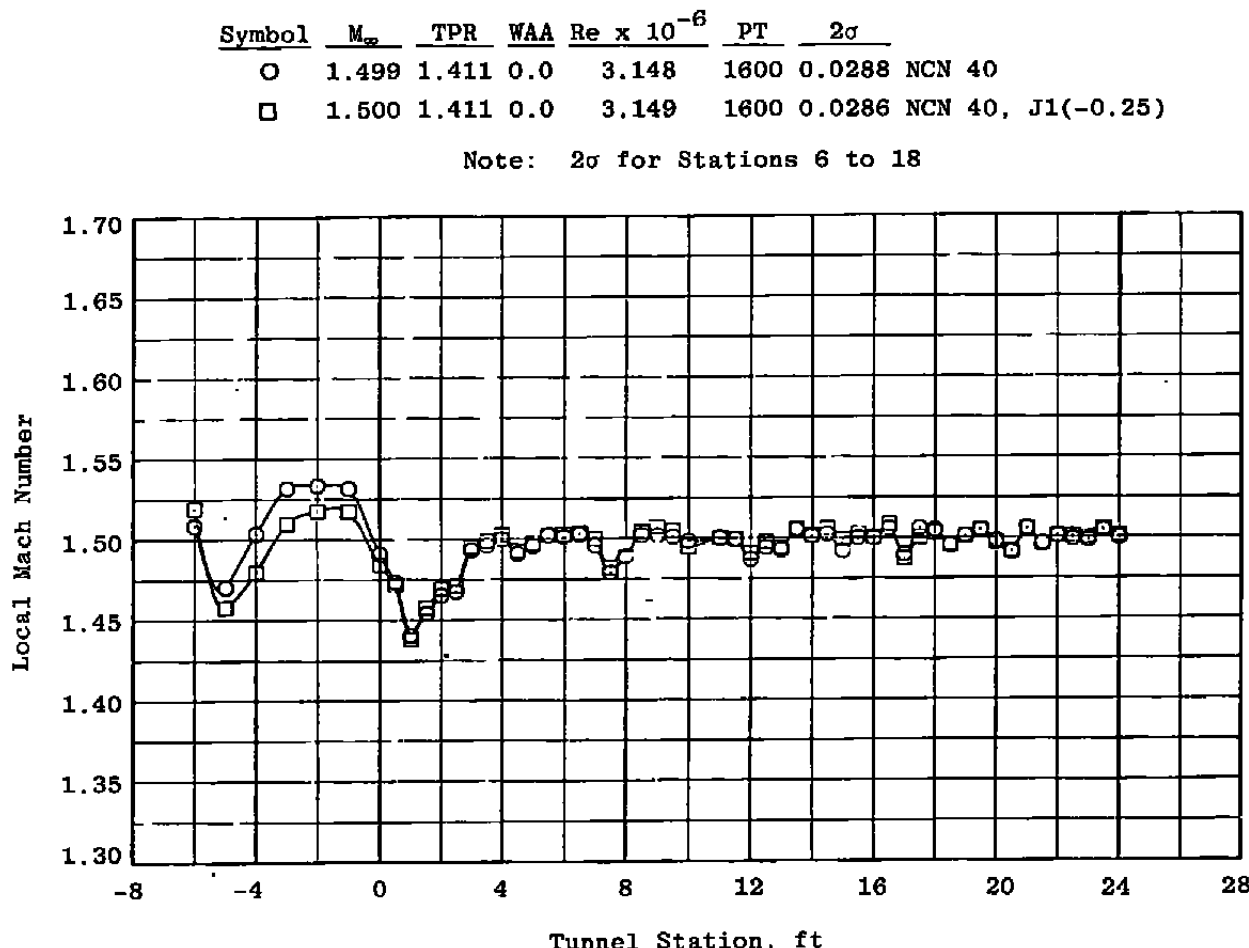


Figure A-5. Effect of perturbing nozzle jack no. 1 on the centerline distribution at  $M_\infty = 1.5$ .

Symbol	$M_\infty$	TPR	WAA	$Re \times 10^{-6}$	PT	$2\sigma$
○	1.600	1.411	0.0	3.075	1603	0.0319 NCN 45
□	1.599	1.411	0.0	3.073	1603	0.0302 NCN 45, J1(-0.25)

Note:  $2\sigma$  for Stations 6 to 18

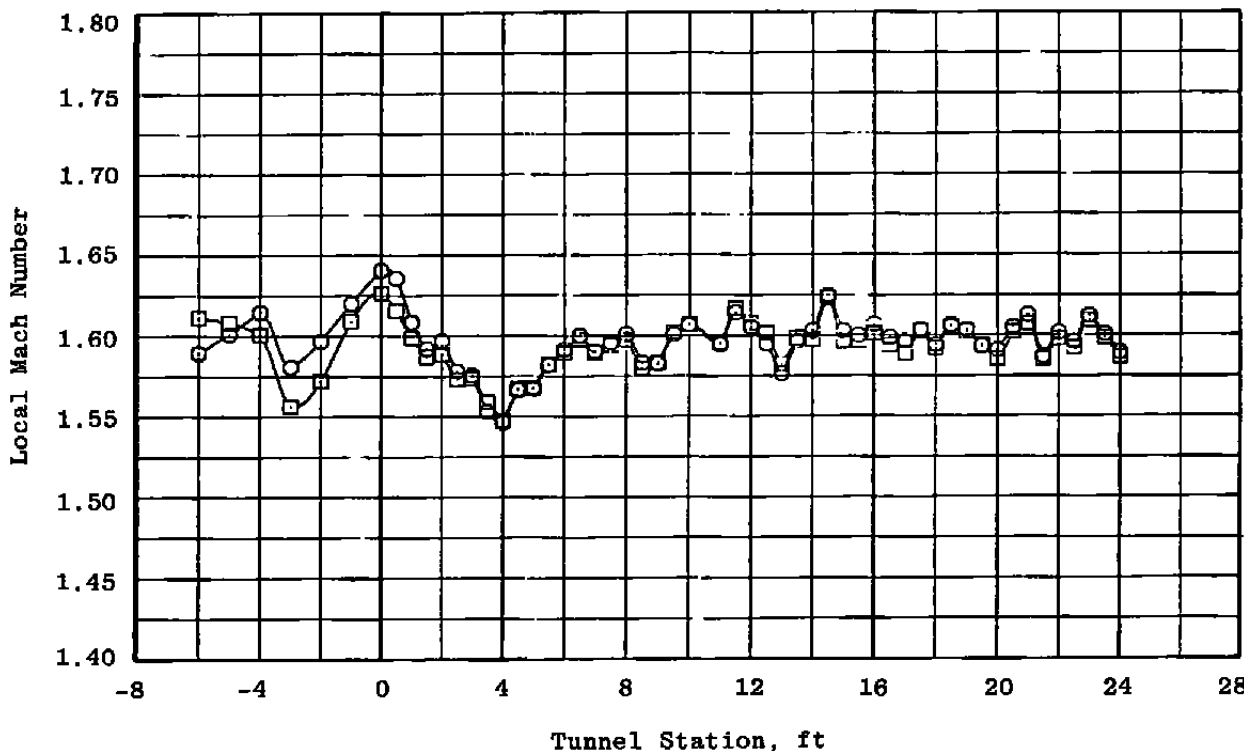


Figure A-6. Effect of perturbing nozzle jack no. 1 on the centerline distribution at  $M_\infty = 1.6$ .

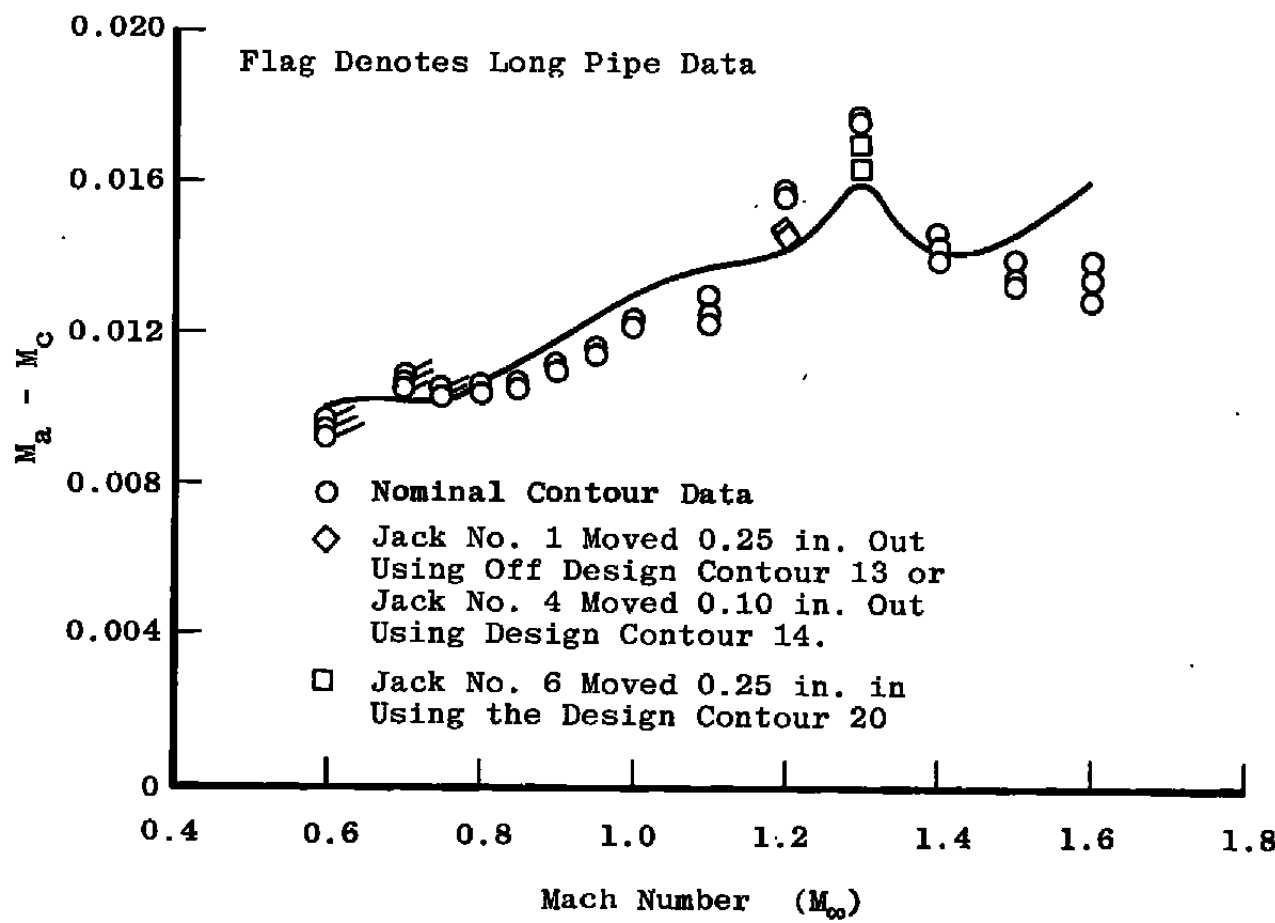


Figure A-7. The effect of nozzle jack perturbations on the calibration with  $\lambda = \lambda^*$ ,  $\theta = 0$ , and  $P_t = 1,600$  psfa.

## NOMENCLATURE

$E_t$	Tunnel total power factor, (total power)/ $P_t$ , MW/psf
$J_i$	Distance nozzle jack number $i$ is moved in in., (positive is toward the nozzle centerline)
$M_a$	Average Mach number from tunnel stations 6 to 18 on the centerline ( $M_a \approx M_\infty$ )
$M_c$	Equivalent plenum chamber Mach number, $f(p_c/p_t)$
$M_{local}$	Mach number calculated at each pressure orifice using isentropic relations
$M_{NA}$	Average nozzle Mach number at tunnel station -4 or -12
$M_\infty$	Free-stream Mach number
NCN	Nozzle contour number
$P_a$	Average static pressure from tunnel stations 6 to 18 on the centerline ( $P_a \approx P_\infty$ ), psf
$P_c$	Plenum chamber pressure, psfa
$P_{nozzle}$	Nozzle average static pressure measured by orifices on the nozzle walls, psf
$P_t$	Tunnel stagnation pressure, psfa
$P_\infty$	Free-stream static pressure, psf
$SH \times 10 + 3$	Test section specific humidity, lb $H_2O$ /lb dry air
$\theta$	Test section wall angle, deg (positive when walls are diverged)
$\theta^*$	Optimum wall angle, deg (Fig. 4)
$\lambda$	Tunnel pressure ratio, ratio of $P_t$ to the compressor inlet pressure

$\lambda^*$

**Nominal tunnel pressure ratio (Fig. 5)**

$\sigma$

**Standard deviation (conventional statistical parameter)**

$\omega$

**Plenum weight flow ratio; plenum weight flow divided by the tunnel weight flow**